Slope effects on liquefaction potential and pore pressure generation in earthquake loading

Katherine Marie deLaveaga

A thesis

submitted in partial fulfilment

of the requirements for the degree of

Master of Science in Civil Engineering

University of Washington

2017

Committee:

Steven L.Kramer

Joseph Wartman

Program authorized to offer degree:

Civil and Environmental Engineering

University of Washington

Abstract

Slope effects on pore pressure generation and liquefaction potential under earthquake loading

Katherine Marie deLaveaga

Chair of the Supervisory Committee:
Professor Steven Kramer
Civil and Environmental Engineering

Loose, saturated sand or silt deposits can often be susceptible to liquefaction deformations during earthquakes. If these deposits are also on or near slopes or embankments, liquefaction events can lead to damages from lateral spreading or embankment failures. The mechanical study of slope effects and initial static shear stresses on liquefaction resistance is still in development. Furthermore, the literature regarding semi-empirical or Factor of Safety approach to liquefaction site analysis is complicated and presents contradictory results, which often leads professionals to ignore slope effects in engineering liquefaction analyses.

However, the standards for characterizing earthquake loading has progressed significantly in the past decades and equipment advances have now made it possible to simulate earthquake loading in soil shear testing. Thus, in addition to summarizing the current standards of liquefaction analyses, this report presents a parametric laboratory study of initial static shear stress on liquefiable sands (with minor emphasis on vertical effective stress, and density). This database is intended to be used as control experimental data on earthquake loading for the development of liquefaction models as part of Next Generation Liquefaction (NGL) project. The parametric program includes a total of 24 simple shear tests on Nevada sands with transient seismic loading on an electromechanical dynamic cyclic simple shear device (EMDCSS). The static shear stress factor (K_α) used in the Simplified Procedure for liquefaction (Seed and Idriss 1975) is empirically investigated under transient loading conditions and corrections for earthquake loading proposed through a regression analysis.

CONTENTS

CHAPTER 1: INTRODUCTION AND BACKGROUND

Despite its important role in soil response to earthquakes, the current state of knowledge of the workings of soil liquefaction events remains incomplete. Further, it is known that these events can cause massive amounts of damage; the 2010- 2011 Christchurch Earthquake sequence in New Zealand alone caused upwards of $40 billion in damages and repairs, with a large component of this damage contributed to residential destruction due to liquefaction (Teara.govt.nz, 2015) This phenomenon poses a hazard in certain soil types, and the mechanics of the event are highly dependent on site conditions and seismic motion characteristics, both of which can be difficult to assess. A clear understanding of the mechanisms of events (triggering, post-liquefaction state, and extent of deformations/damages) is crucial to liquefaction preparation for the creation of resilient communities.

Many site elements contribute to the engineering analysis of liquefaction potential. One of the technical case history issues currently lacking transparent laboratory data is the effect of initial, static shear stress on stress-strain behavior of a soil body before and after the triggering of liquefaction. These initial conditions are often present in slopes and embankments. Some experimental data is available (Seed & Harder, 1990; Boulanger, 2003; Cetin & Bilge, 2015), but there a consensus on the effects of static shear stress has not yet been fully established. As a result, current professional practice commonly ignores its effects in engineering analysis. Thus, it is often hazardously ignored in liquefaction evaluation; liquefaction which occurs on even slight slopes or near embankments can lead to extensive damage due to lateral spreading, cyclic liquefaction failures, etc.

This report is part of a larger geotechnical earthquake research effort known as Next Generation Liquefaction (NGL). This concept was conceived by researchers at the Pacific Earthquake Engineering Research (PEER) center in California and global partnering organizations as a new paradigm for ground failure modelling and research development. Using this paradigm, NGL seeks to create a transparent, centralized repository of information related to ground failure including case histories backed by laboratory data. NGL looks to provide a coordinated framework for supporting studies to augment case history data for conditions important for applications but poorly represented in empirical databases. Finally, NGL seeks to provide an open, collaborative process for model development in which developer teams have access to common resources, concepts, and results during model development, to reduce the potential for mistakes and to mutually benefit from best practices.

The creation of this database draws together the international work of several key players in the field including work done at the geotechnical groups of University of Washington, The University of Texas, and the Norwegian Geotechnical Institute. As part of their project to further the understanding of soil liquefaction hazards, NGL aims to create a holistic and transparent community database of liquefaction case histories and supporting laboratory data for use in developing predictive models for liquefaction and its effects. The essence of this paper is to present a laboratory data from cyclic simple shear tests with harmonic and transient loading—particularly as it pertains to initial static shear stresses—to supplement the sparse existing case history data for triggering of liquefaction under sloping ground conditions.

The effects of static shear stress are particularly well-suited for experimental investigation using cyclic simple shear testing. Such tests offer an easily obtainable and improved understanding on the generation of excess pore pressure and accumulation of permanent strain during

liquefaction. Careful and methodical laboratory testing programs of the static shear stress factor (K_α) on liquefaction resistance have been performed in the past, however these programs consist of cyclic or static loading without real seismic waveforms. Consequently, this paper seeks to investigate the effects of initial static shear stresses on pore pressure generation and liquefaction triggering in liquefiable sands via simple shear testing.

This report is organized into several parts. Chapter 2 presents an overview on the mechanics of liquefaction and current state of the field. Chapter 3 introduces a simple shear testing program investigating the effects of initial static shear stress on liquefaction potential. This program will be composed of seismic simple shear tests for a better translation between laboratory and field events. The tests presented in this paper are high quality and can be used for constitutive modelling calibration. All tests are graphically represented in Appendix A and the digital raw data is stored in an SQL database per the specifications laid out in Appendix C. Access to the database is available upon request to the author. Chapter 4 presents the findings of these testing programs and interprets the results.

CHAPTER 2: MECHANICS AND CONSEQUENCES OF LIQUEFACTION

The term *liquefaction* was brought to the public eye following two major seismic events which resulted in significant infrastructure damage in 1964; first the Good Friday earthquake of Alaska, USA and then three months later a large earthquake in Niigata, Japan. In addition to the expected damage from large magnitude earthquakes, both events were unique in that they triggered an unusual phenomenon in the soil. The soil, subjected to the large seismic loading, suddenly exhibited almost fluid-like behavior. Slopes failed causing debris to flow into streets and houses, buildings sank while buried pipes and objects floated to the surface, embankments spread and settled, and foundations lost nearly all bearing capacity. The final damage resulted in billions of dollars and many deaths. With the consequences of this phenomenon so openly exposed, a new wave of research sought to understand this hazard and identify sites that may be vulnerable to such events.

Many definitions of liquefaction have been presented. The term generally refers to a loss of strength and stiffness in saturated, cohesionless soils triggered by cyclic, seismic, or occasionally static disturbance. With reduced frictional strength between the particles, a soil body can become fluid-like and no longer remain standing on moderately steep slopes. Thus, extensive damage to property, utilities, agricultural lands, levee systems, and heavy infrastructure can occur, as proven by instances of liquefaction damage during earthquakes across the globe (1964 Alaska USA, 1964 Niigata Japan, 1989 Loma Prieta: San Francisco Marina District, 1995 Great Hanshin Earthquake: Kobe Japan, 2010 Canterbury Earthquake series: Christchurch NZ). The difficulty of

accurate predictions is due in part to the unpredictable timing and intensity of the seismic events, and in part to the still emerging understanding of the complex mechanical behavior of liquefiable soils. To better understand the liquefaction susceptibility of sloped sites, further insight into the mechanics of liquefaction is required.

Figure 1: Damage to infrastructure from liquefaction events. (left) River Road, Christchurch New Zealand damaged from lateral spreading in the 2011 earthquake series. (right) A dramatic example of sinking apartment buildings due to the loss of soil shear strength, Nigata, Japan 1964.

The mechanics of these events will be discussed in detail in the background section of this report, but it is summarized here as follows. Saturated soil bodies that may otherwise contract under disturbances are prevented from doing so by the incompressibility of the fluids surrounding the particles (Kramer, 1996). Thus, the pore pressure incrementally increases with continual shaking, reducing effective stress on the soil body until a special state is reached such that the characteristic, or effective, shear strength of the soil body can no longer support the normal loads of the soil-structure system. At this point, the strength of the soil has dropped drastically and, on occasion, disastrously.

Studying liquefaction in the field is difficult as most sampling and monitoring is done post-earthquake. Due to the unpredictable nature of earthquakes, it is very rare to have live sampling of liquefaction events. Instead, evidence of a completed liquefaction event is found through traces left behind; sand boils, lateral spreading of pavements, sunken objects and buried objects floating to the ground surface. Some mapping of liquefaction has been undertaken on a regional scale (Youd, 1991); however, there is little data about the pore pressure evolution and structural reorientation events during a strong motion. This leaves laboratory testing methods as the main source of insight into the mechanics of liquefaction events and spurs the need for this study.

The question of whether liquefaction will be initiated on a site can be addressed in two parts: a) whether a site or soil body contains soils with "susceptible" characteristics and conditions, and b) whether sufficient local shaking can be produced to reach the dynamic loading thresholds necessary to liquefy the susceptible soils. The latter is a question of site response and full analysis is beyond the scope of this report. This report operates under the assumption that any site analysis conducted using these results will already understand the site's shaking capacity, e.g., ranges of intensity, frequency content, and duration of a characteristic earthquake. This report utilizes several arbitrary ground motions pre-proven to reach intensities necessary to breach liquefaction thresholds and seeks to present an illustrative expansion to existing models for liquefaction susceptibility based on inherent soil characteristics.

2.1   Background in Soil Mechanics

In the decades following the 1964 earthquakes, the modern approach to liquefaction research slowly developed as accurate predictions of land subsidence became a major concern in many civil

engineering practices. Early advances in the procedural analysis of liquefaction and its effects, termed the "Simplified Procedure" (Seed & Idriss, 1971), rely on the fundamentals of static and dynamic soil mechanics. The complexities of dynamic analysis were embraced in the early 1970's as onset of the personal computer allowed for accurate and efficient analyses of large testing databases. As the field expanded and branched, so did differing approaches to liquefaction research. The last true consensus of the Simplified Procedure may be considered the series of National Science Foundation workshops from 1996 to 2001 by T.L. Youd and I.M Idriss. Subsequent updates to the procedure diverge from the Simplified Procedure, i.e., the semi-empirical procedure (Idriss I. , 2004).

The early study of liquefaction centered on the triggering mechanisms to determine if a site was likely to be affected in a seismic event. Further development in the field lead research efforts to collect data on liquefaction events worldwide to obtain a better understanding of the consequences of liquefaction including post-liquefaction strength and stress deformation behavior (Youd & Idriss, 2001). This report is largely concerned with the assessment of 'triggering' or 'initiation' of liquefaction which is required to predict strain deformation and damages.

As basic knowledge of soil mechanics is necessary to understand liquefaction mechanisms; a description of liquefaction susceptible soils and a summary of static and dynamic behavior of susceptible soils is provided in the background section. For more detailed information, refer to texts on soil mechanics (i.e., Idriss and Boulanger, 2008; Kramer 1996).

2.1.1 Behavior of coarse soils under uniform harmonic loading

The effects of dynamic stresses on a sand rely on the same fundamentals of behavior as static loading, with a few major differences. This report will draw a distinction between the use of the

term "cyclic", "transient" and "dynamic" loading. *Cyclic* loading will refer to regular uniform harmonic loading in which the frequency of the applied shear deformations is low enough so that there are effectively no dynamic, or inertial, forces to speak of. In DSS tests, this distinction could be as low as a cyclic frequency of 1 hertz with a 2-inch amplitude. For cyclic testing, one can generally load a specimen to more than 20% shear strain. *Transient* loading will refer to stress loading based on a pre-defined irregular pattern with effectively no inertial forces, e.g., a ground motion loaded at a low time scale. *Dynamic* loading, on the other hand, can contain irregular cyclic stress reversals which are applied much more rapidly than—and interact with—static stress conditions, like those in real-time seismic ground motions. The loading induced by earthquakes is often rapid enough that even clean sands can be considered and analysed under undrained conditions.

Cyclic loading characteristics in a laboratory conditions are chose based on the same desired characteristics important in transient and dynamic loading: amplitude, frequency, and duration. Transient motions are often simplified to equivalent harmonic inputs by accumulation procedures to an equivalent number of cycles to liquefaction, N_{eq}, and an applied average shear stress (Seed et al., 1975; Andersen 1976). These loading properties have a direct effect on several aspects of the soil response in strain controlled testing, including:

- Cyclic, average and permanent shear stresses
- Permanent pore pressure accumulation (and inversely the effective stress)
- Shear modulus curve
- Damping
- Post cyclic static shear strength

Figure 2 depicts a typical cyclic testing program. In a stress-controlled test, the pore pressure generation, horizontal strain, and vertical effective stress are measured and plotted to view the results. Initially the specimen is mainly contractive when the pore pressures are low, thus the strain remains minimal. As the pore pressures build and the specimen's stiffness decreases, the strain with each cycle becomes much larger as it builds its hysteresis loop. The greater difference between the contraction and dilation with each cycle indicates increased energy dissipation.
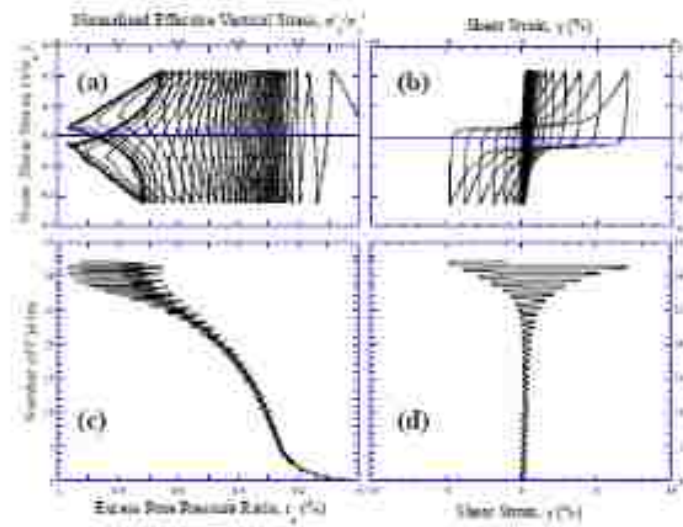
Figure 2: Typical soil response of loose sand to cyclic simple shear testing. CSR = 0.2, Dr = 54%. Monterrey Bay Sand (taken from a study be Wu 2002). (a) a typical stress path of loose sand. Graph (b) stress-strain response. (c) pore pressure generation trend (d) shear strain response over the course of the test.

Figure 3 is a comparative example of what happens to saturated sand strength over a full cyclic program vs a monotonic program. Note that cyclic behavior typically imitates monotonic behavior when allowed to extend without stress reversals for a significant time period until the failure envelope is reached. At this point, phase transformations begin. The shear strains may not necessarily become excessive once the failure line is reached, as dense soils may dilate and follow the failure line, however repeated cycles in some soils may cause pore pressure generation to drop the effective stress to near zero levels. Successive cycles reaching these near-zero levels may cause

large effective stress fluctuations with low stiffness levels due to the rearrangement of the soil fabric, causing low damping and energy dissipation. If loading continues, these samples may reach a point in which liquefaction is triggered. Common definitions of liquefaction triggering will be discussed later in this chapter.
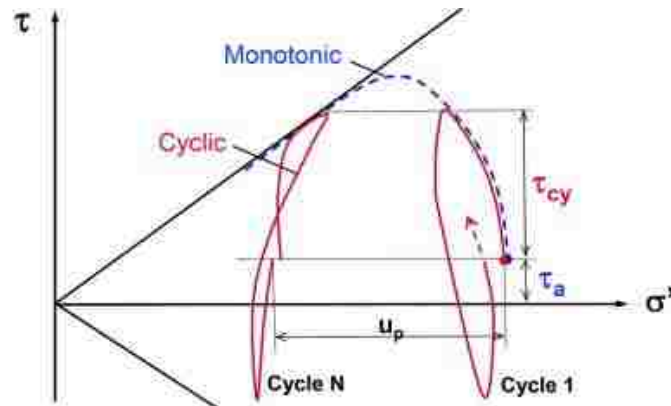

Figure 3: Typical effective stress path for undrained tests, comparison of monotonic curve to cyclic path in a contractive soil. Cyclic behavior imitates monotonic behavior when allowed to extend without stress reversals for a significant time period. T_a denotes static shear stress applied, τ_{cy} is cyclic amplitude, and U_p is permanent pore pressure accumulation at cycle N. Figure from Anderson 2015.

2.1.2   Behavior of coarse soils in transient and dynamic loading

Transient loading, like that from a seismic motion, adds another significant dimension to the complexity of a soil response through rate effects, soil body inertia, etc. Past studies have found that rate effects of clean, liquefiable sands are relatively minor and the leading factor effecting the response is shear loading history. Soils respond with fluctuating degrees of stiffness due to characteristics of the irregular stress reversals. Even as the strain is reduced after each successive stress reversal, in undrained conditions the pore pressures do not dissipate but incrementally build with each stress reversal. This process continues at unpredictable intervals, whether quickly reversing and causing rapid incremental pore pressure generation, or reversing infrequently with more minor pore pressure generation. Thus, an accurate estimate of the principal characteristics

of a typical strong ground motion at a given location—frequency content, intensity, and duration—is crucial to predicting liquefaction potential. These factors are addressed under this report's transient simple shear program.

2.2 Mechanics of Liquefaction

The debate regarding what factors contribute to making a site or soil body susceptible to liquefaction is an ongoing source of contention among leaders of the field. However, it is not enough to have susceptible soils to be determined to be a liquefaction hazard. The liquefaction potential of a soil is two-fold: it depends on characteristic soil capacity *and* locality capacity to produce a threshold loading condition, i.e., there must be also be an energy source within a vicinity capable of producing sufficiently large seismic motions. Then there is the additional question: should the soil body liquefy, what will happen to the soil properties and ultimately the site? Thus, the study of liquefaction is typically divided into three parts: liquefaction *susceptibility* (due to inherent soil body properties), *triggering* (due to loading characteristics), and *consequences* (post-liquefaction strength, permanent strains, failure modes, etc.). This section will address the current state of each of these in turn.

2.2.1 Behavior of coarse soils under static loading

For modelling purposes, a common observation of coarse soils (defined as 95% of the particles are larger than 125 μm) under static stress reveals that the behavior of the specimen can be divided into roughly two regimes: linear elastic behavior at small strain conditions (strain $\gamma < 0.01\text{-}0.04\%$), and non-linear behavior at large strain conditions. In the small strain condition, the modulus of elasticity E, a general measure of stiffness, converges to a maximum as strain levels decrease. This

value E_{max} is regularly used as constant and no volume change is attributed for low levels of strain. In the second regime, large strain conditions, the soil no longer behaves nor can be analysed as a linear, elastic, and purely deviatoric body. It is therefore necessary to use two values of E to describe the stiffness nonlinearity: the instantaneous stiffness modulus E_{tan}, and the average stiffness modulus E_{sec}. The point or range at which the soil enters the second regime and its subsequent reaction to additional stresses varies by soil type. Under static conditions, some soils can exhibit *strain-softening* behavior in which the stiffness of the material decreases, sometimes dramatically, after reaching a final level. In this case the E_{tan} may become negative for a period of time. Permanent strains may develop as well.

Volumetric changes due to stresses can be induced due to the physical effects of grains of soil sliding and rolling around and over each other. Contractive and dilative behaviors, and the conversion between the two with changes in stress conditions (as occurs in cyclical loading), play a large part in the understanding of liquefaction behavior as they can drastically effect the shear strength of a saturated soil. Sands and silts in a dense state are required to physically move up and over each other to accommodate excessive movement, causing the soil body to expand, or "dilate". Soil bodies in loose states, however, tend to "contract" as the body is sheared because particles roll in to fill large voids. The shear strain threshold for volumetric change in relatively non-plastic soils and assuming spherical particles is estimated to be minimal, between 0.01% and 0.04% (Dobry R. , Ladd, Yokel, Chung, & Powell, 1982). Dilation is often resisted by vertical gravitational stresses and frictional inter-particle forces.

It is important to understand the initial and instantaneous "state" of a saturated soil body to begin to understand static, and further, dynamic behavior. Three main state conditions, void ratio, vertical effective stress, and shear stress, can be used to predict susceptibility to liquefaction.

Castro and Poulos (1997) proposed that every soil has a density state in which, if subjected to monotonic loading to very large strains, will reach a steady state equilibrium between contractive and dilative behaviors. The soil shears at constant volume, constant effective stress, constant shearing resistance, and constant strain rate: a point of Critical State Deformation. This steady state can be classified as a *critical void ratio, e_c.* Additional testing revealed that e_c is directly related to a *Critical State Line (*CSL) (Casagrande, 1936) that divides dilative vs contractive soil behaviors based on initial density state. This can be shown well on a void ratio to vertical effective stress graph, commonly called an e-p' curve, like that in Figure 4a. Similar volumetric behaviors is observed under static shear loading as normal loading, therefore the critical state can be viewed as a 3 dimensional CSL on an $e - \tau - \sigma'$ plot as seen in Figure 4b.

(a)   (b)
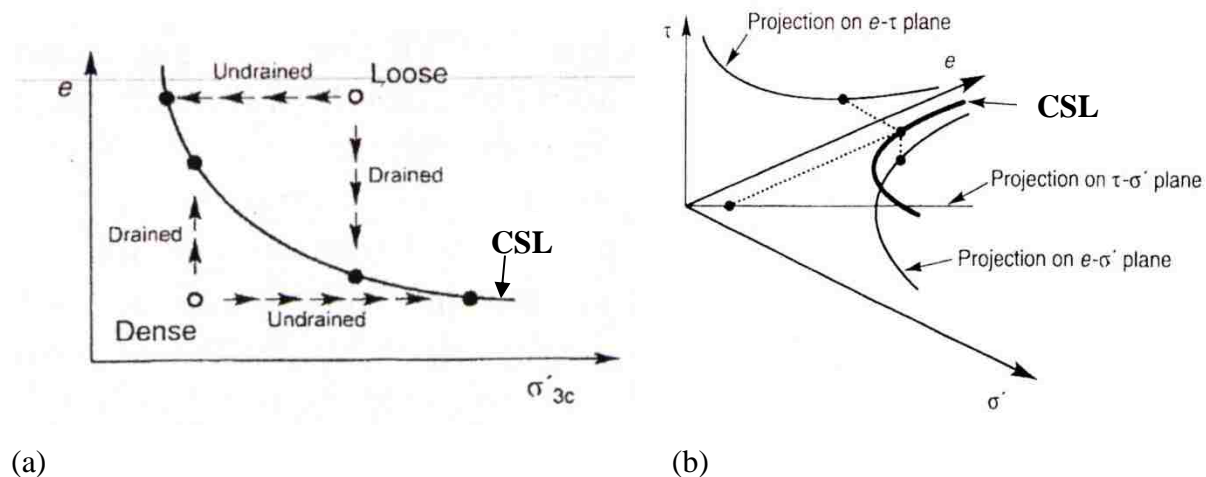
Figure 4: (a) Behavior of initially loose vs initially dense specimens under monotonic loading in drained or undrained conditions. Undrained specimens tend to move toward the critical state line under undrained conditions by sole reduction of effective stresses until the critical state line (CSL) is reached. (b) 3D visualization of the steady state line in a void ratio, shear and normal stress space (from correspondence with S. Kramer)

In drained conditions, loose sands tend to contract upon shearing and mobilize a peak strength before decreasing to residual strength values at large strains (*strain-softening behavior).* Dense sands dilate upon shearing, slowly increasing strength (*strain-hardening behavior*) until the

steady state is reached at large strains. An interesting phenomenon occurs in soils with intermediate density, initially discovered by Castro in 1969 through systematic static and cyclic testing. In intermediate density soils, initial shearing contracts and mobilizes a peak strength followed by strength reduction at low strains as a loose sample would, but subsequent shearing causes an increase in strength and a change to dilative behavior. The point of change between contractive to dilative behaviors was termed the *phase transformation point* (Ishihara 1993). These strain behaviors can be illustrated well by Figure 5.

The capacity of volume change of a soil, its *state parameter,* depends on both density and confining stresses and indicates how far a soil's void ratio plots from its CSL. The state parameter ψ gives an indication of how far a soil begins from its critical state. In the undrained conditions necessary for liquefaction events, void ratio changes are prohibited and thus the effective stress only can change. On an e-p' curve, this is reflected by horizontal movement towards the CSL with loading. Soils with negative state parameters plot below the CSL in the dense range, and thus the dilative tendencies under forced constant volume conditions cause the effective stress (and thus shear strength) of the soil to rise as it moves to its critical state. Conversely, soils positive state parameters plot above the CSL in the loose range, and thus the contractive tendencies cause the pore pressure to rise and the effective stress to decrease as it moves toward its critical state. The distinctions of this behavior undrained behavior on effective stress are crucial to understanding the strength devolution during cyclical and dynamic loading.

The following parameters define state conditions often associated with the change from contractive to dilative behavior in intermediate density soils. These terms are often confused as they occur almost simultaneously in static loading. They are also detailed in Figure 5 and defined as follows:

Phase Transformation Point (PT): point at which a soil under shear is neither dilating nor contracting. The tangent to the effective stress path is parallel to the total stress path. (Ishihara, 1993).

Quasi Static State (QSS): local minimum of shearing resistance from strain softening behavior observed in loaded soils of intermediate densities. QSS often occurs at a point very near the phase transformation and thus is often falsely considered identical to the PT. (Alacon-Guzman et al., 1988).

Minimum mean effective stress (σ'_{min}): local minimum of effective stress in loaded soils of intermediate density.

Ultimate Steady State (USS): shearing resistance at very large strains. The USS is highly dependent on initial void ratio but not on initial effective stress.   (Yoshimine & Ishihara, 1998)
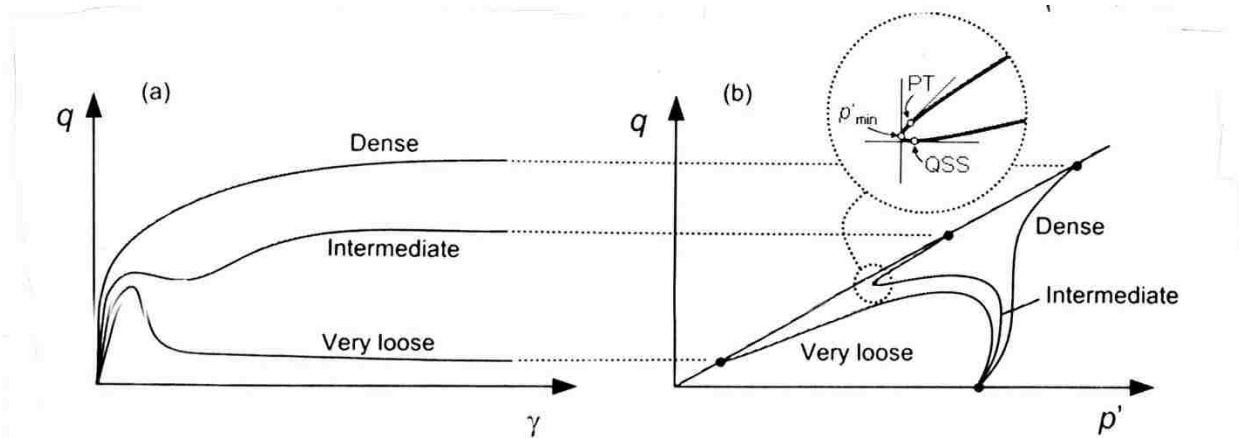
Figure 5: Illustration of effect of state on shear strength and volumetric change behavior in an unsaturated sample as shown on a stress vs. strain graph (or q-γ) (left) and a shear stress vs. normal effective stress graph (or q-p') (right). Typical behavior of loose, intermediate, and dense soils are loaded until failure is reached. Intermediate soils often display a phase transformation (PT) which marks the change from contractive to dilative behavior (from correspondence with S. Kramer).

2.2.2 Liquefaction Susceptibility

Most researchers choose to classify liquefaction susceptibility of a soil body with various emphases on soil composition, state criteria, and saturation. Generally, the following conditions in the field should serve as flags identifying the chance of significant liquefaction susceptibility, discussed in more detail in this section:

- Saturated conditions

- Uniform sands with little fines content; low plasticity

- Normally consolidated deposits; young deposits; fluvial or alluvial fans; loose-medium compacted fills

- Low blow counts in SPT or low tip resistance in CPT testing

- Indications of past liquefaction events present (sand volcanoes, lateral spreading, channeling through layers, etc.)

- Shallow depths (z < 12-15 m)

2.2.2.1 Composition of susceptible soils

This report comments briefly upon composition of susceptible soils here. However, it will present results of studies as proven assumptions rather than subjective stances as susceptibility is not a focus for this report. It should be noted that composition of susceptible soils is a topic of ongoing geological research and this section merely seeks to provide suggestions to further resources.

Geologic considerations play a large part in the composition and state of liquefiable soils, namely composition, deposit age, and site history. First, newly placed soils tend to have large void ratios and contractive tendencies which make them highly susceptible to liquefaction upon saturation. These soils can include fluvial, colluvial, alluvial fan, and Aeolian deposits which tend to deposit large masses of uniform soils in loose states. Young soils, like those deposited in the

Holocene era, tend to have higher susceptibility before the soil body becomes denser with age and the CRR increases correspondingly (deposit can be effected by cementation processes, increased overburden stress with subsequent coverage, occasional dynamic or constant static loading, etc.). Loose, human constructed fills are also likely susceptible to liquefaction for the same reasons (Kramer, 1996). Several investigations (Youd T. , 1984) show that sites with history of liquefaction events have a high likelihood of recurrence upon additional seismic events.

Source of Method	Fines Content by weight	Liquid limit	Water content	Plasticity Index	Commentary
MODIFIED CHINESE METHOD (WANG 1979)	<15%	<35%	>0.9*LL		Outdated. FC shown to be less important than plasticity
ANDREWS AND MARTIN 2000	<10%	*in #40 sieve* <32%			Influenced by Chi—Chi 1999 Earthquake in Taiwan – showed that MCM was unconservative and a definite "threshold" was not appropriate → gradual transition based on FC and LL
BOULANGER AND IDRISS 2001	*always liquefiable*			<3	Uses PI as high plasticity causes the decrease in effective shear stress with cycles of loading to "stall out" before reaching liquefiable levels
	liquefiable given other criteria met			<7	
SEED 2003	*liquefiable*	>37		<12	
	Transition zone: recommend testing	>47		<20	
BRAY AND SANCIO 2006	*liquefiable*	w/LL >0.85		<12	The parameter w/LL can change with the state of the soil.
	Transition zone: recommend testing	w/LL >0.8		<20	

Table 1: Common composition thresholds for liquefaction susceptibility. Soils must meet every criterion to be considered susceptible to liquefaction by said method.

The subject of susceptibility becomes even more sensitive when the question of the effects of fine particles is addressed. It has been determined that sufficient fines content, often represented by the soil type behavior index I_c (T.L. Youd, et al., 2001) also hinders liquefaction. Highly or moderately contractive sands will develop pore pressure much faster than less contractive soils

such as those with high plasticity. High plasticity soils may also experience a loss of strength and stiffness, but in a form different and less severe than the classic idea of liquefaction. These soils reach "liquefaction" state at larger shear strains than clean sands would. The Modified Chinese Criteria (Wang, 1979) first proposed a procedure for determination of a soil's susceptibility by defining a threshold of fines content (FC) by weight and liquid limit (LL) by Atterberg standards. This method was repeatedly modified as subsequent researchers recommended various standards. Over time it was shown that plasticity plays an equally large role in the inhibition of liquefaction, and currently the state of practice is on development of thresholds based on PI. The general consensus of professionals suggests a re-evaluation of these methods. Some of the most well-known criteria are chronologically addressed in Table 1 for reference.

2.2.2.2   Saturation

Full or near-full saturation of a silt or sand body is required for the soil to be considered susceptible to liquefaction. To understand the reasoning for this, consider a non-saturated versus saturated sand under a single cycle of harmonic loading. Volumetric change in a saturated sand is hindered by the incompressibility of the fluid, so the pore pressure response is to increase during contraction and decrease during dilation. Effective shear stress (and consequently shear strength) is inversely proportional to pore pressure. Therefore, the behavior of pore pressure of an intermediate density saturated sand mirrors that of the volumetric change in a non-saturated sand. This logic can be stepped through during a full loading cycle as outlined in Table 2.

The example in Table 2 of a saturated, intermediate-density sand subjected to harmonic loading is well equipped to illustrate the effects hindered volumetric-deviatoric coupling in saturated sands. Figure 6 depicts a typical DSS test as harmonic loading is applied to dry and saturated sands. The dry sample does not affect the effective stress conditions, whereas the saturated sands observe an incremental drop in effective stresses with each cycle. This effect

results from a reduction of effective stress as the normal stress carried by the soil skeleton is transferred to the pore water.
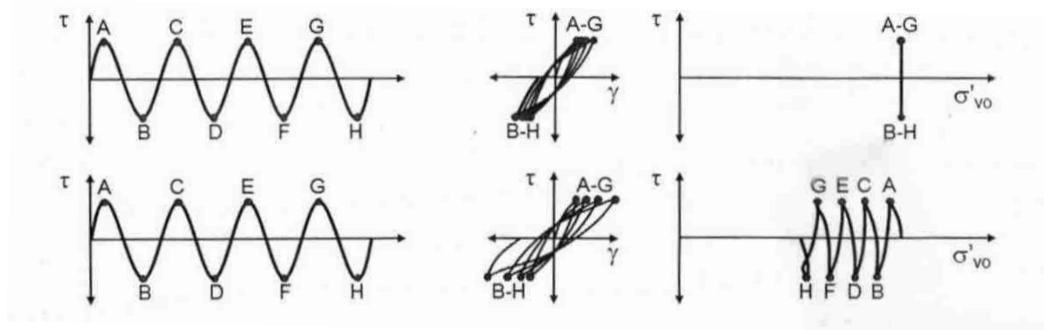

Figure 6: Cyclic degradation of a (top) unsaturated, and (bottom) saturated sand sample. Accumulation of strain γ with each successive cycle as stiffness incrementally decreases. In saturated samples, pore pressure increases and effective stress incrementally decreases, causing stiffness to degenerate at a higher rate and strains to accumulate faster (figure from Kramer 1996)

Stress event	non-saturated sand	saturated sand
SHEAR LOADING BEGINS	Sand begins to contract until phase transformation point is reached, then dilation begins.	Desire to contract then dilate causes the pore pressure to raise then lower.
STRESS DIRECTION REVERSAL	Specimen is looser than beginning of test. Contracts to a state denser than initial state before dilation begins again. Large strains cause particles to reorient to lower stiffness states.	Another cycle of initial pore pressure increase, then a smaller decrease begins. Large strains cause particles to reorient to lower stiffness states.
STRESS REVERSAL IN OPPOSITE DIRECTION	Soil is slightly denser than state at previous stress reversal, therefore contraction and subsequent dilation in this half cycle is slightly diminished from previous. Particles are oriented in opposite direction and now temporarily resists stress in this direction, thus stiffness is briefly increased until particles reorient in opposite direction	Pore pressure increases then decreases after phase transformation point reached. Particles are oriented in opposite direction and now temporarily resists stress in this direction, thus stiffness is briefly increased until particles reorient in opposite direction
CYCLE FINISH	Soil slightly denser than initial state	Pore pressure incrementally higher and effective stress incrementally lower than initial state.
SUBSEQUENT CYCLES	Incremental density drops by cycle causes each cycle to reach the phase transformation point sooner. Accumulation of net contractive strains which slow with each successive cycle.	Desire to accumulate net contraction instead accumulates net pore pressure increase, which slows with each successive cycle.

Table 2: Behavior of saturated and non-saturated, intermediate density sands during a single cycle of cyclic shear testing

2.2.2.3 State conditions of susceptible soils

To understand the importance of state on soil behavior during liquefaction, consider an old lake bed composed of clean sands deposited through settlement of sediments through the water column. This deposit is saturated and loosely packed with a large volume of void, i.e., a high void ratio. Upon initiation of shaking, the soil body will naturally contract into a denser formation, but the presence of incompressible water permits no volumetric strain. The pore pressure therefore increases the same amount which the effective stress, and consequently strength, decreases. Liquefaction may occur upon continued shaking as the effective stress approaches zero. Alternatively, consider a compositionally similar but glaciated sand deposit that has been under hundreds of feet of ice for excessively large time periods. The state of this deposit is now indurated to a dense state, i.e., a low void ratio. Upon shaking, the body may be subjected to dilation before the particles can rearrange and begin contraction, thus a higher loading state would be required to cause deformation. This deposit would not liquefy at the same shaking threshold required to trigger liquefaction in the first loose deposit.

Soil composition alone is not enough to determine the liquefaction potential of a soil. Analysis of state condition variables has provided great insight into prediction of liquefaction triggering which is generally summarized in Table 3. The traditional engineering practice of defining state as a function of relative density D_r (Equation 1) is only so useful for liquefaction purposes. This is because (a) methods for calculating D_r may vary widely depending on practitioner, and (b) soils of the same D_r may still have different void ratios which have a direct relation to the volumetric behavior of a soil under cyclic loading. Thus, the definition of a state parameter, ψ (or sometimes denoted ξ) as the difference between the void ratio and the critical state void ratio (i.e., Δe from the CSL on an e-p' curve) (Been & Jefferies, 1985) is more representative as soils with common volumetric behavior than relative density.

Further detailed indices describing volume change potential which involve both density and confining stress values include the dilatancy index, I_r, as defined in Equation 2a (Bolton, 1986), and the relative state parameter index, ξ_R. These values are normalized by the difference between the maximum void ratio (e_{max}) and minimum void ratio (e_{min}) values that are used to define relative density (Konrad 1988). ξ_R is defined using an empirical relationship for the critical state line, and has the form of Equation 2b.

$$D_r = \frac{e_{max} - e}{e_{max} - e_{min}}$$ Equation 1

$$I_r = D_r(Q - \ln(p')) - 1$$ Equation 2a

$$\xi_R = \frac{R}{Q - \ln\left(\frac{p'}{p_A}\right)} - D_R$$ Equation 2b

Q and R values for quarzitic sands were shown by Bolton (1986) to be about 10 and 1.0, respectively. Considering both composition and state, liquefaction potential is greatest in saturated sands and silts with a high ψ, i.e., a relatively loose fabric which plots above the CSL.

2.2.3   Liquefaction Triggering

Like susceptibility, liquefaction triggering is effected by many factors. It is generally agreed that whether liquefaction is 'triggered' is a balance between the soil's inherent resistance to liquefaction (defined by susceptibility) and the level at which the soil is loaded, i.e., *resistance* versus *loading*.

There are two main types of liquefaction: *cyclic* and *flow* liquefaction. Cyclic liquefaction occurs during active cyclic or dynamic shear loading in which the effective stress on the soil goes to zero and the stiffness drops to negligible levels, causing large, rapid deformations. These types of events often occur in level or lightly sloping liquefied deposits and are responsible for most liquefaction damages. Flow liquefaction refers to an advanced strain softening behavior in the

presence of larger initial static shear stresses which may or may not come about through cyclic shear loading and can often result in large slope stability failures.

2.2.3.1 Definition of liquefaction triggering

An important definition that must be made is the point at which liquefaction is triggered, i.e., failure occurs. In cases of cyclic liquefaction, *initial liquefaction* is historically considered to be the point at which sufficient pore water pressure has built to bring the effective stresses to, or very near, zero. Excess pore pressure, *Δu*, is typically normalized by the total normal stress, σ_{vo}, as a term called the excess pore pressure ratio, r_u, defined as follows:

$$r_u = \Delta u / \sigma_{vo}$$
<div align="right">*Equation 3*</div>

 The maximum value of r_u is 1.0, therefore initial cyclic liquefaction can be defined as the point when effective stress is zero and r_u is 1.0. The stiffness at this point is so low that very large shear strains can develop rapidly, as shown in the cyclic test in Figure 7 by the difference in strain of point A, the point of initial liquefaction where $r_u = 1.0$, and point B, a point quickly following initial liquefaction.

Many classifications of liquefaction initiation which refer to strain thresholds have also been used in laboratory tests. It is typically found that sandy soils and silty soils of very low plasticity tend to experience "triggering" of cyclically induced soil liquefaction at low shear strains of 3% to 6%, but defining initiation at varying points within this range can have a significant effect on the development of the soil's cyclic strength curve. The *double-acting* strain definition suggests that liquefaction is initiated when the cyclic strain amplitude reaches a threshold value or range within a single loading cycle. Ishihara (1993) recommended a 3% single-acting strain for cyclic simple shear tests, and Wu et al. (2004) recommended 6% double-acting shear strain. Typical cyclic simple shear tests use a failure criterion of 3% single-amplitude shear strain to define the

CRR values because the pore pressure values tend to reach their limiting value at this level of shear strain. At this point the pore pressures generally are not expected to increase with further increases in the maximum shear strains.

For the purposes of our harmonic tests, we will infer that liquefaction is triggered when the pore pressure ratio r_u becomes 1, in other words the entirety of the vertical load is being supported by the pore fluids and not by the sand skeleton.
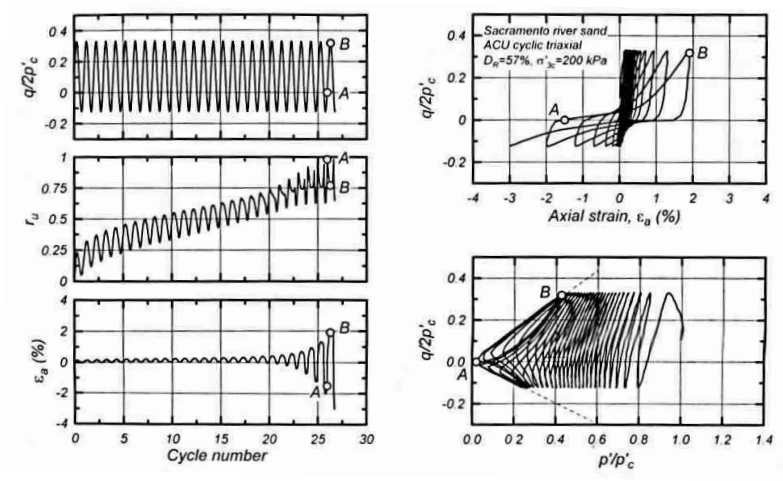

Figure 7: Response of Sacramento river sand to undrained cyclic loading (test from Boulanger and Truman 1996)

2.2.3.2 Loading: semi-empirical approach to triggering liquefaction in clean sands

Site response analysis can approach the topic of liquefaction triggering in one of two ways: the semi-empirical boundary method based on numerous case histories or the Simplified Method which defines a factor of safety against liquefaction. Both approaches are outlined in the following sections.

When evaluating empirical data of liquefaction events, it becomes quickly apparent that a single parameter for the classification of seismic sources which produce liquefaction is

insufficient. Often, initiation is dependent on the shaking capacity of a site which is in turn affected by a wide range of factors with large amounts of uncertainty: site to source distance, event magnitude, acceleration history, and duration of the ground motion, etc. The modern process of Probabilistic Seismic Hazard Analysis is complex, requires advanced equipment and/or advanced algorithms for accuracy, and often has an inherently high degree of uncertainty. Therefore, other methods of site analysis were sought for simplification for standards of practice.

Some studies sought to simplify the identification of liquefiable to a measurable density parameter that can be obtained from a CPT or SPT test. Been and Jefferies (1985) correlate the soil's liquefaction resistance to a state parameter ξr and bounds it by fines content, as shown in Figure 8. This is a practical approach, but does not fully capture the complexities of the factors which effect the CRR.
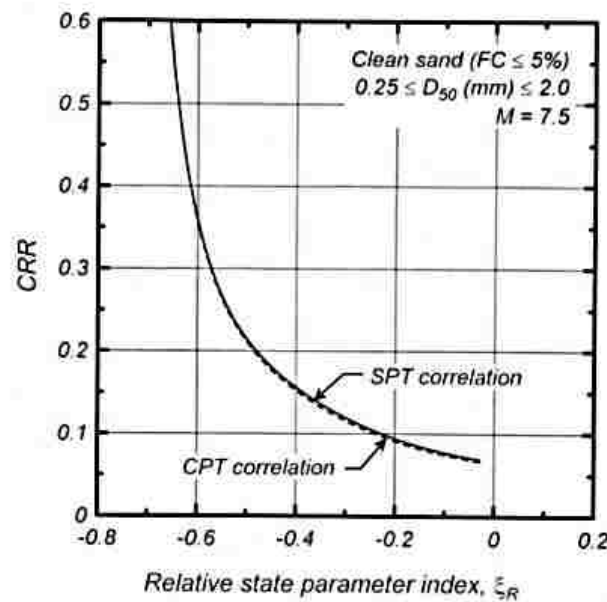

Figure 8: Curve of SPT and CPT correlation of critical resistance ratio and state parameter index. (Idriss and Boulanger 2004)

Other approaches to field liquefaction site analysis involve empirical zonation methods. In the early 90's two major papers were published proposing relationships between residual shear

strength of liquefied soils and normalized blow counts which were easily obtainable. The first

paper by Seed and Harder (1990) was regarded as a landmark paper which could provide field

engineers quick and easy site methods to evaluate liquefaction susceptibility. Their findings used

copious case studies of liquefied sites to develop an empirical threshold of susceptibility using

relative density and SPT blow counts correlations to residual shear strength. The second paper by

Boulanger and Idriss (1991) proposed a series of corrections to this representation, choosing to

present the susceptibility threshold based on CPT or SPT capacities and CSR. Figure 9 depicts

Boulanger and Idriss' compilation of several case history studies of liquefaction boundary curves

over the years, although this does not encompass all relevant databases. The discrepancy between

studies remains a source of contention in the academic field.

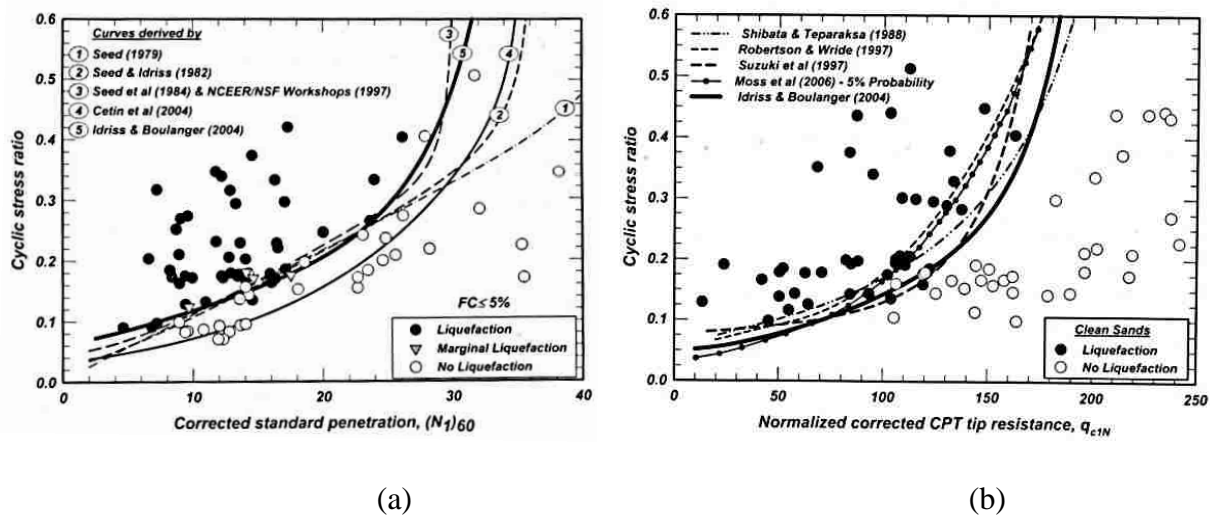<div align="center">(a)   (b)</div>

Figure 9: (a) Curve from multiple studies depicting boundary of liquefaction susceptibility based on CSR versus median values of equivalent clean-sand, normalize SPT blow count. (b) Same curves of found using other studies by normalized CPT tip resistance. M = 7.5 and effective normal stress is atmospheric. (from Boulanger 2008)

The use of field testing is critical for a liquefaction site analysis. The common geotechnical

practice of correlating blow counts using SPT tests have been presented as a measurement of

liquefaction potential subject to given cyclic shear loads. However, field methods for establishing

a blow count are highly variable, and can be highly affected by drilling or boring conditions and equipment. Therefore, parametric laboratory studies are an invaluable tool to validate or categorize the uncertainty inherent in empirical field testing. These databases to classify inherent soil resistance could be compared to the predictive boundary models set forth by Seed & Harder (1990) and Boulanger and Idriss (1991). State factors, effective vertical stress, static shear stresses, soil plasticity, and many others have been examined in detailed studies. Table 3 loosely summarizes the general effects these factors have on liquefaction susceptibility.

Table 3: State and loading factors affecting liquefaction susceptibility in cyclic testing of sands (after Kramer 1996)

Increasing Condition	Liquefaction susceptibility	Testing details
Initial Soil Density (decreasing ψ)	Soil becomes less contractive, pore pressure generation rate decreases, tends to increase liq. resistance	*Clean sands* (DeAlba, Seed, & Chan, 1976)
Initial effective stress	Contractiveness tends to increase which serves to decrease liq. resistance	(Vaid & Sivthayalan, 1996) (Cetin & Bilge, 2015)
Initial shear stress	*Loose Soil* – contractiveness increases and decrease liq. resistance *Medium-dense soil* – tends to increase liq. resistance	(Seed & Harder, SPT-based analysis of the cyclic pore pressure generation and undrained residual strength, 1990) (Boulanger & Idriss, Earthquake groung motions at soft soil sites, 1991)
Soil Plasticity	Damping ratio increases along with stiffness, contractiveness drastically decreases, and liq. resistance increases	(Dahl, 2014)

2.2.3.3 Loading: The Simplified Method

In typical engineering practice, a factor of safety can be used to quantify the potential to trigger liquefaction. This factor of safety against liquefaction *FS$_L$* (Equation 4) is often used as a field standard "simplified procedure" to assess liquefaction potential (Seed & Idriss, 1971). This parameter is defined as a ratio of the soils' inherent resistance against liquefaction to its applied stress conditions. The *FS$_L$* can be broken down into indexes are used to describe the relationship between the soil's natural resistance capacity to liquefaction, the *Critical Resistance Ratio,* or CRR

(Equation 7), and the magnitude and conditions of the loading applied to the soil body, the *Critical Stress Ratio,* or CSR (Equation 5). Multiple probabilistic seismic hazard models have been developed to describe these indexes (Youd et al 2001; Moss et al 2006; Boulanger and Idriss 2008, 2015). These models estimate the probability of liquefaction based on popular soil testing methods like SPT or CPT methods, and use common earthquake intensity measures such as PGA or spectral acceleration. However, these methods do not predict when liquefaction occurs or the consequential induced deformations.

$$FS_L = \frac{CRR}{CSR}$$
Equation 4

If the CSR is equal to or exceeds that of the CRR, the soil body is both characteristically susceptible to liquefaction and in a site capable of reaching above a threshold event, and therefore presents a hazard of liquefaction given the next seismic event.

A fixed criterion of liquefaction is the presence of a seismic source to trigger an event. Empirical data collections of the maximum effected site to source distance around faults capable of producing sizeable motions provide great references for categorizing zones of susceptibility. However, these still can be improved upon as the reproducibility of these relationships is variable by simply considering alternate regions or time periods. Analysing this uncertainty and its effect on the CRR and CSR is beyond the scope of this report, but is a topic of study within the larger NGL movement.

The CSR is often used in factor of safety evaluation as it does not require site-specific information. This index is a function of ground motion characteristics like the peak acceleration a_{max}, magnitude scaling factor (MSF), and condition characteristics like the stress state σ_{vo}/σ_{vo}', and a depth reduction factor r_d. The form is generally taken in the field to be:

$$CSR_{in\_situ} = 0.65 \frac{a_{max}}{g} \frac{\sigma_{vo}}{\sigma'_{vo}} \frac{r_d}{MSF} \qquad \text{Equation 5}$$

where a_{max} is the peak ground acceleration (PGA) of the motion, σ'_{vo} is the vertical effective stress, σ_{vo} is the initial overburden stress, r_d is the depth reduction factor, and MSF is the magnitude scaling factor which increases the CSR for events less than a magnitude 7.5 and decreases them for larger events. There is general agreement to the method of obtaining the soil conditions and the peak acceleration of the ground motion, but the value of $\frac{r_d}{MSF}$ has several publications which offer relationships to deposit depth and moment magnitude. The two most highly utilized relations of these are found in the work of Youd et al. 2001 and Idriss and Boulanger 2004.

In laboratory conditions, the CSR can be interpreted as a function of shear stress amplitude and initial effective stress:

$$CSR_{lab} = \tau_{max}/\sigma'_{vo} \qquad \text{Equation 6}$$

where τ_{max} is the amplitude of the cyclic or maximum shear stress.

Typical field practice is to standardize the CRR based on its corrected blow count, $(N_1)_{60}$, at a normalized pressure state at the surface where vertical loading is 1 STP. An overburden correction factor based on laboratory regression data, K_σ, is applied to compensate for effective stress state. Therefore, the form of CRR simplifies to

$$CRR = CRR_{\sigma'=1tsf, M=7.5} K_\sigma K_\alpha MSF \qquad \text{Equation 7}$$

where $CRR_{\sigma=1\,tsf}$ is a function of $(N_1)_{60}$; K_σ is a correction factor for overburden stress, or vertical effective stress, and blow count; and K_α is a static stress correction factor; and MSF is a magnitude scaling factor based on the design earthquake intensity. Various methods for application of the simplified procedure are discussed in detail in texts by Youd et al. 2001 and Idriss and Boulanger 2008.

In many liquefaction studies, testing using transient or dynamic loading is desired but is hindered by equipment capabilities. In this situation, it is common to use an equivalent number of harmonic cycles to liquefaction, N_{eq}, to approximate soil response to a transient or dynamic motion. The CRR can therefore be thought of as the CSR that is required to reach liquefaction in this number of loading cycles, N (typically 10 cycles). Multiple methods for developing this approximation have been discussed. Anderson (2015) lays out a detailed process for the development of contour diagrams to determine the equivalent number of cycles. Vaid and Sivathayalan (1996) found the relationship between CRR and N_{eq} can be approximated for earthquake engineering purposes as

$$CRR = a * N_{eq}^{-b} \hspace{3cm} \text{Equation 8}$$

where *a* and *b* are determined by regression of experimental data (Boulanger, Wilson, & Idriss, 2011), (Vaid & Sivthayalan, 1996). The value of *b* for clean sands is typically around 0.34, but *a* has a wide range. These relationships can then be used to create liquefaction resistance curves for various soils.

The factor of safety method for evaluation of liquefaction potential focuses on the worst-case scenarios and ignores the potential for multiple event sources, site variability, or time-varying dimension of every earthquake motion. These factors are addressed in Probabilistic Seismic Hazard Analyses (PSHA), but these do not focus on the detailed mechanics of what is occurring during an event. Therefore, if the Simplified Method is to be used, a controlled variable laboratory method is perhaps more appropriate to use for the high-quality evaluation of soil mechanic response due to transient or dynamic ground motions.

2.2.3.4   Resistance: laboratory liquefaction triggering testing methods

Traditional means of evaluating the liquefaction susceptibility of a soil body is carried out by direct field measurements or by sampling for laboratory testing. Several important papers have highlighted the field behavior of liquefiable soils (Boulanger, Wilson, & Idriss, 2011) (Seed & Idriss, 1971). Predominant characteristics of a soil body used to determine susceptibility are saturation levels, grain size distribution, and shear modulus, all of which are quickly assessed through classical laboratory means. Shear modulus reduction in laboratory setting has principally been conducted by means of variations to traditional simple shear tests or triaxial tests (El Mohtar, 2013) (Eseller-Bayat, Gokyer, Yegian, Ortakci, & Alshawabkeh, 2013) . This investigation will follow the testing standards previously set.

Laboratory analysis of liquefaction has been largely limited to resonant column, cyclic simple shear, or triaxial testing in the past. The current standard of practice is to validate the field readings of shear modulus behavior with those obtained in lab tests. Obtaining undisturbed samples is exceedingly difficult therefore reconstituted samples which mimic deposition are more suitable.

The resonant column tests measure very small values of the strain shear modulus by disturbing the base of a soil column and measuring the shear wave velocity response which is directly correlated to the shear modulus of a saturated sand. Sands subject to liquefaction initiation typically begin to undergo large deformation with shear strains exceeding 12-15%. However, due to the nature of the test device, resonant column tests only allow for testing up to 0.01% shear strains before the soil structure degrades to a point which renders shear wave readings unusable. Therefore, for liquefaction studies it is more pertinent to turn to alternative methods which assess a wider range of strain behavior.

Cyclic triaxial tests have been used successfully for these means, but these involve complicated machinery and difficult specimen creation. CSS tests are often preferred over triaxial testing as they more closely approximate the in-situ rotation of principal stress directions expected during earthquake shaking. Therefore, the creation of an extensive database is well suited for a cyclic simple shear testing program like the one conducted in this report.

2.2.3.5 Resistance: initial static shear stress effects

Initial shear stresses, the true focus of this study, can be imposed upon a soil body on a slope or if subjected to some structural loads. To understand the mechanics of a static directional force it is useful to visualize the loading conditions in a cyclic shear test. As illustrated in Figure 10, cyclic loading in a soil with no initial shear stress does not prefer shearing one direction or another, thus should produce any net directional displacement. If an initial static shear is present a preferential shear stress direction is present. This may cause permanent lateral strains to develop upon each successive cycle, termed *cyclic mobility* (Casagrande 1976). In addition, the stress reversals involve changes in stiffness and energy dissipation through inelastic soil behavior.
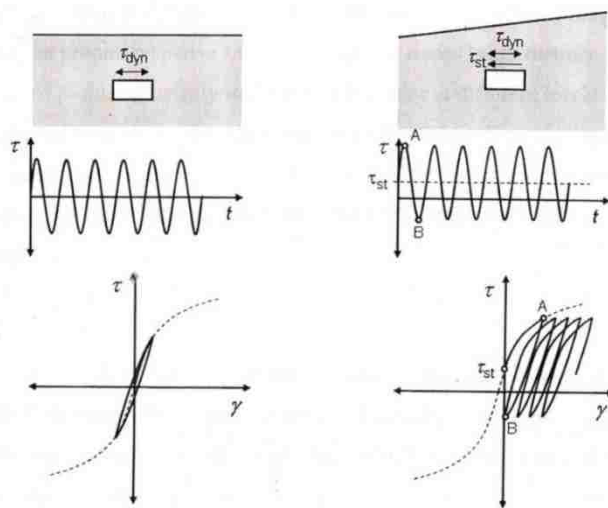

Figure 10: Stress-strain response of cyclic loading of a soil sample (left) with and (right) without an initial static shear stress (from correspondence with S. Kramer)

This directionality from the presence of a static shear produces a strange effect on the pore pressure evolution during an earthquake. Experimental studies have shown that liquefaction can occur more quickly in very loose soils (Dr ≈ 35% or ξr > 0) in the presence of an initial shear stress. In dense soils (Dr ≈ 35% or ξr > 0), K_α increases with increasing α (Boulanger 1991; 2003), and the soil may exhibit many phase transformations but maintain sufficient dilative behavior as to never reach the level of null effective stress required for liquefaction (Blaker & Anderson, 2015). In medium dense to dense soils, however, the presence of an initial shear stress tends to increase liquefaction resistance. This phenomenon is counter intuitive, implying that steeper slopes have a lower liquefaction potential. The current explanation of this singularity can be attributed to the mechanics of phase transformations during liquefaction. Experimental evidence (Dobry et al. 1982, Mohamad and Dobry 1986) indicates that the rate of pore pressure generation increases with the higher quantity of directional stress reversal. During shearing with low stiffness—as occurs near the point of liquefaction—the fabric of the soil reorients itself when the shear stress changes directions and decreases the effective stresses. For an event of the same magnitude or shear level, the shear stress direction reversal may occur less frequently when a static shear stress is present. Therefore, the soil body may not reach the state of zero effective stress so initiation of liquefaction is not as likely. However, this does not mean the body does not experience permanent strain. If subject to even a low static shear stress, the asymmetry of static shear stresses result in cyclic mobility.

It is common to relate static shear stress by relationships between the slope parameter α and the initial static stress factor K_α as defined in Equations 9 and 10 respectively:

$$\alpha = \frac{\tau_o}{\sigma'_{vc}} \qquad\qquad \text{Equation 9}$$

$$K_\alpha = \frac{Strength_{cyclic,\alpha}}{Strength_{cyclic,\,a=0}} = \frac{CRR_\alpha}{CRR_{\alpha=0}} \qquad\qquad \text{Equation 10}$$

where α is the ratio of initial static shear stress to the effective normal consolidation stress on the plane of interest and K_α in a laboratory setting is simply the cyclic strength for some value of α divided by the cyclic strength for α= 0.

Several publications have developed suggestions for the interpretation of the K_α correction factor. Seed and Harder (1990) developed models of K_α by relative density using empirical methods (Figure 11). There was an inherent wide range of uncertainty in the data. Boulanger et al. (1991) proposed that adopted failure (or resistance) criterion play a more important role than previously thought. This study based the results on strength criterion and expressed terms of CRR corresponding to 3% single amplitude (SA) shear strain level, shown in Figure 12. Additional K_α corrections were proposed and were later revised by Boulanger in 2003 (Figure 11a). In 2008 Boulanger again redefined K_α as a function of relative state parameter ξr.

(a) (b)
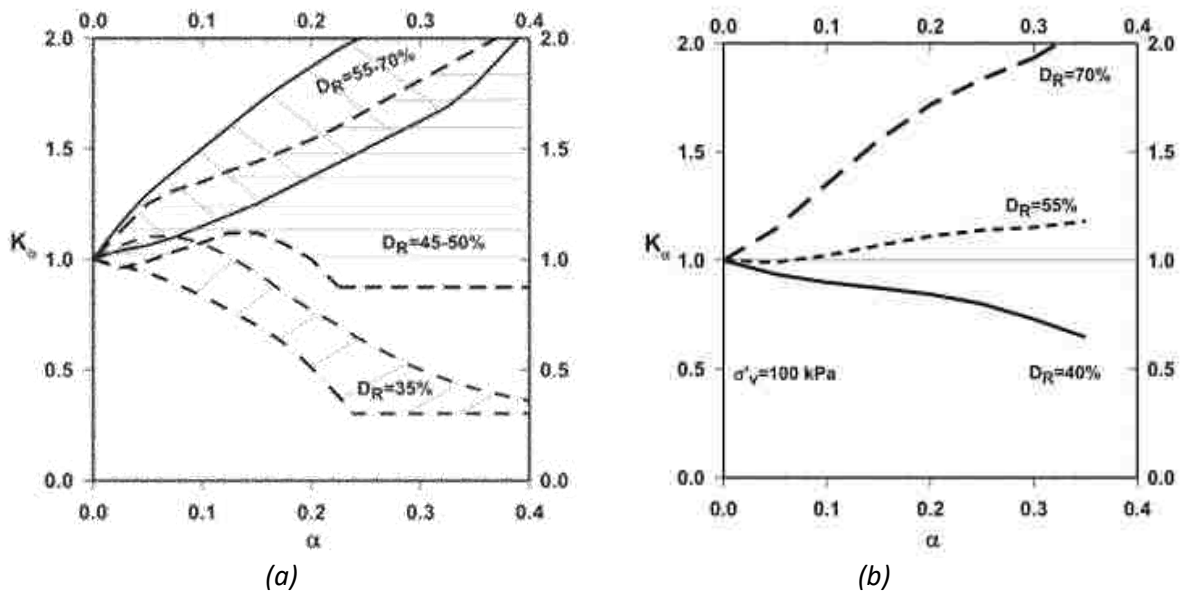
Figure 11: (a) Seed and Harder (1990) and (b) Boulanger corrections (2003) of K_α models. Tested at vertical effective stress of 100 kPa.
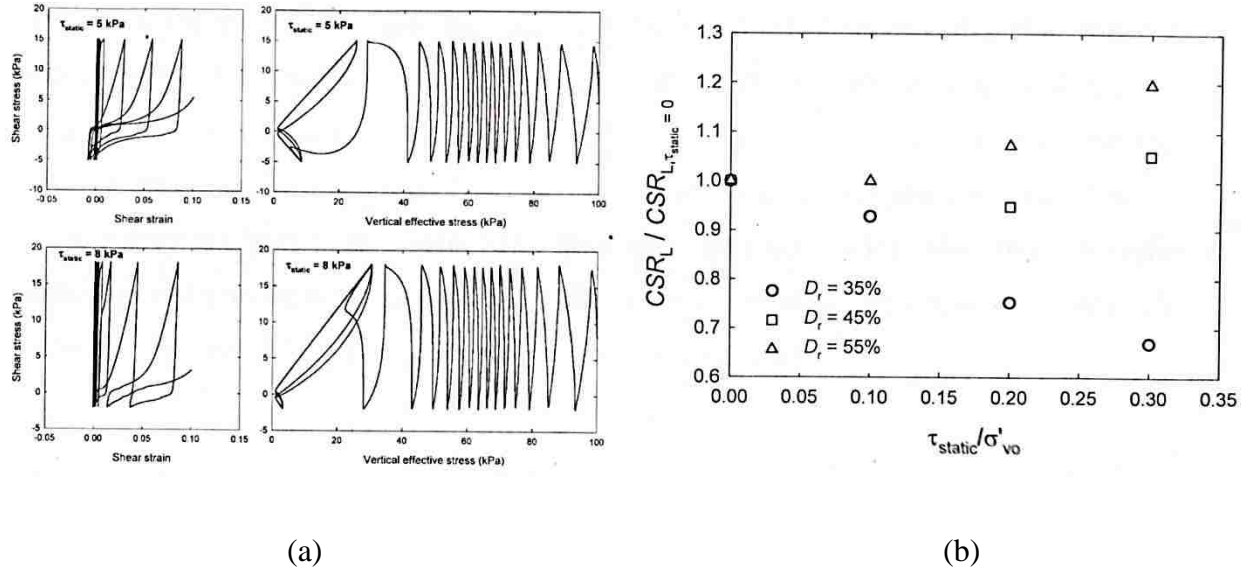
Figure 12: (a) Stress-strain and stress path of soils with initial static shear of 5 kPa and 8 kPa respectively. D_r = 60%. (b) Summarized effect of static shear on CRR. Markings indicate CSR required to produce 3% shear strain in 10-30 cycles of shear. From (Boulanger & Idriss, Earthquake groung motions at soft soil sites, 1991)

Vaid et al. (2001) discovered an interdependency between vertical effective and static shear stress, thus introducing a unified correction factor $K_{\sigma,\alpha}$ to look and both K_σ and K_α corrections simultaneously. His results claimed that Harder and Boulanger's results were over conservative. Wu (2003) and Cetin and Bilge (2015) developed a cyclic testing program using Monterey sands in 2003 to propose yet another set of corrections to the K_α. Cetin and Bilge proposed a final closed form solutions to K_α and α and introduced a factor which also depends on strain amplitude and failure criteria (Figure 13). This form was recommended for ranges of $0.3 \leq \frac{\sigma'_v}{P_a} \leq 4.0$, $0 \leq \alpha \leq 0.35$ and $0 \leq SRR \leq 2.0$. More studies include Vaid and Chern (1985), Mohamad and Dobry (1986).

Although not all these studies tend to agree on the true shape of the initial static shear factor, they do agree that several important parameters are important in defining laboratory K_α behavior. These include:

- Soil state (dependent on relative density or confining stress)

- Failure criteria (or definition of point of liquefaction initiation for determining cyclic resistance)

- Somewhat influenced by the laboratory test device used to find K_α (Harder & Boulanger, 1997).

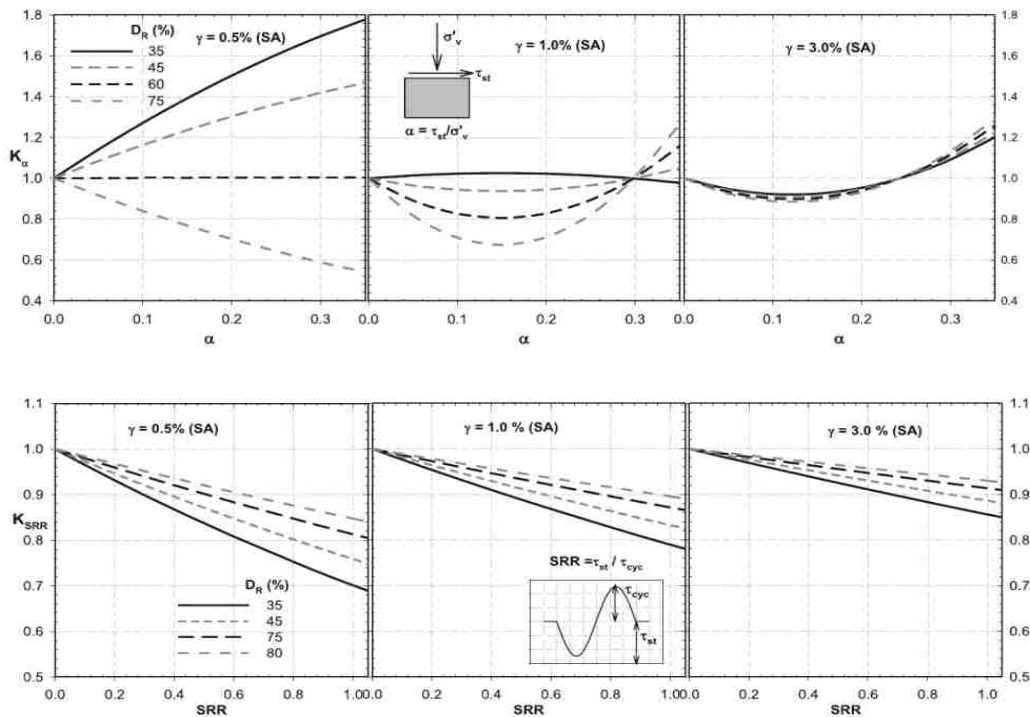with the primary contributors to the value of K_α being the state parameter.

Figure 13: Static shear stress correction factor correlations and closed form solutions of a correction factor $K_{\sigma,\alpha,SRR}$ which accounts for overburden and static shear stress as well as the ratio of static stress to cyclic amplitude (SRR). Determined that K_α depends on strain rate. (Cetin and Bilge 2015)

The complexity of defining an appropriate critical state line without advanced field sampling has led to a lack of consensus on K_α effects on the factor of safety against liquefaction, Models of FS_L can range up to a factor of two on clean sands and a factor of three on silty sands (Boulanger 2008). Furthermore, there is some disagreement as to the form of K_α itself. All models agree that soils experience an increase of resistance with increased relative density, but there is some disagreement as to the effects of increased α. Some models predict an exclusive increase in

resistance with increased α while others do not present as definitive trends. Thus, it is no surprise that current engineering practices typically disregard slope effects in liquefaction analyses. This report presents a coherent cyclic and transient database to build supporting evidence regarding the effects of normal effective stress and static shear stresses for empirical liquefaction models.

2.2.4   Liquefaction Consequences

There are many possible consequences to triggering liquefaction. It is typical to find that soils experience a dramatic drop in shear stiffness to nearly zero levels once liquefaction is triggered. This in turn allows large cyclic deformations in flat slopes which can be compounded with permanent strains in the presence of initial static shear stresses. In situ behaviors of liquefied soil bodies can exhibit damaging consequences evidenced by (though not limited by) to:

- *Sand boils:* The liquefiable layer is trapped under a non-liquefied layer. The pore pressure escapes through small holes in the top layer, pushing soil up along with escaping pore fluids to create sand-volcanoes at each hole.

- *Settlement:* Low liquefied shear strength causes settlement and/or a dramatic decrease in bearing capacity of structures. Post-liquefied deposits may settle into denser states.

- *Buried object buoyancy*: Liquefied deposits take on the properties of the pore fluids, thus buried utilities and structures can become buoyant during the earthquake and begin to rise to the surface.

- *Lateral Spreading:* Soil bodies subject to initial static shear stresses like those near embankments or on slopes may exhibit large permanent strains which result from shear loading with a directional preference. This can cause pavement cracking, slope failures, etc.

CHAPTER 3: RESEARCH METHODOLOGY

The primary purpose of this research effort was to perform and interpret the results of a series of tests on the effects of initial shear stress on liquefaction triggering. The direct simple shear devices logged cyclic and transient liquefaction tests which were compiled into a database. After vetting this information, the data is intended to be posted online as part of the NGA Ground Motion database.

To carry out a full enquiry, it was necessary to explore the effects of several secondary characteristics such as vertical effective stress, sample preparation procedures, and loading characteristics. These effects were studied by means of a parametric testing program, the results of which are stored in an SQL database discussed in Appendix C.

3.1   Program Design

These tests are designed based on the results of several recent studies, namely a transient simple shear program on Nevada sands at the University of Texas (Kwan 2015) and a centrifuge program at the Renssealaer Polytechnic Institute in 2013 (Sideras 2013).

Low to intermediate density saturated sands under uniform loading were tested on a NGI DSS device and transient tests were tested using a GDS EMDCSS device. The details of these devices are discussed in Chapter 3.2.1. The cyclic simple shear (CSS) test was chosen for several

reasons. CSS tests are simple in nature and allow for easy preparation of controlled, repeatable specimens. Additionally, the applied shear stresses from simple shear tests approximate the stresses from vertically-propagating, earthquake shear waves. CSS tests can also be subject to the wide variety of loading conditions needed to evaluate seismic liquefaction stability and shear strain degradation under cyclic loading.

The following sections provide the details regarding the transient CSS program at NGI. The reasoning for selecting these methods is also discussed. The design of the final testing program is sought to encompass the following parameters:

Design of Transient Simple Shear Test Program

- o 2 distinct ground motions (Palm Springs and Landers)
- o 2 ranges of soil density (30-50%, 60-85%)
- o 4 levels of initial static shear ($\alpha = 0$, 0.05, 0.1, 0.2)
- o 4 amplitudes of applied cyclic shear stress (5 kPa, 10 kPa, 15 kPa, and 20 kPa)
- o 1 amplitude of applied vertical effective stress (100 kPa)

The final database included 20 parametric transient tests. In addition, 4 transient tests were conducted to test for repeatability, pre-shearing effects, dynamic rate effects, cycle history, etc.

3.1.1   Sand selection

For the sake of simplicity and a reasonable scope of study, this liquefaction testing program targeted soils which are already known to be readily liquefiable. Thus, Nevada sands were selected as a clean, uniform, liquefiable sand to optimally consider the mechanics of liquefaction. This medium-coarse sand was used in several previous liquefaction studies (Kwan 2015, Sideras 2013), which simplifies the validation of results. The grain size distribution and important characteristics

of the sands are reported in Table 4 and Figure 14. A liquefaction resistance curve for Nevada sand

by relative density developed by Kwan (2015) is reported in Figure 15. This curve suggests loosely

packed Nevada sand has a low resistance to liquefaction and denser packing has a slightly higher
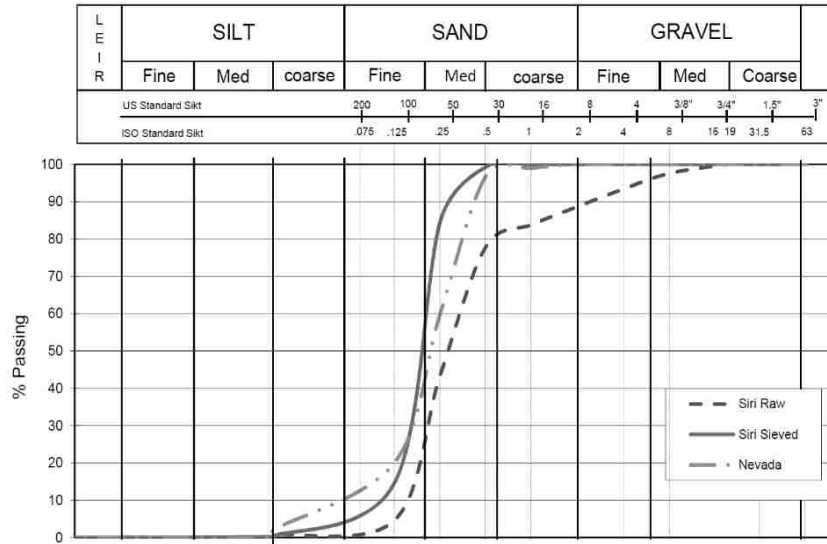
resistance.

 Figure 14: Grain size distribution of Nevada sand used in this program. Similar Siri sand included for reference.

	Nevada Sand	
Min. density	14.8	kN/m^3
Max density	16.8	kN/m^3
e max	0.72	
e min	0.51	
Specific gravity	2.6	
Coef. Of Uniformity,	2.7	
Soil friction angle, Φ	36°	

Table 4: Characteristics of Nevada sands
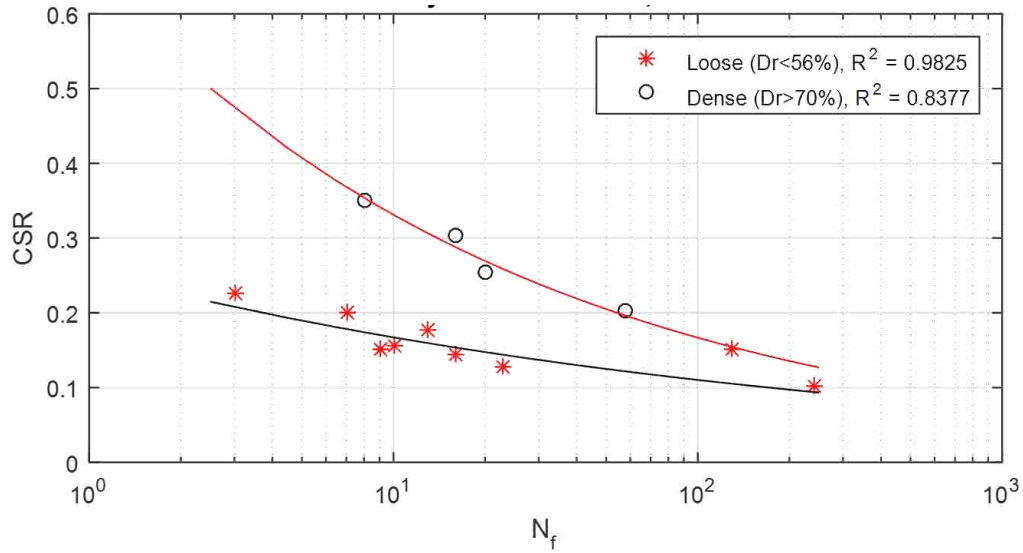
Figure 15: Liquefaction resistance curves for loose and dense Nevada sand specimens. CSS study from W.S. Kwan 2015.

3.1.2 Selection of transient shear loading

The influence of phase transformation behavior in the presence of initial static shear stress must be assessed to adequately predict the effects on the amplitude of instantaneous and permanent strain induced from a loading event. The program focuses on transient loading of irregular patterns for the emulation of true earthquake motions. All tests were conducted under undrained conditions to simulate the condition of nearly all liquefaction events. Stress controlled testing methods were used to capture the directional static shear loading seen in a sloped environment.

The characteristics of a seismic motion are more difficult to capture than a simple harmonic series. The current standard practice of characterizing earthquake loading using peak parameters and a magnitude scaling factor are not sufficient to capture the information necessary to predict the liquefaction reaction of a soil deposit, nor to determine the range of soil deformation following a seismic event. Based on numerical analyses, Kramer and Mitchell (2006) suggested the use of

Arias intensity or cumulative absolute velocity above 5 cm/s (CAV_5) to reduce the uncertainty in performance-based evaluation of liquefaction hazard.

Following a similar manner of Ishihara and Yasuda (1972), the transient tests' shear loading histories were chosen to be scaled versions of selected acceleration ground motion records. Each motion was scaled to a ratio of peak shear stress to vertical stress of 0.15 (i.e., CSR = 0.15 indicating the peak shear stress is of 15% of the vertical overburden stress). This report quantifies the intensity development of a stress record by a stress intensity index, I_s. This parallels the method in which Arias intensity quantifies the development of an acceleration record (Kwan, 2015). I_s is defined as the integral of the shear stress square as an intensity measure (Equation 11). This can be normalized to its final state for direct comparison of records (Equation 12). This measure allows for an analysis of the building-up of absolute stress magnitude over time.

$$Stress\ intensity:\ I_s = \int_0^t \tau^2\ dt \qquad\qquad \text{Equation 11}$$

$$Normalized\ Stress\ intensity:\ I_{s,n} = \frac{\int_0^t \tau^2\ dt}{\int_0^{t=\infty} \tau^2\ dt} \qquad\qquad \text{Equation 12}$$

The two selected motions in Figure 16, Palm Springs 1986 and Landers 1992, are compared to several famous seismic events. The intensity measures, duration, and frequency content are compared in Table 6 and their intensity measure development and spectra are shown in Figure 17 and Figure 18, respectively. The number of equivalent cycles, N_{eq}, is also included. The N_{eq} refers to the number of equivalent of uniform cycles in a laboratory test which, if applied to an element of soil in the field, would have the same effect on the soil strength as the transient earthquake motion. The N_{eq} values listed in Table 6 are found using the Seed and Idriss (1971) model.
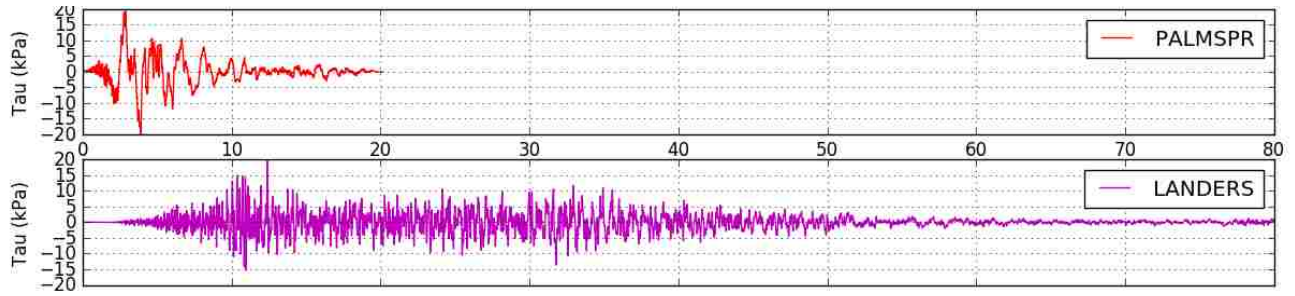
Figure 16: Selected Earthquake shear stress vs. time records. Scaled to a peak shear stress of 20 kPa

Motion	PEER NGA#	Location	Year
PALMSPR_MVH135	527	North Palm Springs, USA	1986
LANDERS_MCF_000	880	Landers, USA	1992

Table 5: Selected Earthquake Characteristics

MOTION NAME	Mag	PGA unscaled (g)	Arias intensity	CAV$_5$	Duration	Neq Seed and Idriss 1971	Pulse description
PALMSPR_MVH135	6.06	0.75	0.62	2.57	20 s	7.29	low frequency pulse and late large pulse
LANDERS_MCF_000	7.28	0.46	0.36	3.93	85 s	12.86	tapers up to peak pulse then tapers down. High frequencies
GREECE_PLK_NS	5.00	1.01	0.22	1.21	22 s		Pulses near peak amp, short duration
COYOTELK_G04360	5.74	1.05	0.50	2.61	28 s		large early pulse
HECTOR_ MMP090	7.13	0.49	0.23	2.40	62 s		low f pulses overlain with high f
KOCAELI_CNA000_H2	7.51	1.09	0.48	3.85	90 s		8-9 pulses near peak amp

Table 6: Intensity measures, duration, and frequency content of selected ground motions and others
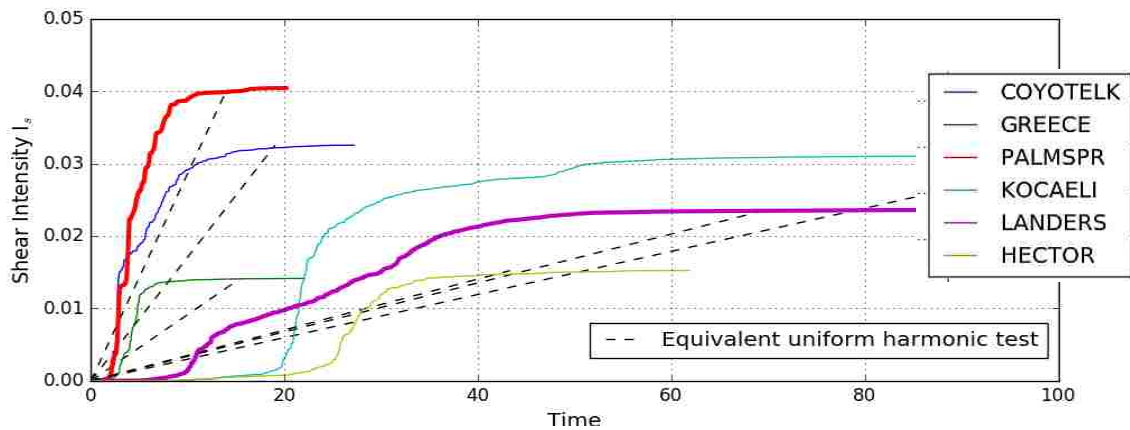
Figure 17: Intensity measurement development of the cumulative stress. An equivalent uniform harmonic test run at 65% of the motion's peak shear amplitude in included for reference.
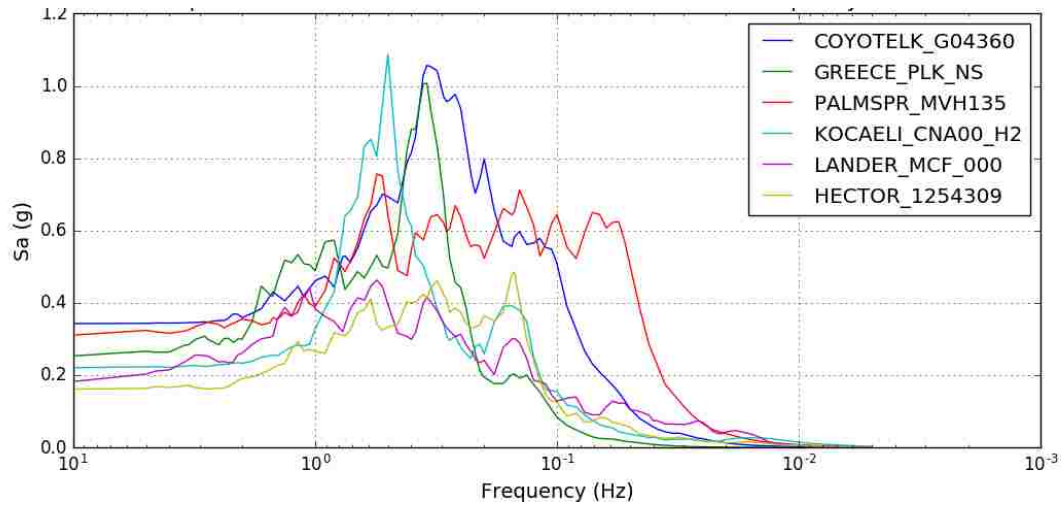
Figure 18: Selected earthquake spectra with corner frequency of 3 Hz

3.2   Laboratory Procedures

The consolidated constant-volume (CCV) laboratory procedures developed by Bjerrum and Landva (1966) were used for the cyclic simple shear testing. These standards follow ASTM D 6528-07 standards for consolidated undrained direct simple shear testing.

3.2.1   Laboratory testing equipment and data acquisition

The NGI Direct Simple Shear (DSS) device used in this testing program was originally developed by Bjerrum and Landva (1966). The active height control in CCV combined with the use of wire-reinforced membranes has several advantages over constant load methods. First, the K_o condition through constant area can be enforced uniformly throughout the specimen. Additionally, it is possible to test dry or partially saturated samples by assuming the vertical load required to hold the constant volume condition is equal to the pore pressure generated in a saturated sample. The validity of this assumption is supported by Bjerrum and Landava (1996). This allows for

simplified, easy testing without the use of cells or back-pressure procedures needed for direct pore pressure measurement.

Like any testing method, DSS tests are subject to a few limitations. Neither the lateral stresses in the wire-reinforced membrane nor pore pressures can be directly measured and therefore must be inferred from measurement of vertical load. Also, losses in vertical load can allow for platen-soil slippage.

Transient and dynamic loading tests required the use of the GDS Electromechanical Dynamic Cyclic Simple Shear Device (EMDCSS). This device was a plane strain device which induces horizontal movement at the bottom of the sample relative to the top. The specimen setup was composed of a short cylinder enclosed by wire-reinforced rubber membrane and sandwiched between two porous stones affixed to caps as constant volume testing requires free drainage for pore fluids. This allowed for consolidation in conditions close to K_o conditions, i.e., with no lateral strain.

The diameter of the sample remains constant due to the restraints provided by the custom NGI wire-reinforced membrane, therefore any change in volume can only result from vertical movement of the top platen. The system is also designed to simulate undrained, constant-volume conditions by continuously adjusting the vertical load by a pneumatic air pressure regulator that operates on a feedback loop which keeps the specimen height constant. The change in vertical stress is assumed to be equal to the change in pore water pressure that would have occurred during a truly undrained test. Comparative tests at NGI have shown that this assumption is valid (Dyvik et al., 1987).

The EMDCSS system uses electro-mechanical actuators, active height control, and stiff crossed-roller bearings for axial and shear linear guidance. An 8-channel DCS system is used for

automatic logging. Unlike the NGI CSS devices, the EMDCSS have much greater control over the constant height condition, thus the stress path curves become sharper and better defined at low effective stresses near failure. Schematics for the EMDCSS can be found in Appendix D.

3.2.2 Sample preparation

Numerous studies have shown that reconstituted laboratory samples can give lower strength than "intact" samples. However, it is possible to mimic the cyclic behavior of young silty or clean sands. Vaid and Sivathayalan (1999) discovered that monotonic undrained responses of reconstituted specimens using water-pluviation qualitatively and quantitatively approximated the behavior of undisturbed alluvial sand specimens common in liquefaction. They found that samples prepared using moist-tamping and dry-pluviation both showed strain softening when sheared monotonically under undrained conditions. In contrast, samples prepared using water-pluviation showed strain hardening and created uniform specimens in clean sands. Studies conducted at NGI on silty sands also recommend the use of water-pluviation over moist tamping specimens for approximation of in-situ samples (Hoeg et al., 2000; Anderson 2009).

Mulilis' (1977) study of cyclic strength curves suggests that sample preparation methods of water-pluviation and moist tamping techniques (Figure 19) yield only slightly differing strengths at low CSR. Therefore, it is possible to compare the results of cyclic tests on samples prepared using these two methods. Mulilis tested specimens at vertical effective stress of 100 kPa, a shear stress amplitude of 14 to 15 kPa, and an initial static shear stress of 10 kPa. He defined liquefaction triggering as the point at which a 2.5% single amplitude strain was reached. To assess the validity of Mulilis' assumption that air-pluviation roughly mimics—if not slightly depreciates—the liquefaction potential, two identical CSS tests on Siri sands were conducted. One used air-pluviation specimen preparation and the other used water-pluviation. Under the same

stress conditions as Mulilis's tests, the air-pluviated and water-pluviated specimens failed at 14 and 16 cycles respectively. This is consistent with Mulilis' assumption that air-pluviated specimens are slightly less resistant to liquefaction that water-pluviated specimens.
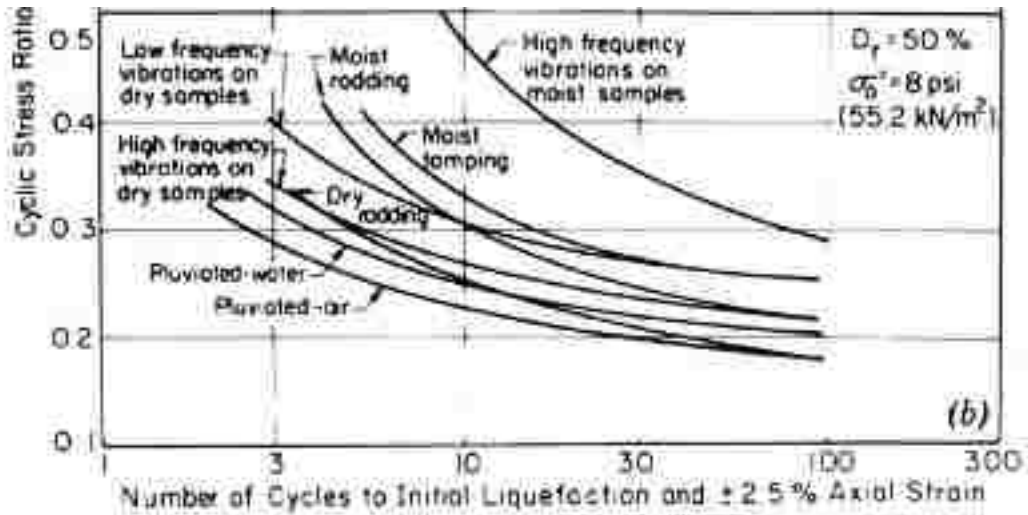

Figure 19: Effect of sample preparation techniques from Mulilis et al. 1977a

Water-pluviated samples for medium-dense specimens were created in the following manner: a wire mesh was placed on the 35 cm^2 base DSS platen. A specimen height of 20 mm was targeted to ensure the grain sizes are <10% the height of the specimen. Wire-reinforced membranes served as horizontal confinement and lubricant silicon oils and O-rings sealed off the membrane and the platens to prevent leakage during sample preparation and loading. Samples were funneled into a cylindrical mold onto the wire mesh full of demineralized water using a small drop height less than a centimeter. Once the sand was dispersed evenly, the mesh was slowly raised through the specimen such that the grains fell through slowly and dispersed throughout the mold evenly and engaged the membrane. The raining of sand serves to simulate the deposition method of natural alluvial deposits through water. Water pluviation best mimics natural fluvial deposits, but it is very

difficult to obtain densities less than 50% in a lab environment. Therefore, water-deposition preparation procedures for high and medium density specimens were used in lieu of water-pluviation, e.g., the screen was held just above the water level and the sand was rained through it. This method created samples with the lower densities required for loose set specimens under $D_r = 50\%$.
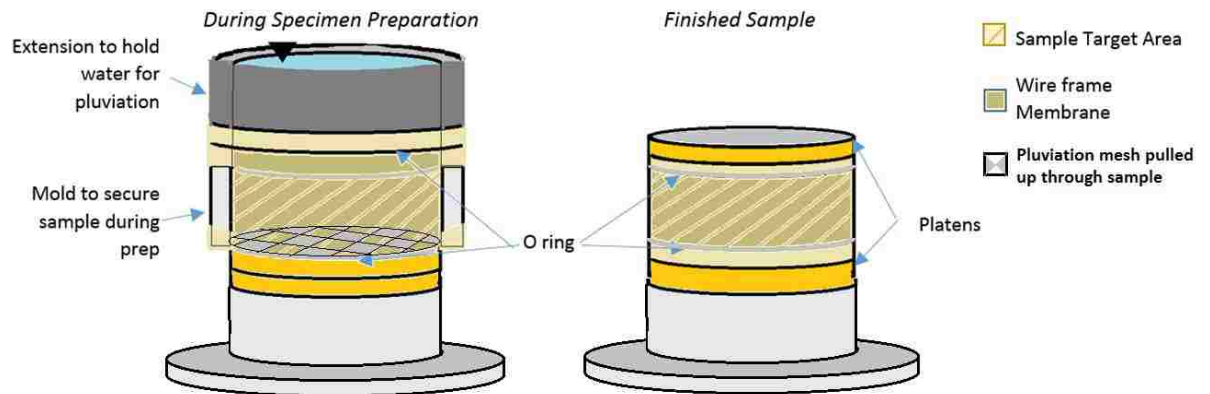

Figure 20: Water-pluviation and moist tamping set up for specimen preparation. Mold and extension was filled with water than sand rained through funnel.

3.2.3 Consolidation

The program tested specimens at an initial vertical overburden stress of 100 kPa which reflects the shallow depths in which liquefiable deposits are typically found. The consolidation characteristics are defined by the virgin, unloading, and reloading moduli. The volume change behavior of a sand is influenced by its state, which is a function of density and vertical effective pressure. These characteristics can be determined for clean sand in a consolidation test via the flow resistance in filters and tubes, which may be high compared to the low flow resistance in the sand specimen.

Each specimen was monitored during vertical consolidation. It is impractical to reproduce the long-term effects of consolidation in the laboratory, but for these clean, uniform sands with significantly high permeability, primary consolidation typically was completed within 45 minutes.

However, the specimens consolidated for greater than 4 hours before shearing began, after which a final flush was conducted to ensure adequate saturation levels and remove any residual bubbles from the pore spaces. The valves only on the bottom platform were opened to allow flow in and out of the specimen at low heads, preventing channelling and disturbance of the pluviated soil structure which can occur in loose or fine sand specimens. Due to the nature of constant volume testing, back pressuring of the specimen to ensure a high B value was not necessary.

The equipment automatically logged data of the consolidation process. Specimens were consolidated at a constant rate of 10 kPa per minute until final vertical loading of 100 kPa was achieved, then the final flush was conducted. (See Appendix A.2 for more details and an example of a typical consolidation curve for Nevada and Siri sands).

This report assumes that the critical state line for sands is parallel to the consolidation curve, in which case the state parameter remains constant when the effective stress changes. However, it should be noted that some studies suggest that the critical state line is steeper as a sand becomes more contractive at higher effective stress levels (Kramer 1996). Other studies have shown minor correlations of measured strength and consolidation time (Mulilis, Seed, Chan, Mitchell, & Arulanandan, 1977a).

3.2.4   Pre-shearing

There is some debate regarding the applicability of pre-shearing soil specimens in liquefaction shear tests. Advantages and disadvantages for pre-shearing reconstituted soil samples in DSS are summarized in Table 7.

Although pre-shearing is typically desirable to homogenize and set specimens for cyclic testing in dense specimens or those with high vertical load, this is not always the case for testing in liquefiable soils. Problems in infrastructure due to liquefaction are typically seen in relatively

young, recently deposited sands, which have not been exposed to previous earthquake shaking and often are in a virgin state. Studies have shown that pre-shearing of sands (even very weak cyclic shearing of around 1% of overburden stress) can significantly increase liquefaction resistance. This happens even when there is no change in density and no change in shear wave velocity. Pocino et al. (2009) conducted a series of tests on the NGI-style DSS device, which found that small amounts of pre-shearing on a specimen render the specimen more resistant to liquefaction than virgin specimens, irrespective of density index value. Further studies on silica and carbonate sands backed these findings (Finn et al. 1970; Lee and Albaisa, 1974; Seed et al. 1977; Shamoto et al. 1978; Kaggwa, 1988).

Table 7: Advantages and Disadvantages of Pre-shearing in liquefaction DSS testing.

	ADVANTAGES TO PRESHEARING	DISADVANTAGES TO PRESHEARING IN LIQUEFIABLE DEPOSITS
SETTINGS	*An improvement of the settings between grains and the platens*	
SOIL STRUCTURE	*Homogenization of stress* concentrations incurred during consolidation as particles rearrange into a more uniform manner	Pre-shearing can destroy *the initial delicate soil matrix* of a water-pluviated specimen or densify a specimen past desired target. Liquefiable deposits are typically young, weak, and have never seen any past shearing
PORE PRESSURE GENERATION	*Removal of any initial static equipment miscalculation* of the confining stress which may cause an error in initial pore pressure generation.	Even small amounts of pre-shearing can increase liquefaction resistance. (Pocino et al. 2009)
PAST LITERATURE	Nearly all past DSS testing of sands conducted at NGI are pre-sheared.	Majority of liquefaction DSS databases do not employ pre-shearing. There is no guarantee of the accuracy of these corrections without an additional testing program.

To address the concern of an initial misreading of lateral confining stress in DSS tests, a set of tests were conducted to determine whether pre-shearing was required. In sands, this initial misreading can be evidenced in an initial rapid rise in pore pressure upon initiation testing or during

the first sufficiently-sized pulse of loading which does not match the behavior of the following cycles (Dyvik, 1984). A series of tests were run on identical Siri sands specimens (to the extent possible) with different level of pre-shearing—0 and 1% of overburden stress amplitude with 0, 20, or 200 cycles—labelled tests A, B, and C respectively—to compare the effect on liquefaction generation. The pore pressure generation of these tests are compared in Figure 21. The specimens were moist-tamped using Siri sand at Dr = 35% and sheared at a CSR=0.1. By comparing pore pressure generation normalized to the time to liquefaction, all cyclic tests are seen to roughly follow the pore pressure development curve r_u by De Alba (1975) of the form:

$$r_u = \frac{1}{2} + \frac{1}{\pi} sin^{-1}\left(2\left(\frac{N}{N_L}\right)^{\frac{1}{\alpha}} - 1\right)$$

Equation 13

where N_L is the number of cycles to liquefaction and α is an empirical shape factor measured to be 0.5 for Siri sands. This indicates that all tests followed the typical pore pressure generation pattern common in harmonic uniform tests. Test C liquefied at 12 cycles while Tests A and B liquefied at 11 cycles. Although there were no dramatic differences between A and B, the higher levels of pre-shear in C did seem to increase the liquefaction resistance. Thus, it can be concluded that normal levels of pre-shearing (i.e., 200 cycles) may not be appropriate for liquefaction testing.

The next question to ask is whether specimens without pre-shearing are effected by the initial misreading of the confining stresses during the initiation of shearing, which would be seen by an initial large jump in pore pressure generation in the first cycle. This initial higher rate is found in almost all cyclic tests. To measure the contractiveness of the soil, the derivative of the pore pressure ratio r_u with respect to shear stress τ was taken to evaluate the change in behavior by cycle. In almost all cyclic cases, $\frac{\delta r_u}{\delta \tau}$ revealed minor differences of scale at a factor of around 1 to 1.5 in the initial loading cycle. The question then becomes: how much of this initial higher pore pressure generation is due to the misreading of the confining stresses and how much to typical

initial high contractiveness of loose virgin soils?   Cyclic triaxial tests have shown that the contractiveness of sands is higher in the first few cycles in specimens constructed by moist tamping, water-pluviation, and by air-pluviation. Liquefiable deposits are typically found in such loose states that there are many particle contacts that are tenuous (or metastable). Thus, small particle movements associated with rearrangement of these contacts causes the soil to be quite contractive initially, which could reasonably be reflected by an increase $\frac{\delta r_u}{\delta \tau}$ first one or two cycles. As more stable contacts develop, the contractiveness reduces. Therefore, initial $\frac{\delta r_u}{\delta \tau}$ scaling factor of 1.5 in initial cycles can likely be attributed to the initial contractiveness of soil upon shearing initiation.
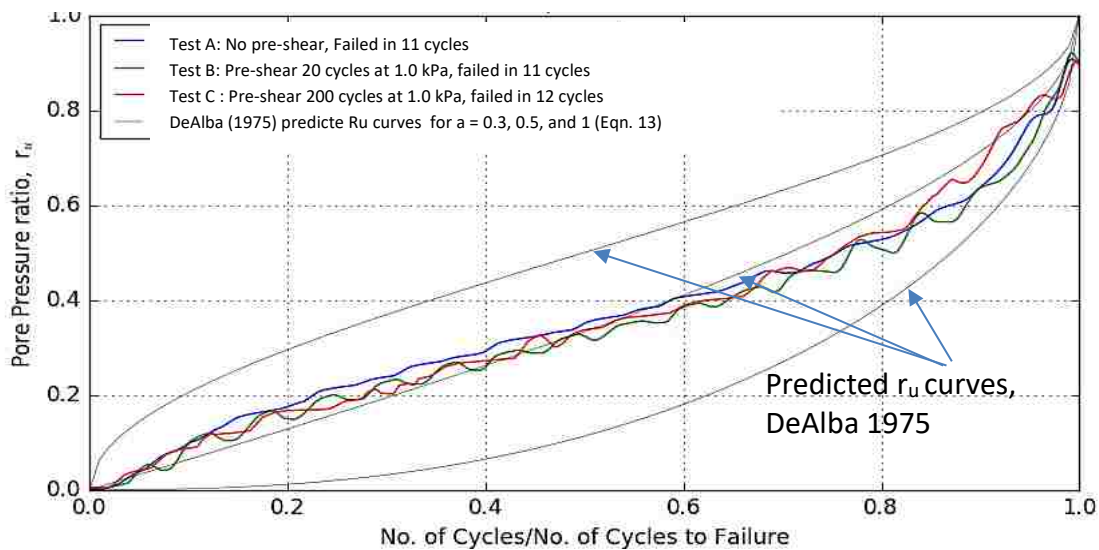
Figure 21: NGI CSS tests evaluating effects of pre-shearing level before cyclic testing. All tests normalized by time to liquefaction failure. All tests subject to: D_r = 35% Siri Sand, σ'_v = 100 kPa, $\tau_{o,static}$ = 0 kPa, CSR = 0.1.

Weighing the advantages and disadvantages outlined previously, it was decided that typical pre-shearing methods (around 100-200 cycles at 5-10% of vertical overburden stress) as used on dense or over consolidated sands would not be appropriate for this liquefaction CSS program. The

transient and dynamic tests on the GDS stands as its own database, and thus will have no pre-shearing for ease of comparison to past liquefaction tests done on Nevada sands (Sideras 2013, Kwan 2015).

3.2.5   Shearing

After the soil consolidated, a final measurement of height was taken and initial relative density calculated.   For cases in which initial static shear stress was greater than 0, e.g., not level conditions, the desired initial static shear τ_o was applied for 30 minutes before shearing began.

Chapter 2 addressed the effects of static shear stress by defining relationships between α and the initial static stress factor, K_α. Most test sites have some degree of sloping ground, thus an understanding of the effects of initial static shear in addition to cyclic or transient loading is crucial to replicating in-situ behavior. Recognizing the importance of stress reversals on behavior, this cyclic testing program chose α values to represent three levels of relationship between loading and initial static shear: no static shear (e.g., α=0), directional reversal of static shear (e.g., α<CSR), and no reversal of shear stress (e.g., α ≥ CSR). To capture these desired conditions, tests for four levels of α were performed: α = 0.20, 0.10, 0.05, and 0.

The transient and dynamic shear histories were taken to be scaled versions of the ground motion's acceleration PEER record scaled to have a maximum shear stress of 15% of the vertical stress on the specimen. In transient tests, the scaled shear records were applied at a speed 1/4th that of real-time to avoid inertial forces between grains such that the DSS equipment could maintain adequate constant height control as the liquefied soil stiffness becomes exceedingly low. A few dynamic tests were conducted at real-time to investigate rate effects. These the tests were typically conducted until (a) liquefaction or (b) a strain threshold of 20 mm had been reached.

A uniform stress series is often used to compare the shaking load of a seismic motion to an equivalent laboratory cyclic testing program. This uniform stress series is defined by three ground motion parameters: amplitude, frequency content, and duration. The standard equivalent uniform stress amplitude is typically taken to be 65% of the peak shear stress of the earthquake time history. Frequency content is evaluated to determine if it falls within the range of engineering interest which is shown to have a significant effect on liquefaction, and duration is characterized in terms of a number of equivalent cycles. A magnitude scaling factor MSF (Equation 14) is applied to the CSR of dense specimens to account for differential durations (Liu, Stewart et al., 2001). The MSF (Equation 15) is derived from the number of equivalent uniform stress cycles and applied to the CSR to normalize a CSR for some magnitude, M, to a CSR corresponding to M = 7.5. As similar CSR values indicated similar peak shear stress amplitudes and MSF gives some indication of energy intensity, the value of CSR/MSF represents a CSR with a duration corresponding to a common reference magnitude of 7.5. The simplified evaluation procedure (Seed & Idriss, 1971) can be used to find the appropriate MSF for each motion, derived in the equivalent number of cycles to liquefaction.

$$Magnitude\ Scaling\ Factor: \quad MSF = \left(\frac{N_{M=7.5}}{N_M}\right)^b \qquad\qquad \text{Equation 14}$$

$$CSR\ for\ a\ Mag.\ 7.5\ earthquake: \quad CSR_{M=7.5} = \frac{CSR_M}{MSF} \qquad\qquad \text{Equation 15}$$

The curve fitting parameter b was calculated by W. S. Kwan (2015) for Nevada sand to be 0.298 which is closely comparable to the value of 0.337 of uniform clean sands measured by Idriss (1999). $N_{M=7.5}$ is 15 cycles, as defined by Seed and Lee (1966); the number of uniform stress cycles for a magnitude 7.5 earthquake. N_{eq} is the number of equivalent cycles, and CSR in this report was taken to be the motion's peak shear stress divided by the initial vertical effective stress:

$$CSR \text{ in transient } CSS \text{ tests:} \qquad CSR_M = \frac{\tau_{peak}}{\sigma'_{vo}} \qquad \text{Equation 16}$$

For the purposes of these tests, liquefaction was 'triggered' when the pore pressure ratio r_u became greater than 0.98. In other words, the point which nearly all the vertical load is supported by the pore fluid and not by the sand skeleton. Loading was terminated at the point in which either (a) liquefaction had obviously been triggered for an extended period or (b) shear strains exceeded +/-15% indicating full failure of the material.

3.3   Data Corrections and Calculations

3.3.1   Membrane correction

The NGI wire-reinforced membranes require a correction factor to account for any vertical loads that are supported by the rubber membrane instead of the soil skeleton. The NGI membrane correction, C_m, is based on a curve from the 1992 study by Brylawski and Berre shown in Figure 22 which is based on membrane elasticity and stiffness. The 35 cm^2 membranes for cyclic testing had a stiffness coefficient of C = 1.25 for transient and dynamic testing. The correction was later revised in 1997 with a scaling factor f, of the form:

$$f = (t + 0.0306)/0.6 \qquad \text{Equation 17}$$

where t is the thickness of the membrane in mm. The corrected initial vertical stress applied to the soil was taken to be $\sigma'_{vo,corrected} = \sigma'_{vo,measured} - C_m$. Table 8 shows the calculated membrane correction factors used for each transient test.
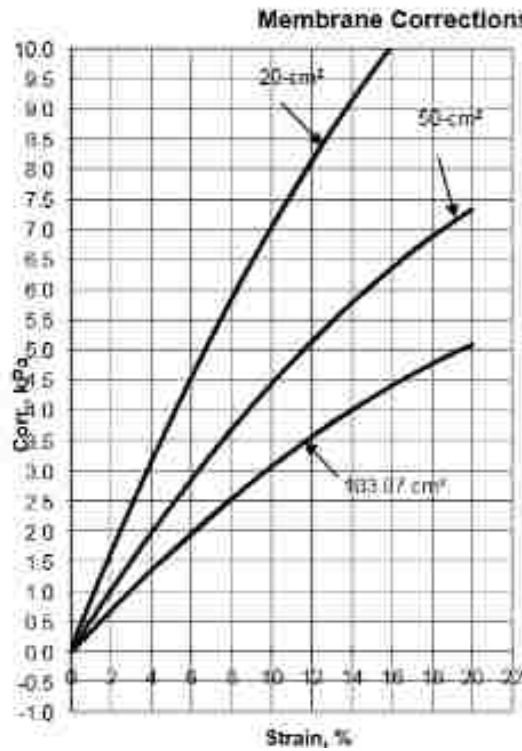
Figure 22: NGI DSS wire-reinforced membrane correction curve. From (Brylawski & Berre, 1992, rev. 1997)

Measured Vertical Stress, $\sigma'_{vo,measured}$	100 kPa
Vertical strain in consolidation	5-7%
Membrane correction factor from Figure	3.5 kPa
Membrane thickness, t	0.65 mm
Revised scaling factor, f	1.19
1997 Revised membrane correction factor, C_m	**4.2 kPa**

Table 8: Revised wire-reinforced membrane correction factors for 35 cm² specimen.

On the GDS, the membrane corrections are calibrated according to vertical strain during consolidation as well. It was found that for 100 kPa of vertical loading on Nevada sands, the specimens consolidated 5-7%. This corresponds to a membrane correction of 4.2 kPa.

3.3.2   GDS loading control lag

Due to the nature of the physical movement of oil through the motor, there is always some inherent lag between the stress command given to the motor and its subsequent response. The GDS

hardware lag can be minimized to an acceptable level by reducing the rate of testing and calibrating the GDS motor to correspond to the stiffness of the tested soil.
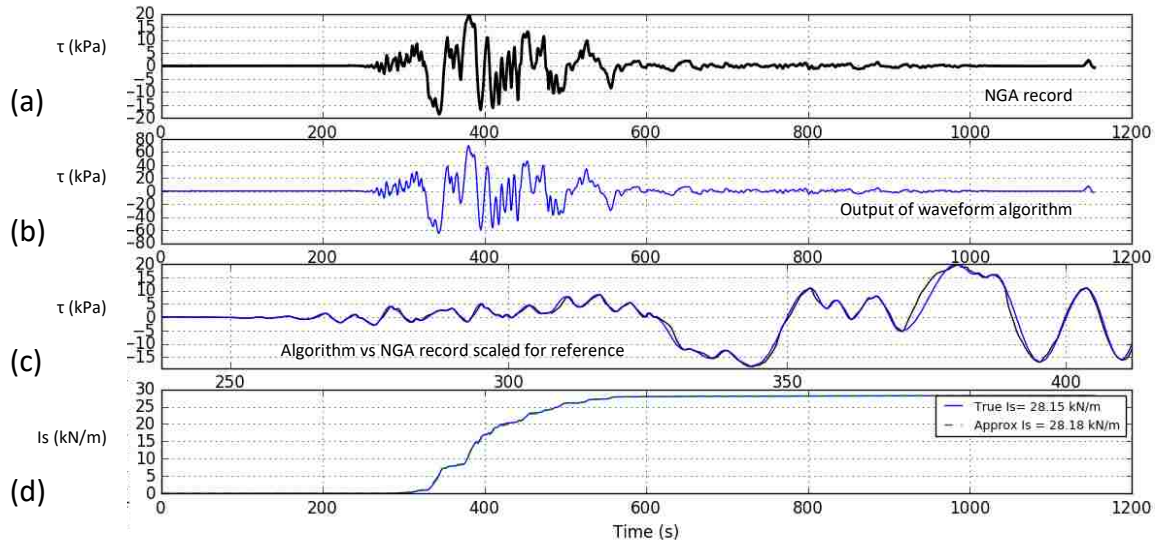
Figure 23: Stress history output of transformative algorithm from the Palm Springs, CA PEER NGA record to a GDS Profile Editor record. (a) The original NGA acceleration record which has been directly scaled to stress record with a peak stress of 20 kPa. (b) A direct comparison of these two can be seen in the time-amplified plot in (c). (d) Comparison of the two motion's stress intensities, I_s.

In addition to the hardware lag, an algorithm was written to deal with the software incompatibility with a time history record. The algorithm transforms a PEER NGA acceleration record into a series of maxima and minima connected by half-sinusoids with a time period corresponding to the time between data points. Due to software limitations, a record which contains more than 1000 data points must be broken into successive records each containing 1000 pts. Therefore, the Palm Springs and the Landers motion were broken into 5 files and 9 files respectively, with each file run consecutively over a 100 second period. The algorithm approximates this record well, as seen in an example of the Palm Springs record in Figure 23. Appendix B describes the logic behind the algorithm and contains all figures of transient stress motions in this study.

3.3.3 Calculation of shear stiffness

The stiffness of the soil structure can be measured by the shear stiffness parameter G. G is defined by the derivative of the shear stress with respect to the shear strain. Measurement of instantaneous stiffness, G_{tan}, can be defined in Equation 18, and the overall stiffness as it corresponds to the whole test, G_{sec}, is defined in Equation 19.

$$G_{tan} = (\tau_i - \tau_{i-1})/(\gamma_i - \gamma_{i-1}) \qquad \text{Equation 18}$$

$$G_{sec} = (\tau_i - \tau_0)/(\gamma_i - \gamma_0) \qquad \text{Equation 19}$$

where τ_i is the shear stress and γ_i is the shear strain at each data point *i*.

Soil stiffness in monotonic/static tests is often described in a secant shear modulus reduction curve. In uniform, harmonic testing, it is typical to see the instantaneous shear stiffness modulus, G_{tan}, of a liquefied specimen vary dramatically over the course of a single cycle. In the case of a liquefaction failure, the stiffness can rapidly drop to very low, near zero values, leading to large cyclic strains, termed in this report as *cyclic liquefaction*. This behavior can appear in the tests in which α is significantly lower than CSR, i.e., the loading may cause the specimen to cyclically fail along its failure plane and reach zero effective stresses. In cases where CSR is less than α, permanent strains are expected to develop over the course of the test and the specimen may fail in *cyclic mobility*. In these cases, the stiffness may decrease at failure, but G_{sec} may never reach levels as low as those reached in cyclic liquefaction failure.

CHAPTER 4. RESULTS OF TESTING PROGRAM

This chapter presents the tests performed for this report. Section 4.1 presents the transient and dynamic tests performed on the GDS device. Details and graphic representations of all conducted tests after post-processing can be found in their corresponding Appendices. Section 4.2 addresses the level of uncertainty and possible sources of error inherent in these simple shear tests. The last section addresses the level of uncertainty and possible sources of error by human error and error inherent in these simple shear tests.

All raw data for tests was stored for ease of access in an SQL database and in simple text file format. Requests for database access can be made through University of Washington Library or directly through the author at kdelavea@uw.edu.

4.1   Transient Database

All transient DSS tests on Nevada sands were subjected to shearing of one the following ground motions, *PALMSPR_MVH135* or *LANDERS_MCF_000*. The transient and dynamic DSS tests are summarized in Table 9. Several additional tests were run to check for rate effects, density effects, loading history, and pre-shearing. Supplemental cyclic tests investigating the equivalent number of cycles are shown in Table 10. All raw digital testing data is stored in individual test txt. files and in the SQL database NGI_Trans_Kalpha_2016.db described in Appendix C.

Testing performed at the University of Texas found that in irregular loading the order of loading cycles has a strong influence on pore pressure generation (Kwan, 2015). For example, in a cyclic test a shear stress pulse will produce a much smaller increment of pore pressure than if it has been preceded by a larger shear stress pulse. Kwan (2015) found that ground motions with a

lower frequency content tend to have a greater effect on the liquefaction triggering. Kwan's results suggest that the general approach of using a typical intensity measure or summing the total level of loading that occur during a ground motion as a parameter to predict strain-induced deformations of a liquefied soil may not be sufficient. Instead, strain-induced deformations are more closely affected by the level of loading that occurs after triggering of liquefaction. Thus, a more involved understanding of pore pressure generation during a motion is required to predict exactly when liquefaction may occur. History of loading is even more important in irregular earthquake loading, a factor investigated in this study.

Table 9: Summary of transient and dynamic simple shear tests on Nevada sands. Test graphically shown in Appendix A at given index. All transient tests run at one quarter of real-time speed, dynamic tests at real-time.

GROUND MOTION	TEST ID	RELATIVE DENSITY (%)	COMMENTS	MSF	α	CSR	CSR/MSF	APPENDIX FIGURE
PALMSPR_MVH135	N0403	55.1	(e)	1.24	0	0.148	0.120	A.1
	N0404	45.6		1.24	0.042	0.147	0.118	A.2
		44.0	(b)	1.24	0.045	0.152	0.122	A.3
		42.1	(d)	1.24	0.044	0.154	0.124	A.4
		69.6	(a)	1.24	0.048	0.127	0.102	A.5
	N0405	42.0		1.24	0.100	0.130	0.105	A.6
	N0406	43.8		1.24	0.199	0.128	0.103	A.7
	N0407	65.1		1.24	0.002	0.149	0.120	A.8
	N0408	62.9		1.24	0.042	0.149	0.120	A.9
	N0409	64.3		1.24	0.092	0.148	0.119	A.10
	N0410	64.7		1.24	0.193	0.155	0.125	A.11
	N0423	91.1	(e)	1.24	0.101	0.151	0.122	A.20
	N0419	43.9		1.24	0.042	0.057	0.046	A.21
	N0420	39.7		1.24	0.043	0.097	0.078	A.22
	N0421	63.9		1.24	0.042	0.147	0.118	A.23
	N0422	73.3		1.24	0.045	0.020	0.016	A.24
LANDERS_MCF_000	N0411	59.8		1.05	0.004	0.115	0.109	A.12
	N0412	62.7		1.05	0.047	0.098	0.093	A.13
	N0413	62.2		1.05	0.096	0.137	0.130	A.14
	N0414	58.2		1.05	0.213	0.168	0.16	A.15
	N0415	55.6		1.05	0.002	0.143	0.136	A.16
	N0416	59.1		1.05	0.044	0.153	0.146	A.17
	N0417	60.7		1.05	0.100	0.118	0.112	A.18
	N0418	55.6		1.05	0.187	0.135	0.129	A.19

COMMENTS:

(a) Dynamic Test, run at real-time, but with low logging resolution
(b) Run in reverse
(c) Pre-sheared at 20 cycles and 0.05 kPa
(d) Run to test repeatability
(e) Consolidated past target density

Table 10: Supplemental cyclic harmonic tests on Nevada Sands

TEST ID	RELATIVE DENSITY (%)	CSR	A	APPENDIX FIGURE
N0500	50.5	*0.10*	0.0	A.25
N0501	87.4	*0.09*	0.0	A.26
N0502	46.7	*0.045*	0.112	A.27
N0503	58.7	*0.045*	0.112	A.28

4.1.1 Parametric studies under earthquake loading

There is much to be learned from direct comparisons of transient tests. Table 11 summarizes the figures presented in this section which compare specific tests on Nevada sands. Following the same logic used in the cyclic parametric study, tests are compared directly by level of initial static shear stress (Figures 24 to 31), density (Figure 32-33), and loading amplitude (Figure 33-37). Additional tests were performed to investigate secondary parameters which may affect pore pressure generation in a liquefiable deposit. These factors include:

Investigation of loading history:

A motion was run in reverse with respect to time under otherwise identical conditions (Figure 38-39) to test the soil response of a motion with identical intensity measures but different orders of loading.

Investigation of rate effects:

Several motions were run at real-time speeds to investigate the effects of dynamic forces present in real-time seismic loading (Figure 40).

Table 11: Reference table for parametric comparisons of transient and dynamic tests on Nevada sand at σ_{3c} = 100 kPa

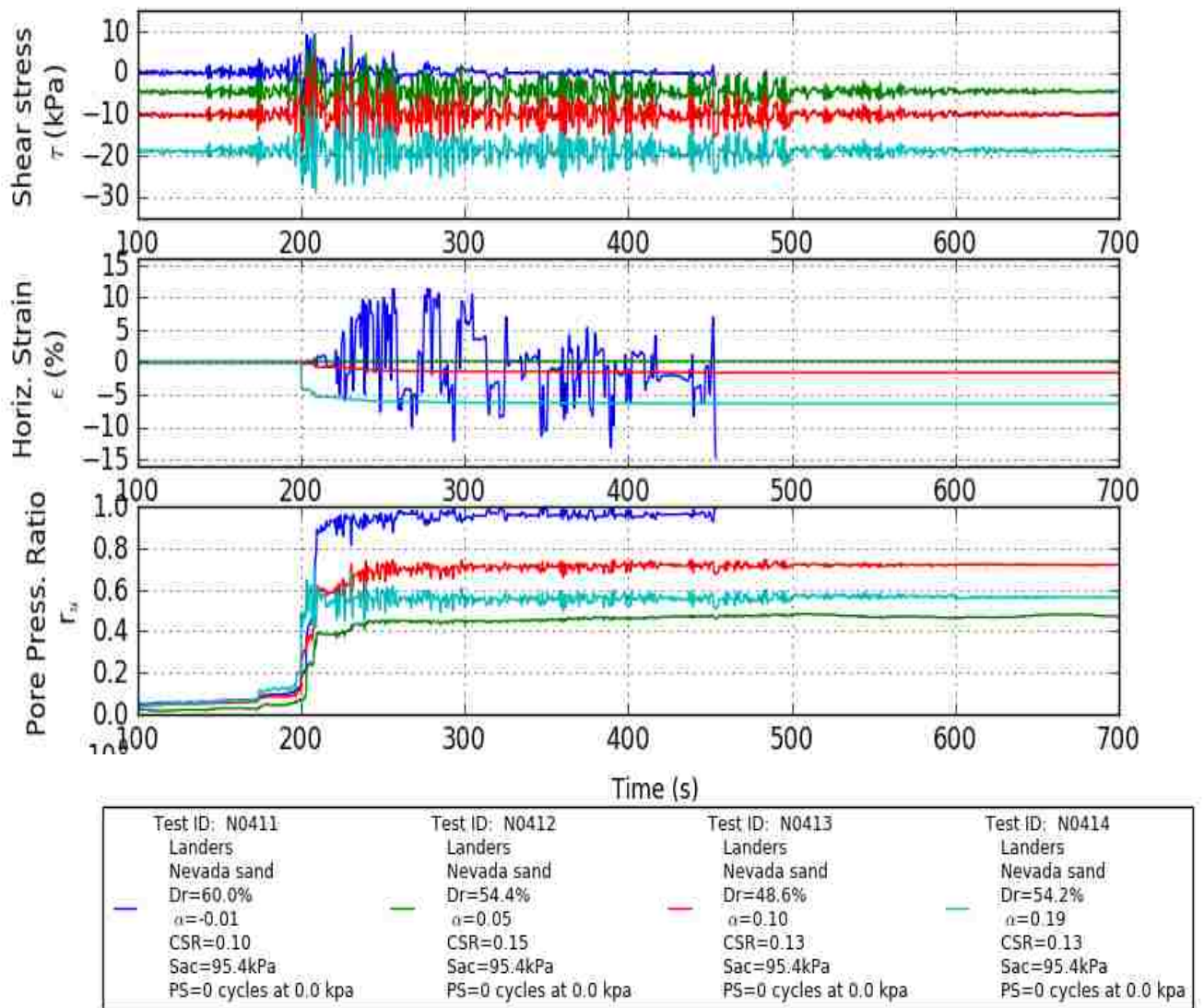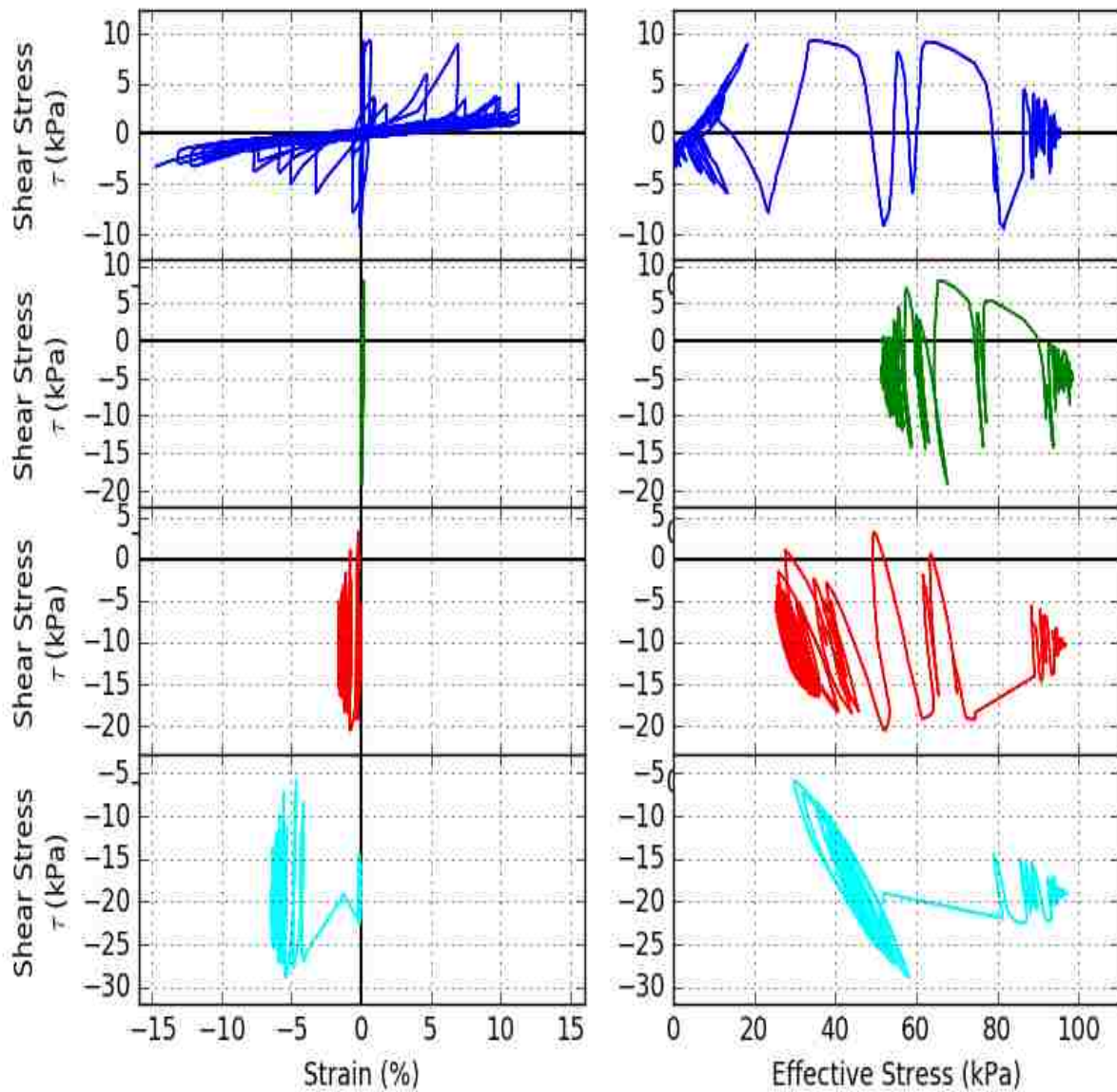| Variable to compare	Motion	Density	CSR	A	Figure No.
INITIAL STATIC SHEAR STRESS, A	Palm Springs	Loose	0.15	Variable	24-25
	Palm Springs	Dense	0.15	Variable	26-27
	Landers	Loose	0.15	Variable	28-39
	Landers	Dense	0.15	Variable	30-31
LOADING LEVEL, CSR	Palm Springs	Loose	Variable	0.05	34-35
	Palm Springs	Dense	Variable	0.05	36-37
SOIL STATE, DENSITY, D_R RELATIVE	Palm Springs	variable	0.15	0.1	32-33
ORDER OF CYCLES	Palm Springs	Loose	0.15	0.05	38-39
DYNAMIC RATE EFFECTS	Palm Springs	loose	0.15	0.05	40

Figure 24: Compare α in loose-medium dense specimens. Time history and soil response. Nevada Sands. Palm Springs Motion. CSR = 0.15. Run at 0.25 x real-time. Dark blue test represents level conditions, green is tested at α<CSR, red at α=CSR, and light blue at α>CSR.

Figure 25: Compare α in loose-medium dense specimens. Stress-strain and stress path. Nevada Sands. Palm Springs Motion. CSR = 0.15. Run at 0.25 x real-time.
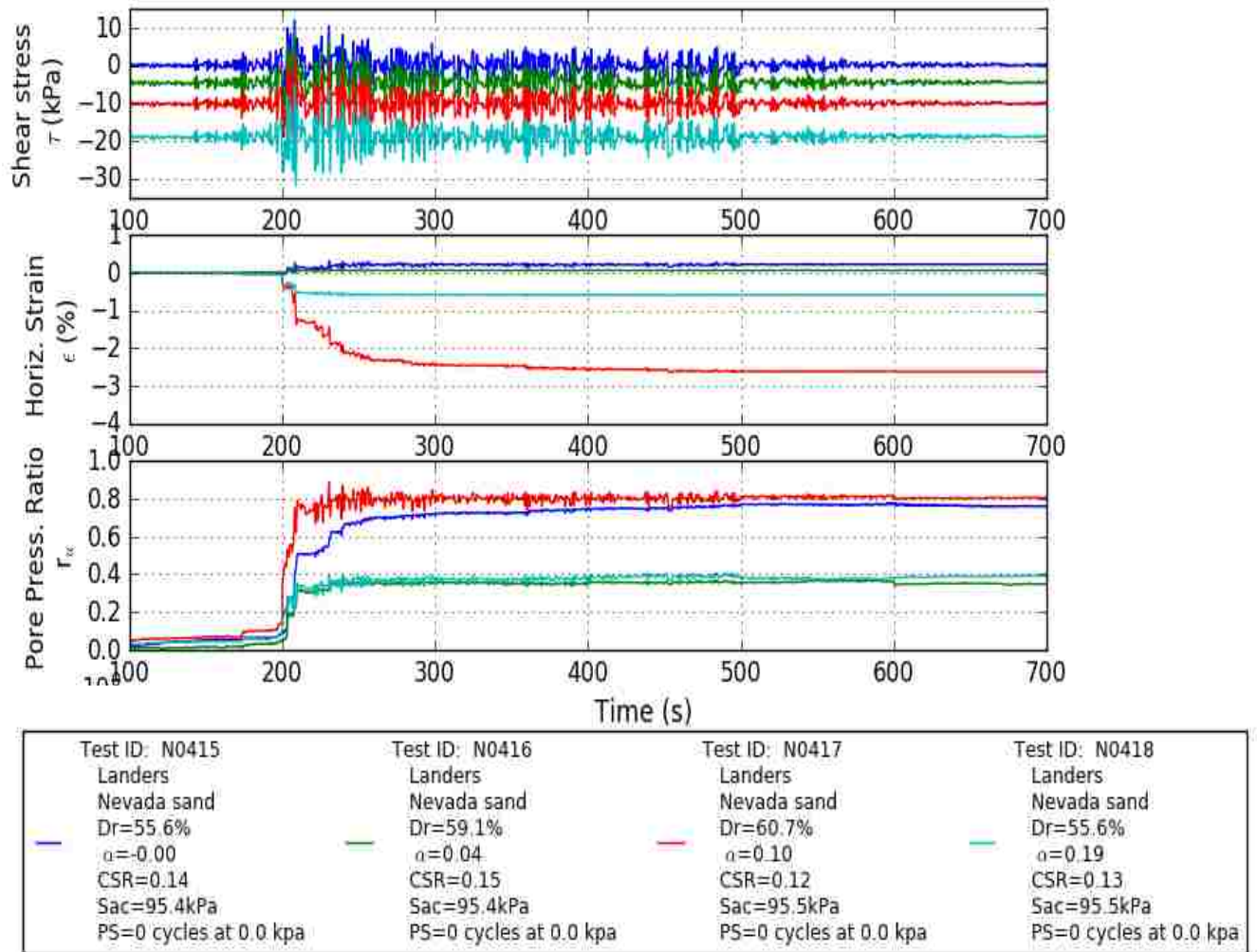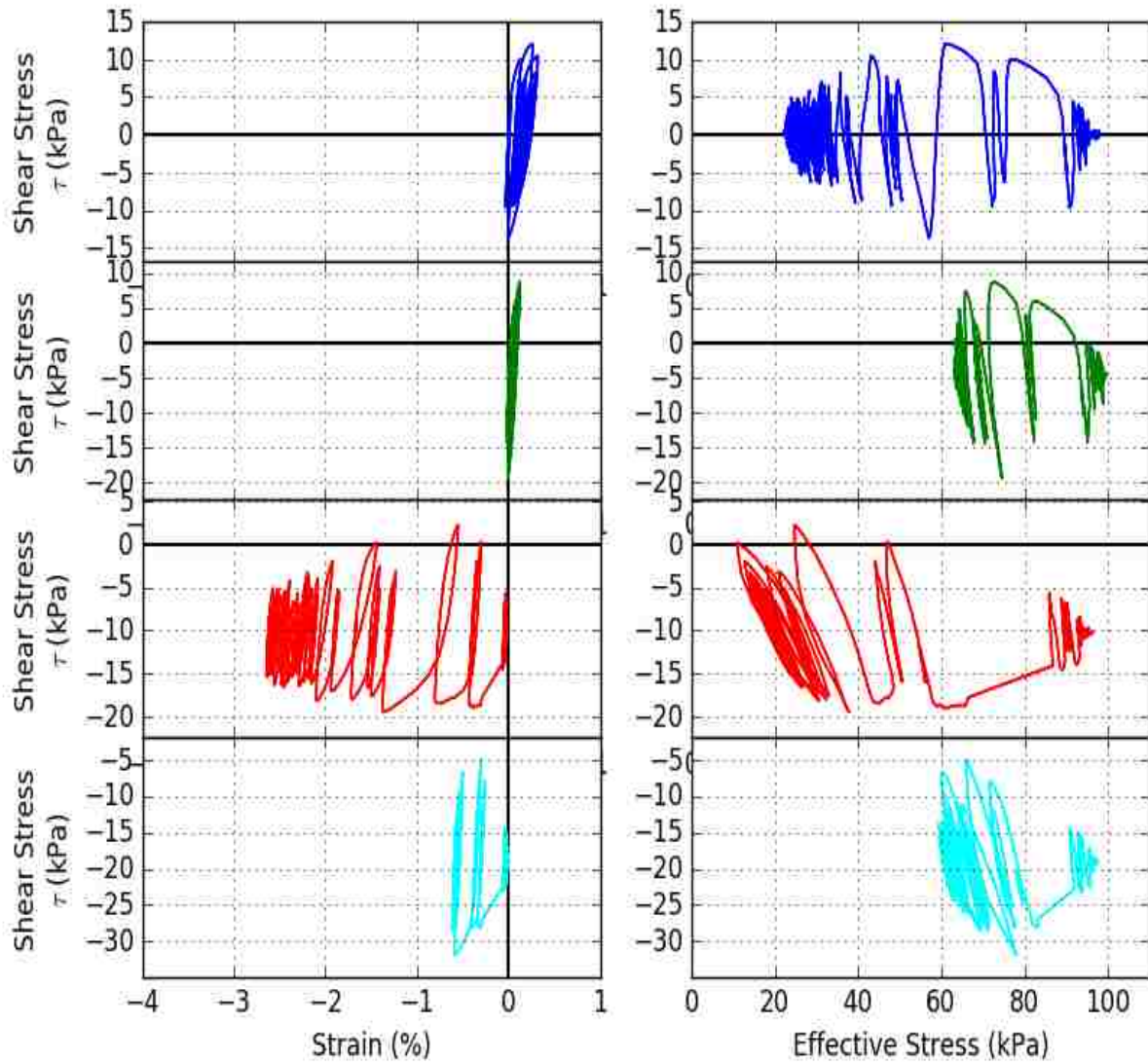
Figure 26: Compare α in dense specimens. Time history and soil response. Nevada Sands. Palm Springs Motion. CSR = 0.15. Run at 0.25 x real-time.

Figure 27: Compare α in dense specimens. Stress-strain and stress path. Nevada Sands. Palm Springs Motion. CSR = 0.15. Run at 0.25 x real-time.

Figure 28: Compare α in loose-medium dense specimens. Time history and soil response. Nevada Sands. Landers Motion. CSR = 0.15. Run at 0.25 x real-time.

Figure 29: Compare α in loose-medium dense specimens. Stress-strain and stress path. Nevada Sands. Landers Motion. CSR = 0.15. Run at 0.25 x real-time.

Figure 30: Compare α in dense specimens. Time history and soil response. Nevada Sands. Landers Motion. CSR = 0.15. Run at 0.25 x real-time.

Figure 31: Compare α in dense specimens. Stress-strain and stress path. Nevada Sands. Landers Motion. CSR = 0.15. Run at 0.25 x real-time.
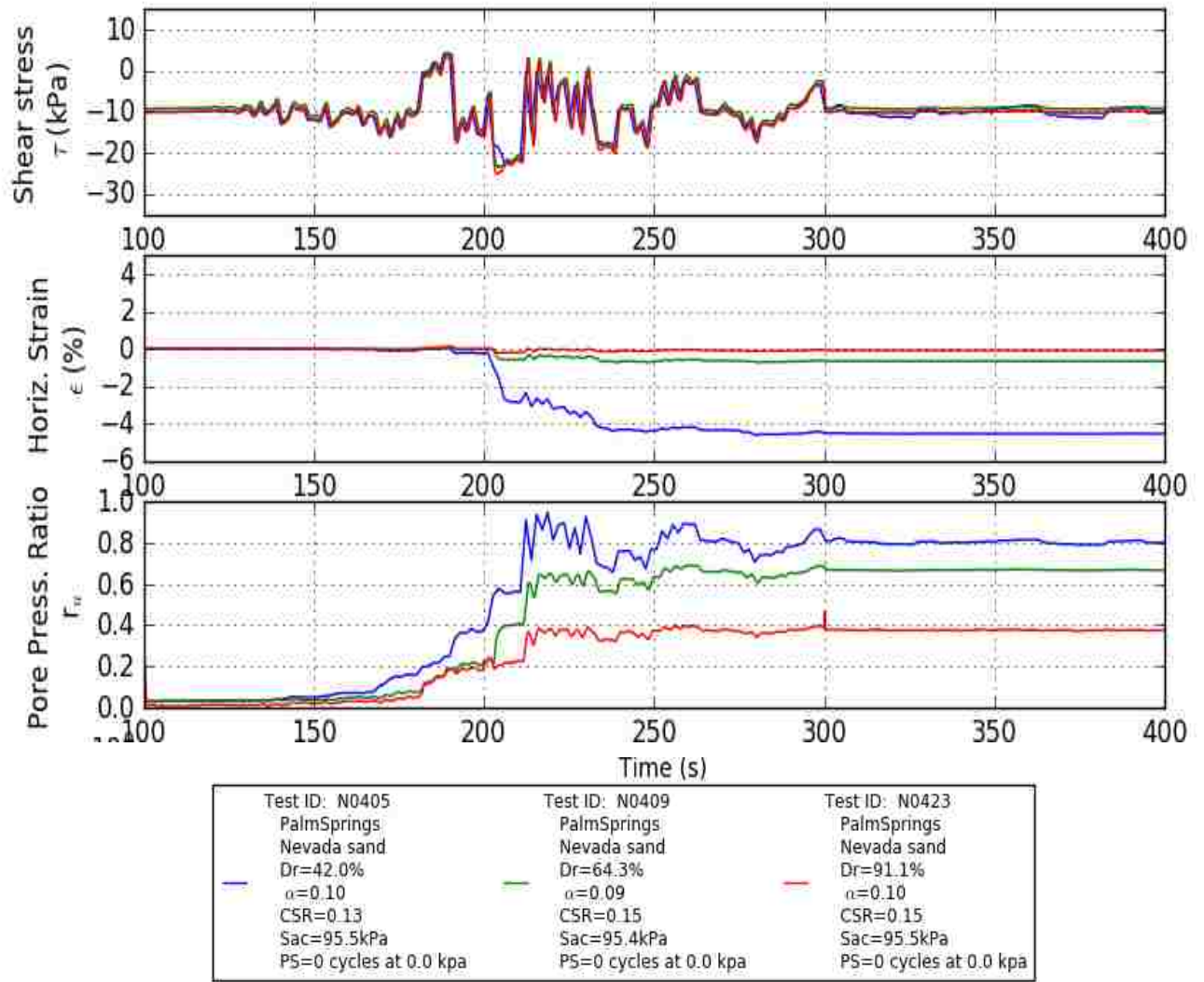
Figure 32: Compare soil state by relative density. Time history and soil response. Nevada Sands. Palm Springs Motion. α = 0.10. Run at 0.25 x real-time.
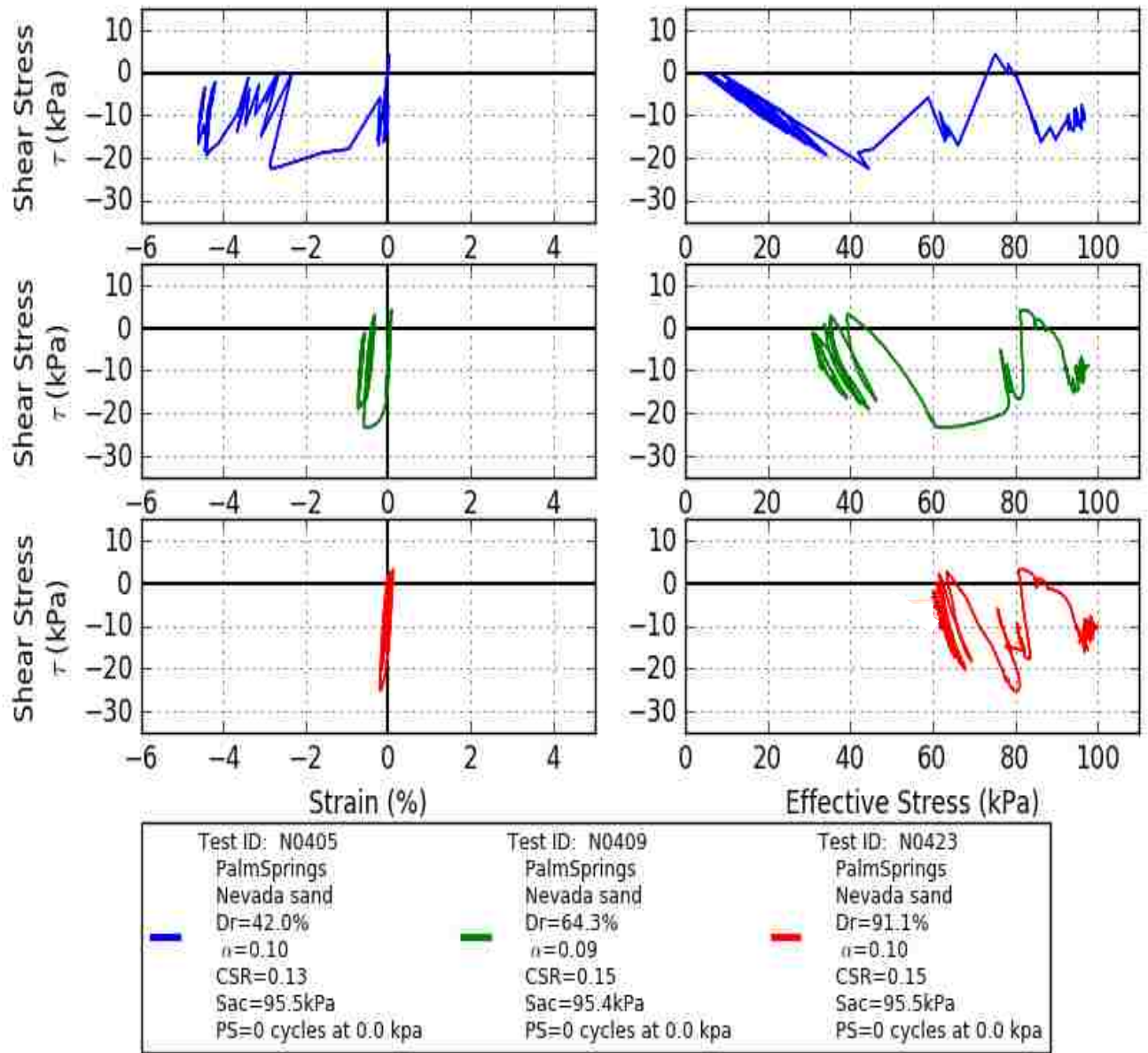
Figure 33: Compare soil state by relative density. Stress-strain and stress path. Nevada Sands. Palm Springs Motion. α = 0.10. N0405 run at real-time speeds, N0409 and N0423 run at 0.25 x real-time.
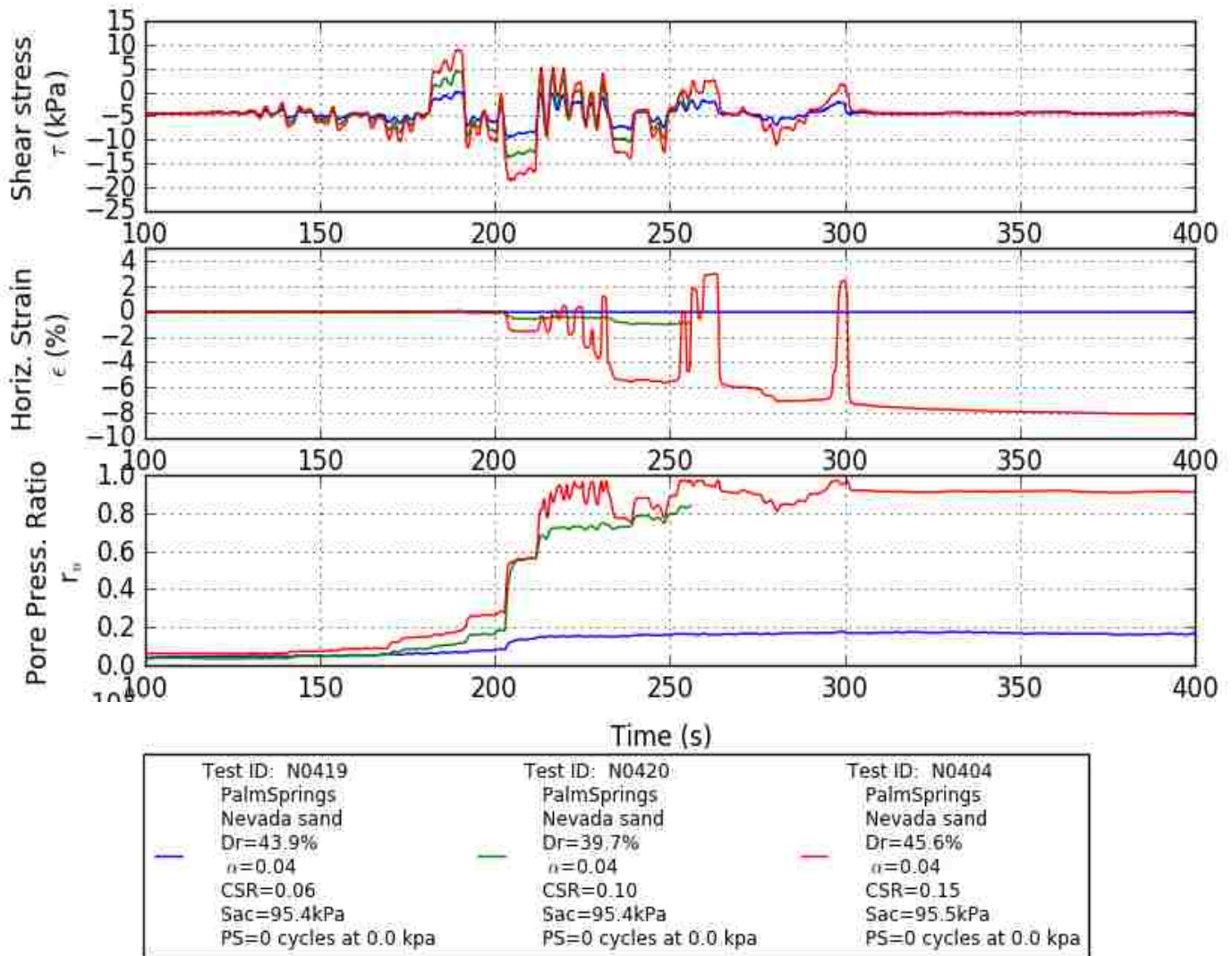
Figure 34: Compare CSR. Time history and soil response. Nevada Sands. Palm Springs Motion. α = 0.05. N0405 run at real-time speeds, N0409 and N0423 run at 0.25 x real-time.
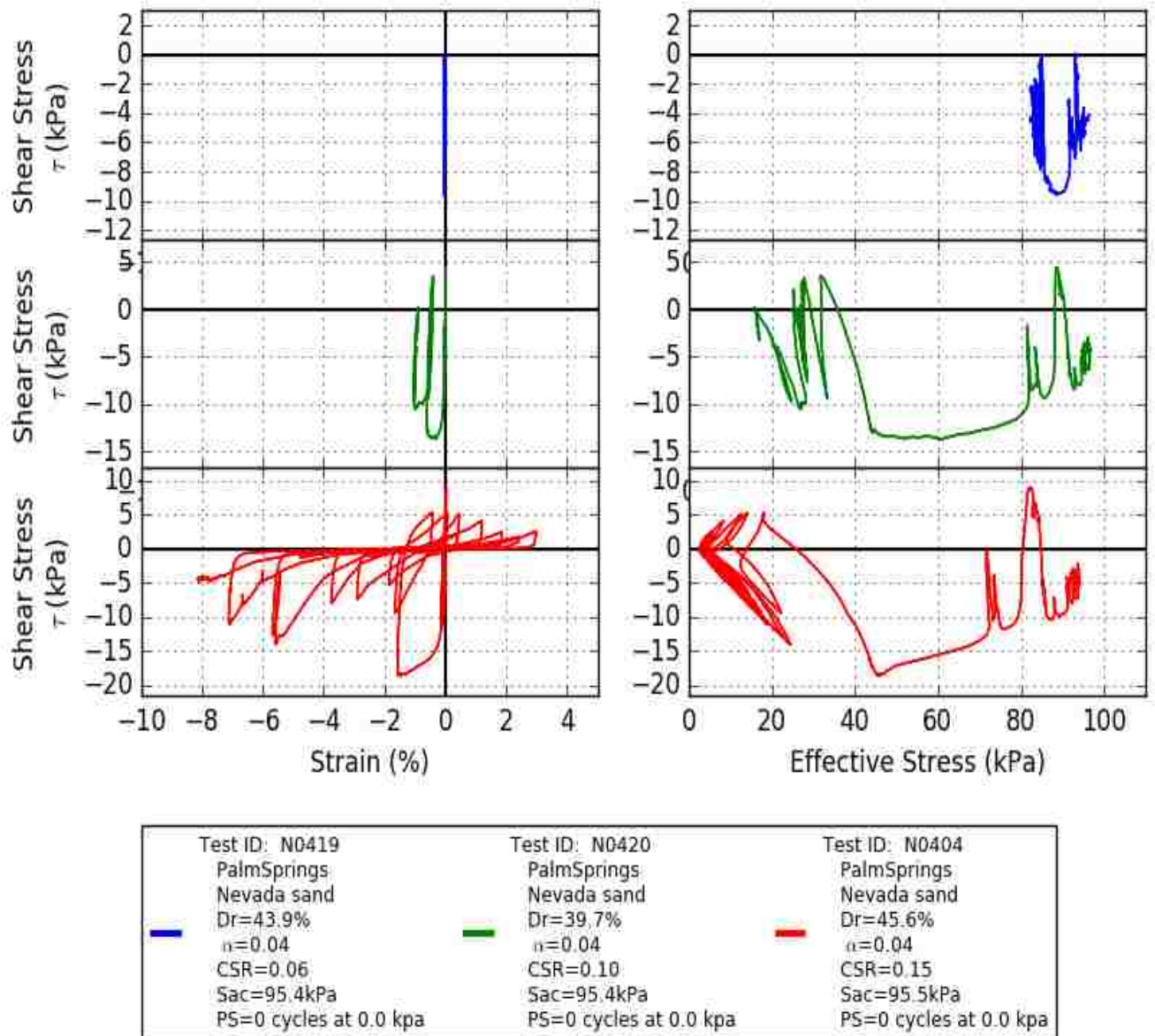
Figure 35: Compare CSR. Stress-strain and stress path. Nevada Sands. Palm Springs Motion. α = 0.05. Run at 0.25 x real-time.
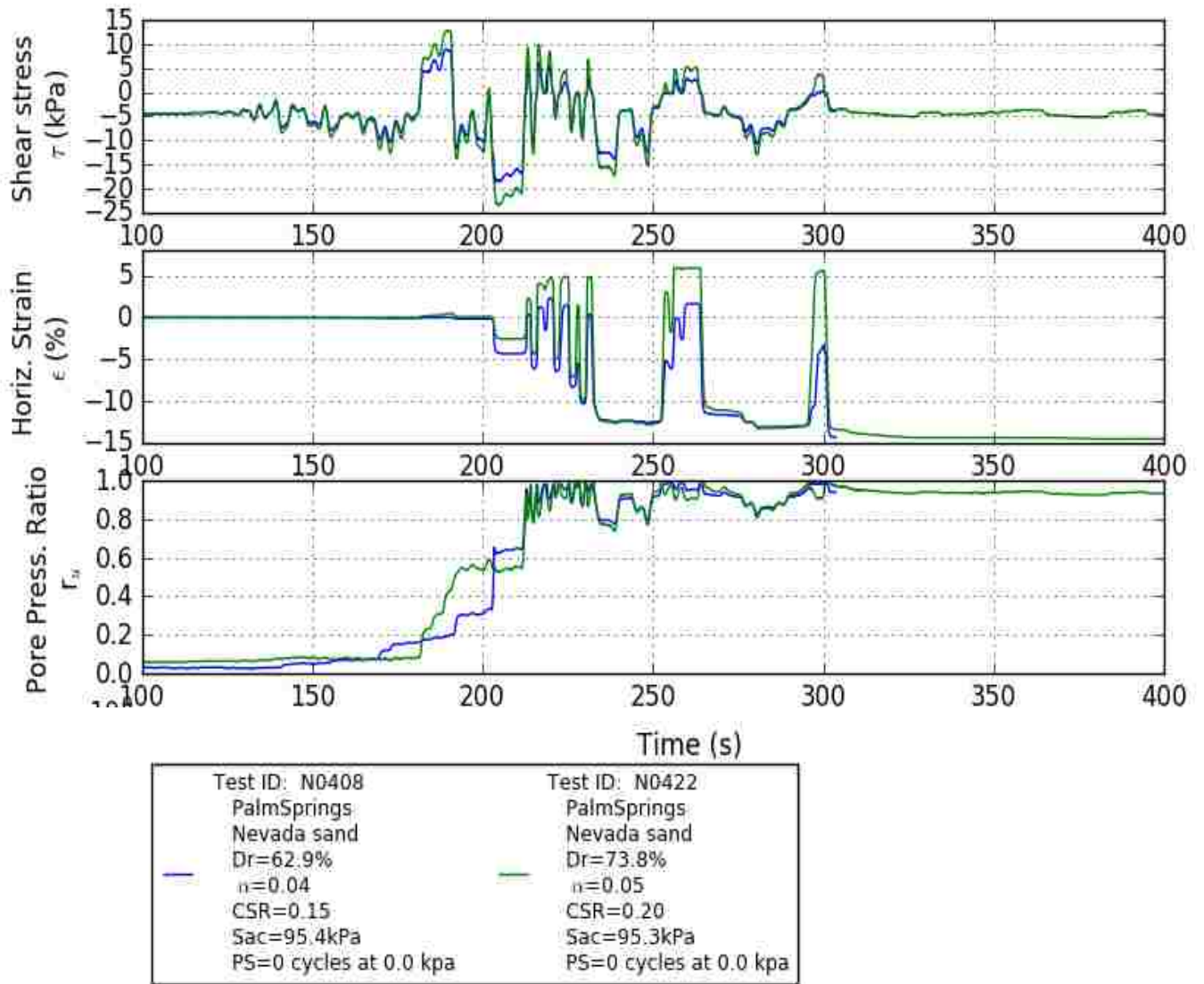
Figure 36: Compare CSR in dense tests. Time history and soil response. Nevada Sands. Palm Springs Motion. α = 0.05. Run at 0.25 x real-time. NOTE: due to testing error, horizontal strain capped at +5.5%
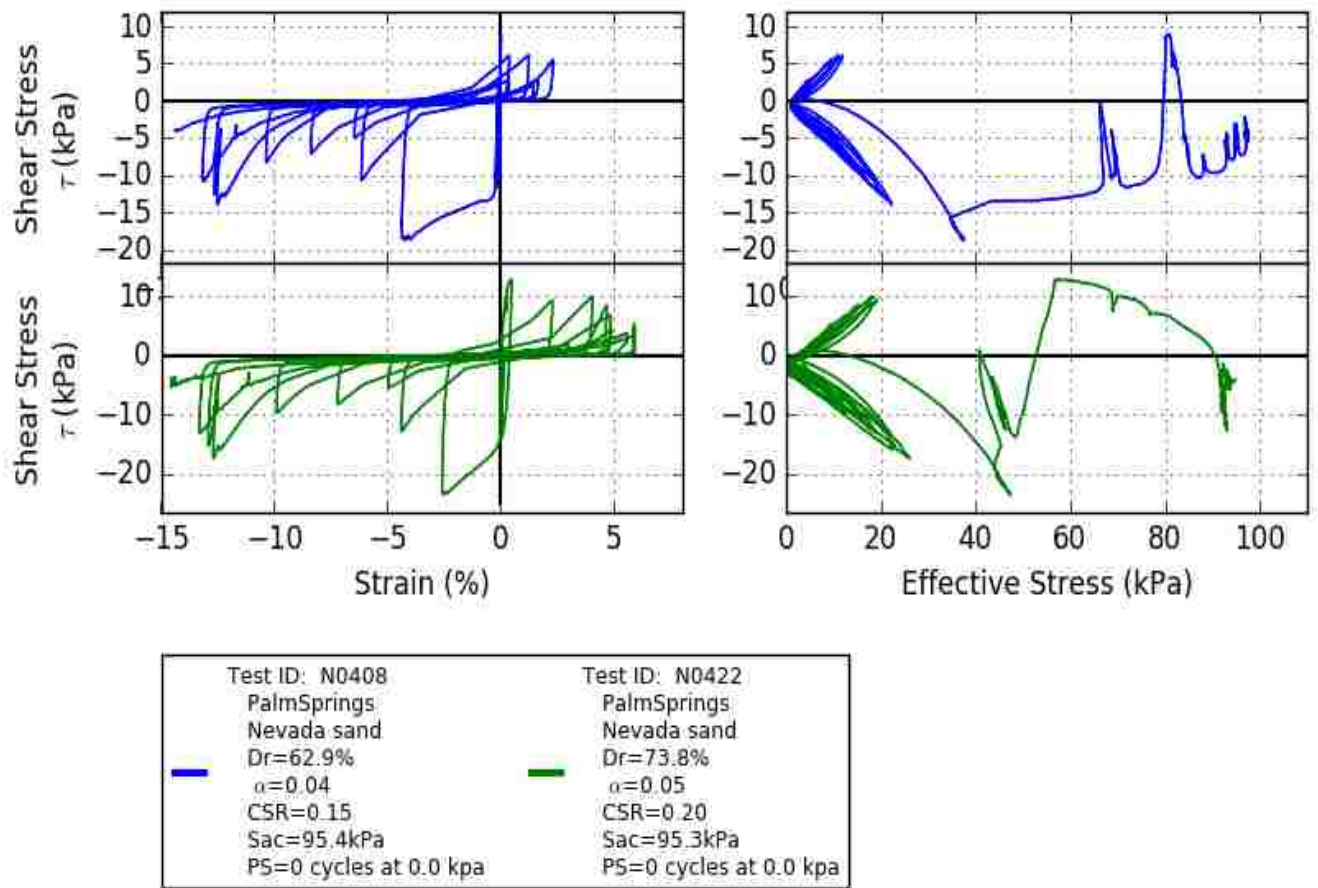
Figure 37: Compare CSR in dense tests. Stress-strain and stress path. Nevada Sands. Palm Springs Motion. α = 0.05. Run at 0.25 x real-time.
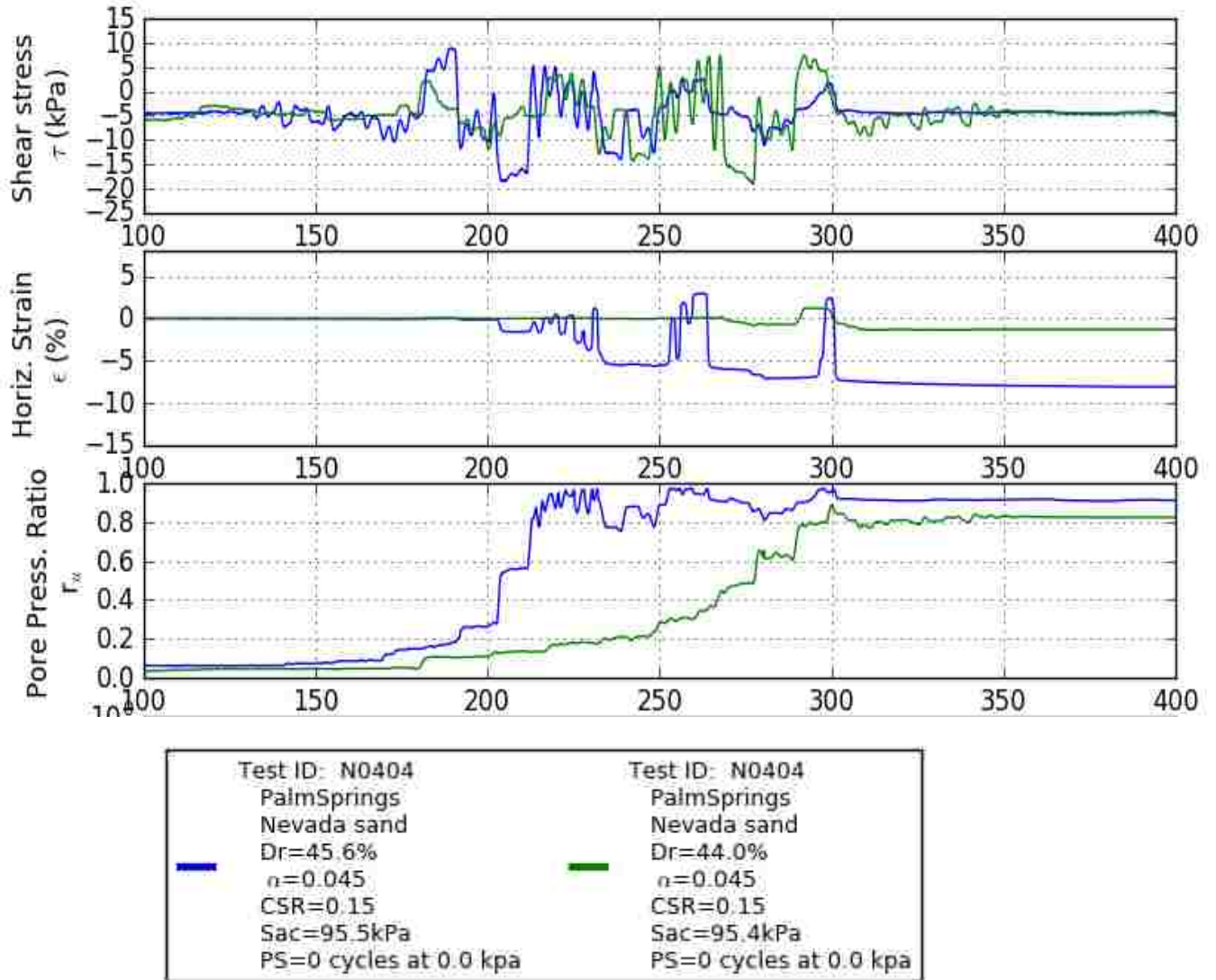
Figure 38: Effects of order of cycles. Time history and soil response. Blue and Green tests included to validate repeatable testing. Palm Springs motion run in forward and reverse with respect to time, same energy content. Nevada Sands. Palm Springs Motion. CSR = 0.15. α = 0.045. Run at 0.25 x real-time.
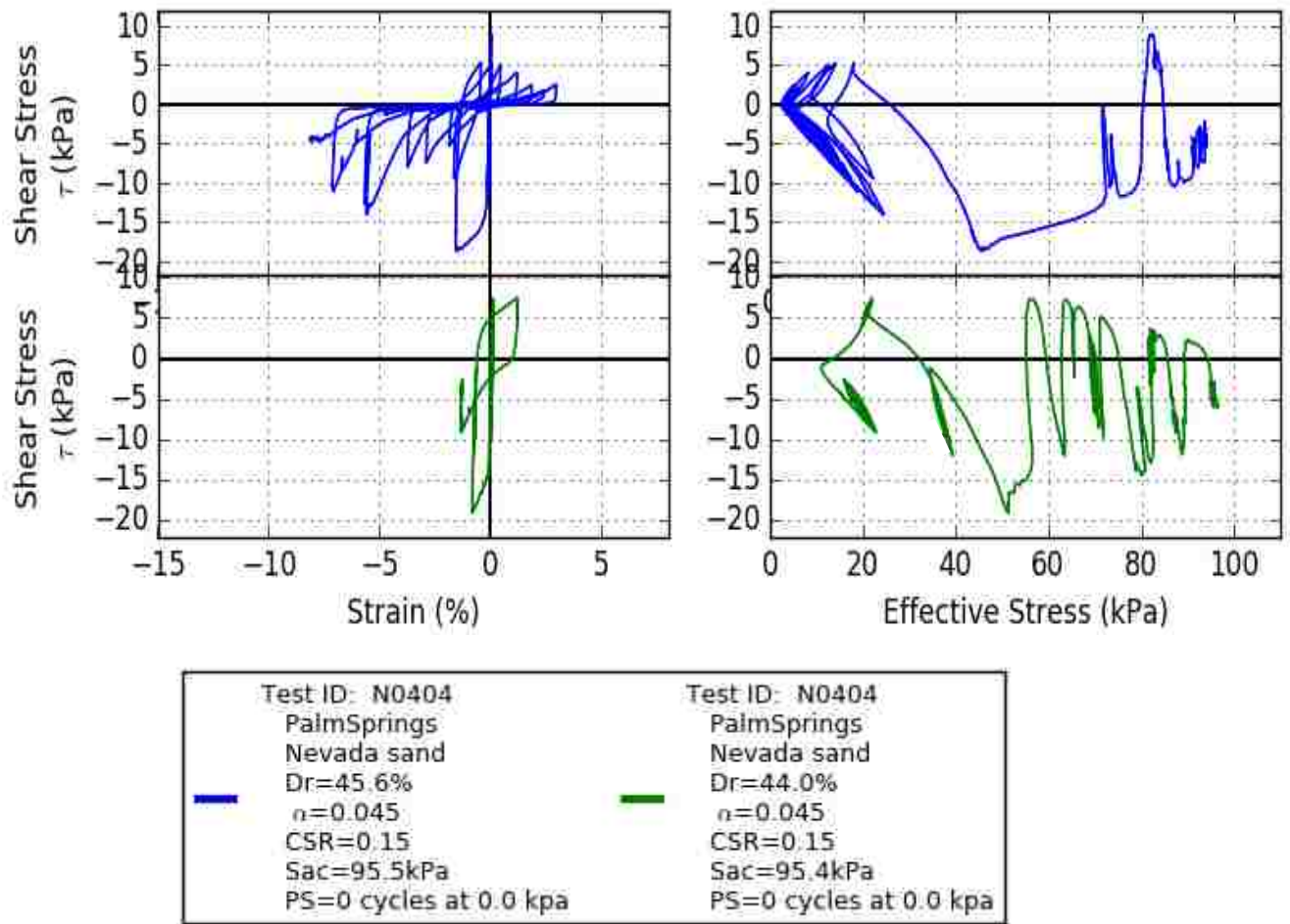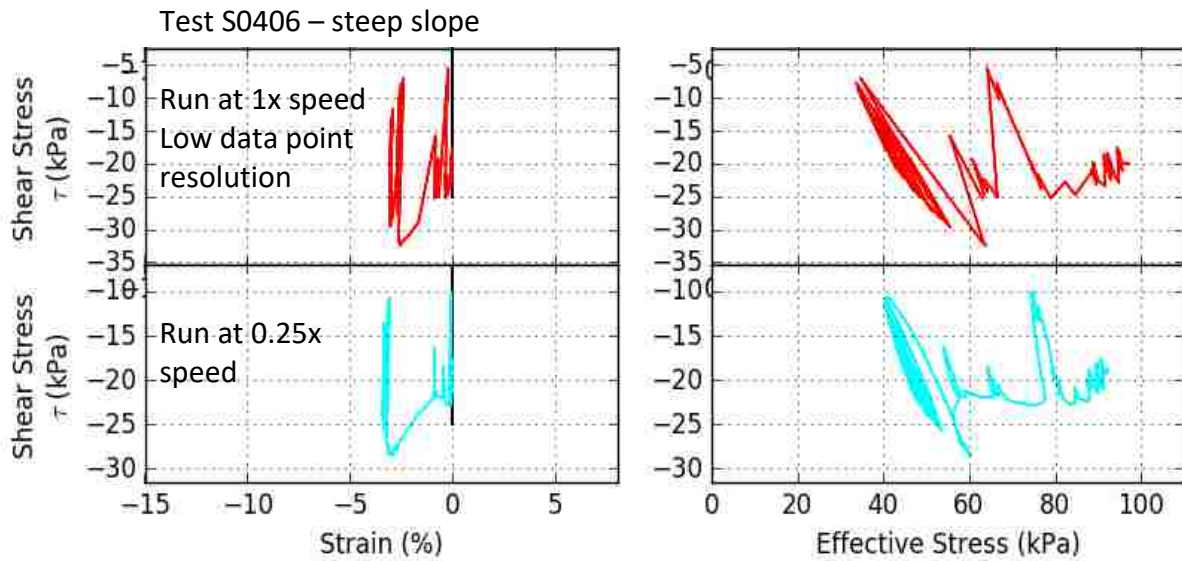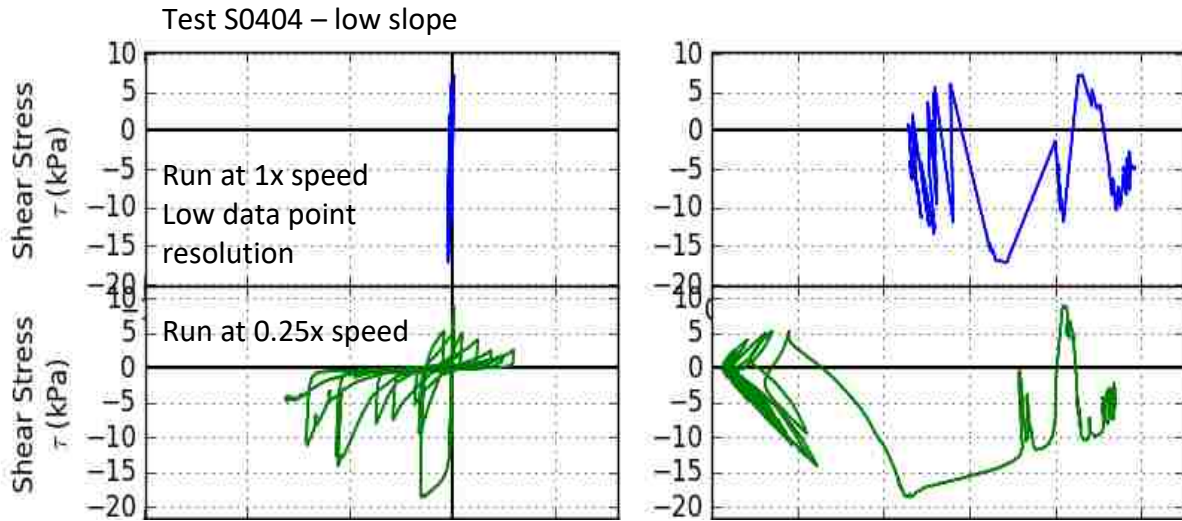
Figure 39: Effects of order of cycles. Stress-strain and stress path. Blue and Green tests included to validate repeatable testing. Palm Springs motion run in forward and reverse, same energy content. Nevada Sands. Palm Springs Motion. CSR = 0.15. α = 0.05. Run at 0.25 x real-time.

Test S0404 – low slope

Run at 1x speed
Low data point
resolution

Run at 0.25x speed

Test S0406 – steep slope

Run at 1x speed
Low data point
resolution

Run at 0.25x
speed

Strain (%)

Effective Stress (kPa)

| | Test ID: N0404 PalmSprings Nevada sand Dr=69.7% α=0.05 CSR=0.13 Sac=95.4kPa PS=0 cycles at 0.0 kpa | | Test ID: N0404 PalmSprings Nevada sand Dr=45.6% α=0.04 CSR=0.15 Sac=95.5kPa PS=0 cycles at 0.0 kpa | | Test ID: N0406 PalmSprings Nevada sand Dr=43.8% α=0.20 CSR=0.13 Sac=95.5kPa PS=0 cycles at 0.0 kpa | | Test ID: N0406 PalmSprings Nevada sand Dr=40.8% α=0.19 CSR=0.10 Sac=95.4kPa PS=0 cycles at 0.0 kpa |

Figure 40: Check rate effects. Nevada Sands. Palm Springs Motion. α = 0.05. Green and light blue tests run at 0.25 x real-time, blue test run at real-time.

4.2   Uncertainty in Testing

In liquefaction studies, testing using transient and dynamic loading is desired but often hindered by equipment capabilities. The reliability of the transient tests on the GDS device are subject to the precision factors defined in Table 12.

	GDS device
Horiz. and vert. displacement logging	0.1% at 10mm strain
load cells	0.1 N
Initial Relative Density	3%

Table 12: Precision factors of testing equipment

The GDS device are subject to uncertainty in the initial measured relative density of the prepared sample. The GDS device logs the direct axial height at placement and axial displacement during consolidation, thus the main uncertainty stems from small jostling while placing the specimen in the machine. Table 13 estimates the uncertainty in each measured value of the simple shear tests.

	GDS device
Measured Axial Displacement	0.01 mm
Measured horiz. displacement	0.1% at 10 mm strain
Measured Axial load	+/- 0.1% max load
Measured horizontal Load	+/- 0.1% max load
Measured initial Relative Density	+/- 3%

Table 13: Estimated uncertainty quantification

CHAPTER 5. TEST INTERPRETATION AND SOIL RESPONSE TO CYCLIC VERSUS EARTHQUAKE LOADING

This chapter synthesizes observations and conclusions drawn from an analysis of the cyclic and transient tests presented in Chapter 4. This chapter is broken down into several topics. Section 5.1 addresses the observed soil strain responses subject to uniform versus irregular loading and proposes explanations for the strain behavior. Section 5.1 also goes into detail regarding individual parametric effects on the pre-liquefaction pore pressure generation. Section 5.2 investigates the current models of the Simplified Method's initial static shear stress factor, K_α, by evaluating K_α for each cyclic test and comparing them to previously proposed models. The differences between cyclic and one-dimensional transient testing are explained in Section 5.3. Finally, a regressive form of K_α fit to the transient DSS tests is proposed and discussed in Section 5.4.

5.1   Soil response to cyclic testing

The presence of an initial static shear stress adds complexity to the stress-strain response. Pore pressure generation is aided by particle reorientation which occurs more readily at low shear stresses when inter-particle friction is at its lowest (Kramer, 1996). Thus, quantification of soil response to static shear stress can be defined by four regimes that depend on the level of cyclic shear stress relative to the level of initial static stress: no initial static shear stress (**α = 0**)**,** shear stress changes signs (**α < CSR**), shear stress goes to zero but does not change sign (**α = CSR**)**,** and

shear stress never changes signs and never reaches zero (**α > CSR**). Figure 41 illustrates typical soil response to increasing levels of initial static shear in a cyclic laboratory test.

No initial static shear stresses (Figure 41a): Typical cyclic soil response involves a high initial rate of contractive behavior and rate of excess pore pressure generation. This is followed by a period of reduced contractiveness and rate of excess pore pressure generation in which the effective stress decreases at a relatively constant rate. During these stages, the shear modulus remains close to its initial value. At the onset of phase transformation or high levels of pore pressure, contractiveness increases and, consequently, the rate of excess pore pressure generation again increases. This behavior is reflected in the development of increasingly large cyclic strains as low levels of effective stress are reached and continues until failure. In tests performed in this analysis, the main contributor to the development of excess pore pressure generation is the soil's volumetric behavior and its tendency for particle reorientation at every stress reversal.

Initial shear stress with stress sign change (Figure 41b): In tests with low initial static shear stress, the initial high and subsequent reduced rate of excess pore pressure generation is often similar to that observed in tests with no initial static shear stress. However, due to higher maximum shear stress levels, the soil (a) reaches the phase transformation point sooner, consequently beginning dilative behaviors earlier and (b) begins dilative behavior in one shear stress direction before the other, leading to asymmetric behavior and cyclic mobility. The tendency for cyclic mobility, combined with preferential peak shear stresses in a particular direction, results in the build-up of permanent shear strain with each cycle of loading. After liquefaction is triggered, the cyclic strains remain similar in amplitude to the test without initial shear stress cases but permanent strain increments are amplified. In these tests, the driving contributor to pore pressure generation can be attributed to the earlier onset of dilative behaviors and the reorientation of particles at low

effective stresses. In loose soils, cyclic tests with initial shear stresses often fail sooner than tests without initial shear stresses. In contrast, in denser soils, tests tend to fail in the same or greater number of cycles than tests without initial shear stresses. This may be because phase transformation is triggered later in denser soils (the angles of the failure line and phase transformation line are steeper), and therefore these effects of dilation are less pronounced then loose tests.

Initial shear stress with no shear stress sign change and zero effective stress reached (Figure 41c): A logical consequence of higher maximum shear stresses is that the rate of excess pore pressure generation is greater. Like the case where $0 < \alpha < CSR$, higher shear stresses lead to earlier onset of phase transformation—effectively decreasing the length of the reduced rate of excess pore pressure generation section—and causing asymmetric strain behavior. Cyclic mobility and permanent strains once again develop, but as the stress never changes signs, cyclic strains only develop in single direction. In this case, we see that the initial rate of excess pore pressure generation and subsequent section of reduced generation rate are both greater than the previous cases where $\alpha < CSR$. The driving factors for rate of excess pore pressure generation are high shear stresses and particle reorientation

Initial static shear stress where effective stresses never reach zero and shear stress never changes signs (Figure 41d): In this case, the initial high levels of shear stress result in a high initial rate of excess pore pressure generation which primarily drives the pore pressure generation throughout the test. The high levels of shear stress also lead to large initial permanent strain which slows as the effective stresses dip near its failure envelope. The effective stress cannot go to zero in this case, so the stiffness cannot go to an extremely low value like that of the other cases. The non-zero level of effective stress means that the rate of excess pore pressure generation

is no longer as driven by particle reorientation and rate of excess pore pressure generation and does not increase at the onset of phase transformation as it does in the other cases. When the failure envelope is reached, the material cycles along a stress path envelope in 'football' shaped curves driven by alternating, but equal, periods of dilation and contraction. In these cases, the driving contributor to pore pressure generation may be the high initial shear stress.
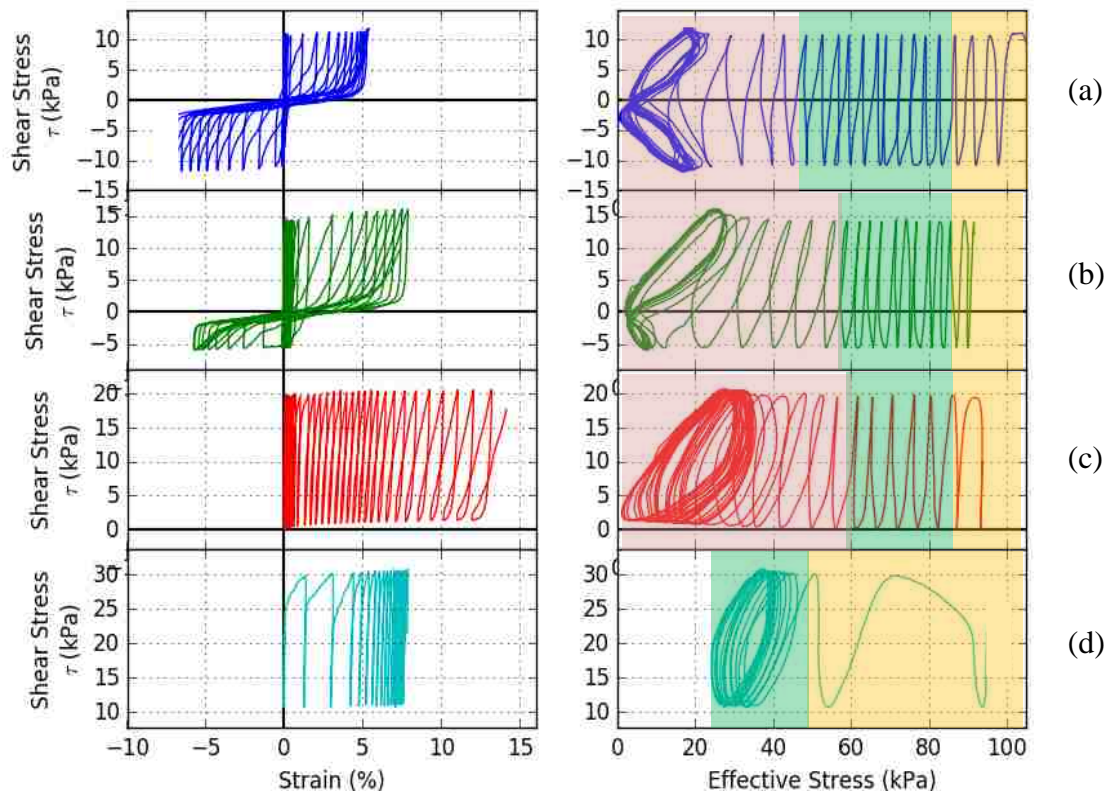

Figure 41: Typical soil response to initial static shear stresses in cyclic laboratory tests. Tests conducted on Siri sand at $\sigma'_{vo} = 100\ kPa$, Dr = 50%, and CSR = 0.1. Yellow shading indicates zone of higher rate of excess pore pressure generation, green shading indicates lower rate of excess pore pressure generation, and red indicates increased rate of excess pore pressure generation. (a) $\alpha = 0$, (b) $\alpha < CSR$, (c) $\alpha = CSR$, and (d) $\alpha > CSR$.

5.1.1 Cyclic strength curves

A cyclic strength curve is a common way of displaying the liquefaction resistance found from a cyclic liquefaction test. A cyclic strength curve shows the level of cyclic shear stress (expressed by the CSR), to the number of cycles to liquefaction, N_L. The CSR required to trigger liquefaction in 15 cycles is commonly referred to as the cyclic resistance ratio, CRR. Cyclic strength curves are often established by applying several levels of CSR to identical specimens. Such tests typically show that a power function can be fitted well to the CSR vs N_L curve. Therefore, the CRR can be written as a function of N_L as:

$$CRR = a * N_L^{-b}$$
<div align="right">Equation 20</div>

where a is a scaling factor and b defines the slope of a straight line on a log(CRR) versus log(N_L) plot. A higher a reflects a higher liquefaction resistance, and a low b value indicates a low sensitivity to the level of cyclic stress. For the case of some sloped tests, the soil will fail in cyclic mobility rather than reach a state of initial liquefaction.

To illustrate some behavioral trends of cyclic testing, Figures 42 to 43 show the results of a sister study conducted on Siri sands from the North Sea sieved to reflect a grain size distribution of the Nevada sands used in the transient tests. The parametric cyclic simple shear tests (Table 14) followed a typical program to define cyclic strength curves of a sand at $\sigma'_{vo} = 100$ kPa. Individual test results are grouped by similar level of initial static shear stress (Figure 42) or by density (Figure 43). The fitted lines are cyclic strength curves (Equation 20) derived from CSS tests without initial static shear stresses on Siri sands at $\sigma'_{vo} = 100$ kPa. The parameters a and b calculated for each level of initial static shear stress are recorded in Table 15.

Table 14: Cyclic simple shear tests on sieved Siri sand. Results plotted in Figures 42-45.

| Test Name	Dr [%]	α	CSR	N_L (where r_u > 0.98 or reaches peak value)	Failure type ($r_{u, peak}$ > 0.98)
S0120	37	0	0.053	142	Liquefaction
S0002	38	0	0.104	12	Liquefaction
S0103	49	0	0.101	18	Liquefaction
S0105	40	0	0.154	1.9	Liquefaction
S0106	53	0	0.154	3.5	Liquefaction
S0107	69	0	0.150	5	Liquefaction
S0108	33	0	0.215	1.7	Liquefaction
S0110	85	0	0.202	6	Liquefaction
S0301	40	0.05	0.098	14	Liquefaction
S0302	48	0.10	0.101	11	Liquefaction
S0303	35	0.22	0.102	10	Strain limit reached
S0305	34	0.11	0.162	2	Liquefaction
S0306	32	0.21	0.160	1.5	Strain limit reached
S0307	34	0.05	0.202	2	Liquefaction
S0308	34	0.10	0.203	2	Liquefaction
S0309	39	0.21	0.209	2	Strain limit reached
S0310	53	0.05	0.105	19	Liquefaction
S0311	52	0.10	0.102	24	Liquefaction
S0312	45	0.21	0.105	14	Strain limit reached
S0313	61	0.05	0.152	53	Liquefaction
S0314	52	0.10	0.156	4.5	Liquefaction
S0315	46	0.21	0.154	3	Strain limit reached
S0316	50	0.05	0.202	2	Liquefaction
S0317	54	0.11	0.207	2	Liquefaction
S0319	70	0.05	0.107	18	Liquefaction
S0321	63	0.21	0.104	30	Strain limit reached
S0322	66	0.05	0.151	7	Liquefaction
S0323	66	0.10	0.149	17	Liquefaction
S0324	72	0.18	0.133	8	Strain limit reached
S0325	67	0.05	0.223	2	Liquefaction
S0327	55	0.21	0.204	1.7	Strain limit reached
S0341	100	0.20	0.099	35	Strain limit reached
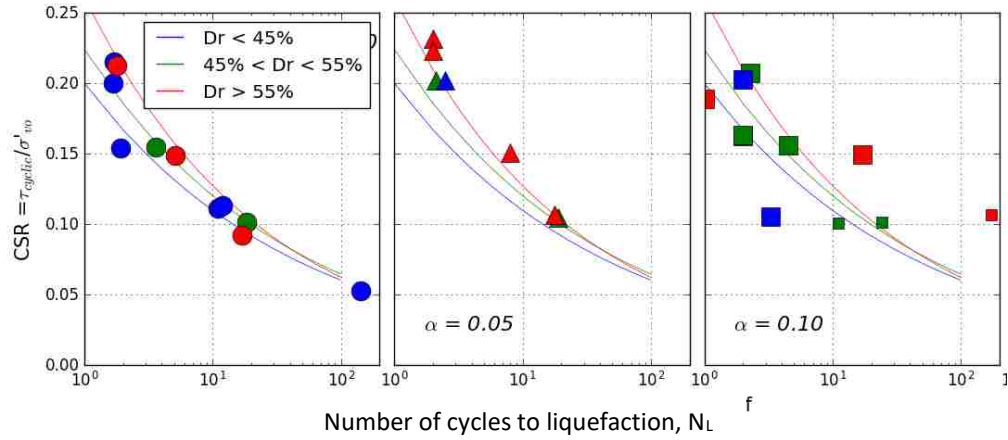
Figure 42: CSR vs. N_L values for tests from cyclic program of Siri sands. $\sigma'_{vo} = 100$ kPa. Cyclic strength curves for tests without initial static shear stresses included for reference. Tests compared by initial static shear stress levels.
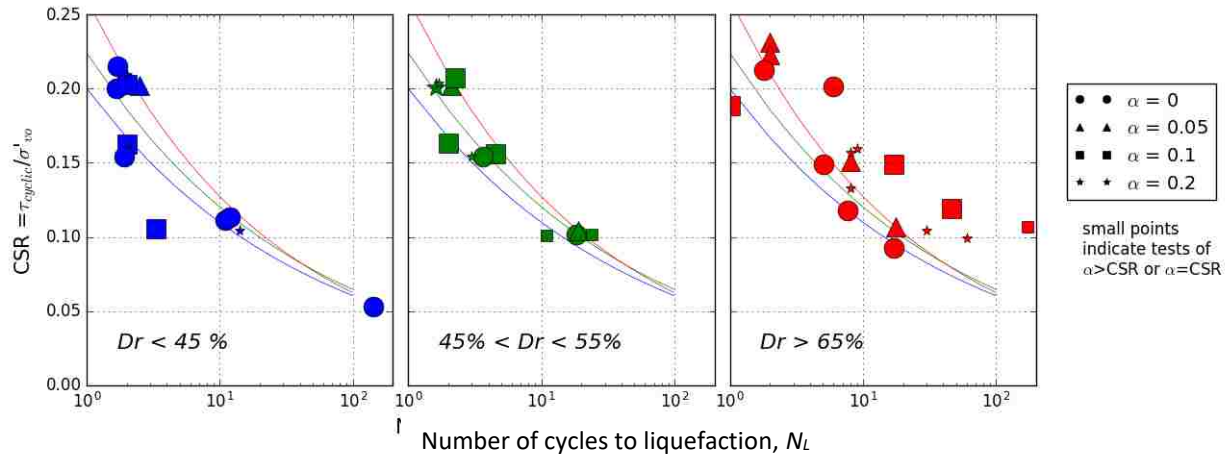

Figure 43: CSR vs. N_L values for tests from cyclic program of Siri sands. $\sigma'_{vo} = 100$ kPa. Cyclic strength curves for level conditions included for reference. Tests compared by relative density levels.

Dr	σ'_{vo}	a	b
45%	100 kPa	0.200	0.260
55%	100 kPa	0.224	0.270
>55%	100 kPa	0.306	0.330

Table 15: Parameters for cyclic strength curves of sieved Siri sands in tests with no initial static shear stress

Tests with initial static shears stresses are shown to have similar or higher liquefaction resistance than tests without initial shear stresses. This behavior is consistent with most existing forms of K_α. However, the range in the results of Figures 42 and 43 reveals that relative density, although commonly used in engineering practice, may not be a sufficient index to adequately

determine liquefaction behavior. Volumetric behaviors have been shown to have stronger correlations to liquefaction resistance than density or vertical effective stresses individually. Therefore, Figures 44 and 45 present the same tests as Figures 42 and 43, but grouped by similar levels of initial dilative behavior expressed by the dilatancy index, I_r (Equation 2a). The fitted cyclic strength curves are representative of the tests without initial static shear stress. These curves can be defined by the *a* and *b* parameters defined in Table 15. Figure 44 is grouped by level of initial static shear stress while Figure 45 is grouped by level of I_r.
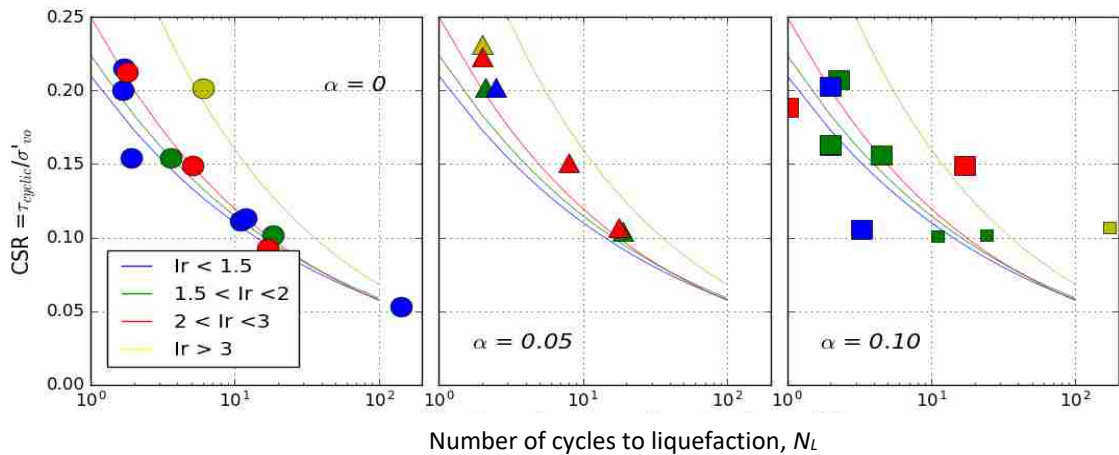

Figure 44: CSR vs. N_L values for tests from cyclic program of Siri sands. Cyclic strength curves for level conditions by dilatancy index I_r are imposed. Shown by increasing level of initial static shear. Higher levels of I_r indicate greater dilative behavior.
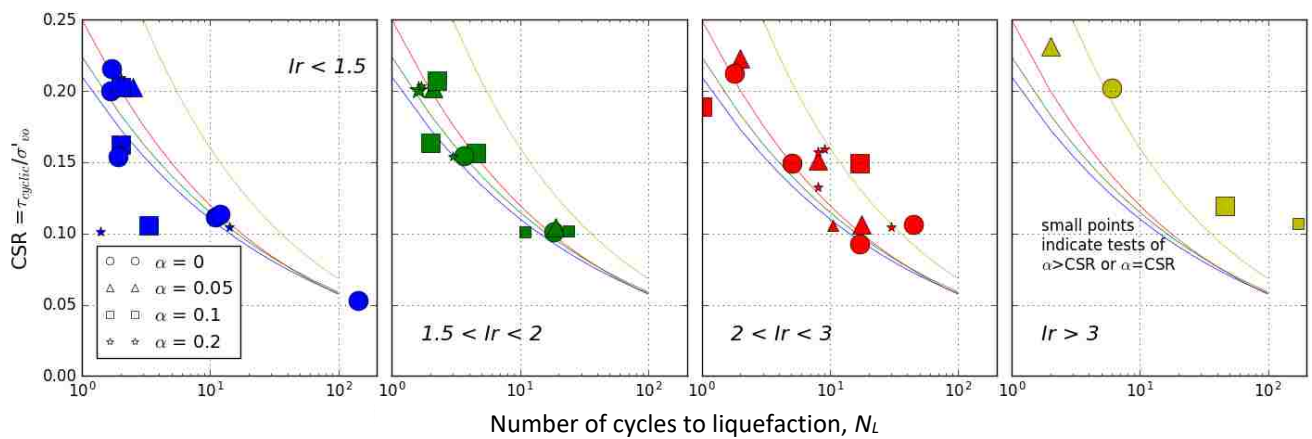

Figure 45: CSR vs. N_L values for tests from cyclic program of Siri sands. Cyclic strength curves for level conditions by dilatancy index I_r. Shown by increasing level of I_r.

As expected, tests shown in Figure 46 with high dilative tendencies (i.e., high I_r) correspond to the greatest liquefaction resistance with increasing initial static shear stress, while high contractive tendencies (i.e., low I_r) correspond to similar or even decreased liquefaction resistance.

Table 16 summarizes the results of the CSS study conducted on Siri sands compared to CSS studies on similar, uniform, clean sands from past liquefaction studies. Figure 44 displays the cyclic strength curves defined by the a and b parameters shown in Table 16. Soil state has been determined to have a direct effect on soil strength, thus many tested soils are tested in differing levels of density.

Figure 44 indicates that Siri sands are more susceptible to liquefaction than Nevada sands and those of other sand studies. This is to be expected as the Siri sands were sieved of fines to increase uniformity and thus decrease liquefaction resistance, a procedure to create a readily-liquefiable sand composition for this study on liquefaction mechanics. The lower resistance but similar GSD of sieved Siri sands would manifest itself in a cyclic strength curve as having a similar shape (*b* value) as Nevada sands, but a lower amplitude (*a* value) than sands in their natural conditions such as Nevada and Monterey 0/30, as seen in Table 16 and Figure 44.

Table 16: Parameters for cyclic strength curves of sands in level conditions corresponding to Equation 20.

| REFERENCE TO FIGURE 44	STUDY	SAND	Dr	σ'_{vo}	a	b
A	This report	Siri Sand sieved	32-38%	100 kPa	0.200	0.260
B			48-53%	100 kPa	0.224	0.270
C			62-68%	100 kPa	0.306	0.330
D	Kwan 2015	Nevada Sand	60%	100 kPa	0.254	0.181
E			80%	100 kPa	0.658	0.298
	Idriss 1999	'clean, sand-like soils'	NA	NA	Variable	0.337
F	Wu 2002	Monterey 0/30	45%	80 kPa	0.27	0.14
G			60%	80 kPa	0.38	0.18
H			80%	80 kPa	0.84	0.27
I	DeAlba 1976	Monterey 0/30	54%	80 kPa	0.3	0.18
J			68%	80 kPa	0.38	0.19
K			82%	80 kPa	0.43	0.12
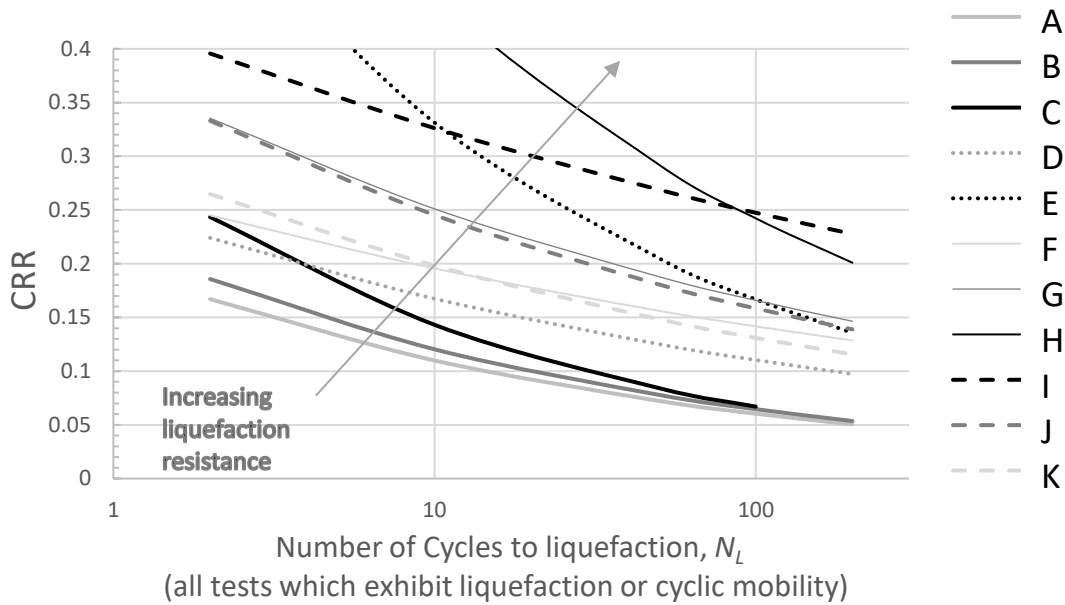
Figure 46: Comparison of Siri cyclic strength curves to other cyclic testing programs. All tests with no initial static shear stress

5.2 Soil stress-strain models

Typical stress and strain response of cyclic and transient tests before liquefaction have been well-modelled by the hysteresis behavior defined by the modified Masing (1926) stress-strain models. This model was built off the Ramberg-Osgood model characterized by a backbone loading curve and an assumed non-linear cyclic degradation of the material. The virgin backbone curve takes on the form:

$$F_{bb}(\gamma) = \frac{G_{max}\gamma}{1+|\gamma|*\left(\frac{G_{max}}{\tau_{max}}\right)}$$

Equation 21

The Masing model adds additional stipulations for the shape of unloading and reloading curves. This model states that at each stress reversal the origin of the backbone curve can be transposed to the stress-strain point and subsequent unloading would follow an unloading curve, while reloading would follow the shape of the reloading curve. Assuming γ is the shear strain state and τ is the

shear stress state, if a stress reversal happens at point (γ_r, τ_r) then the stress-strain behavior would be expected to follow the unloading curve defined by:

$$\frac{\tau - \tau_r}{2} = F_{bb}\left(\frac{\gamma - \gamma_r}{2}\right)$$ Equation 22

where $F_{bb}(\gamma)$ is the backbone shape function in a stress-strain space, G_{max} is the initial shear modulus, and τ_{max} is the limiting shear stress that the soil can resist. In other words, the unload-reload curves are the same shape as the backbone curve but the origin is transposed to the new reversal point and the curve is expanded by a factor of two in both stress and strain. Figure 47 illustrates the generalized shape of a Ramberg-Osgood backbone curve and Masing unloading and reloading curves.
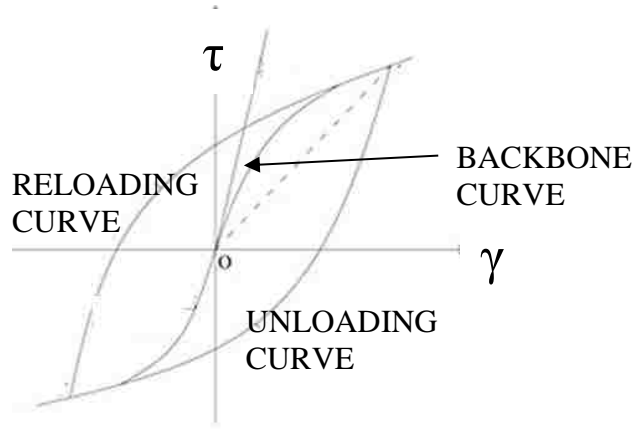

Figure 47: Typical stress-strain response in cyclic testing. Backbone curve in hysteric loading for a backbone curve defined in the Ramberg-Osgood model and unloading and reloading curves from the Masing model.

The extended Masing model can be used to address the additional complications of irregular cyclic loading. The Masing model and subsequent Finn (1977) corrections follow the framework of the Masing model, with several rules imposed:

a. If the curve is at a state larger than the maximum past strain and intersects the backbone curve, the behavior will follow the backbone curve until the next stress reversal.

b. If the curve should cross the path of a previous cycle, the stress-strain curve will follow that of the previous cycle.

The predictive forms of the instantaneous shear modulus G_{tan} of the unloading and reloading curves are defined in Equations 23 and 24 respectively. However, it is not appropriate to assume that G_{max} is constant over the course of the full test. This would imply the soil body is a perfectly elastic system which would follow unloading-reloading curves ad-infinitum under cyclic loading with no increase in cyclic shear deformations. Soils, however, are not purely elastic and thus the shear modulus degrades over the course of the test. As G degrades, the backbone curve the slope of the stress-strain curves decreases.

$$G_{tan,unloading} = \frac{G_{max}}{\left(1+|\gamma|*\left(\frac{G_{max}}{\tau_{max}}\right)\right)^2} \qquad \text{Equation 23}$$

$$G_{tan,reloading} = \frac{G_{max}}{\left(1+|\gamma-\gamma_r|*\left(\frac{G_{max}}{2*\tau_{max}}\right)\right)^2} \qquad \text{Equation 24}$$

The backbone form of the Masing model holds until phase transformation behaviors begin and a soil begins to experience periods of dilation. At this point, the reloading curves would begin to curve backward and up, creating the typical 'banana' shaped hysteresis which are characteristic of the early onset liquefaction in cyclic simple shear testing.

5.3   Soil response to transient and dynamic loading

Past studies on the form of K_α have been primarily conducted using constant amplitude cyclic testing. Earthquake loading involves additional influencing factors for soil liquefaction response

including dynamic rate effects, three-dimensional shearing, motion intensity and characteristics, history of past events or loading, etc. This section discusses the effects of these secondary factors and observations made in the transient CSS investigation of slopes.

The current standards of engineering laboratory approach for determining liquefaction potential are based on empirical correlations and often do not account for the secondary characteristics of an earthquake. Earthquake load histories are normally non-symmetrical and irregular, and therefore are often transformed in engineering analyses into simplified, more regular forms which can be characterized by cyclic laboratory tests. For instance, many earthquake soil models modify procedures of stress-controlled P-M material fatigue methods and use an equivalent number of uniform cycles, $N_{eq,}$ and *weighting factor curves* (Seed et al., 1975; Arango, 1996) to simplify soil response predictions.

Weighting factor curves can be thought of as normalized cyclic strength curves which compare the CSR normalized by the CSR required to liquefy the sand in one cycle (CSR$_1$) to the N_L normalized by a reference number of cycles, N_{ref}. Figure 48 displays the weighting factor curve used by Seed et al., (1975). Seed took N_{ref} to be 15 cycles. There are inherent assumptions in this model: (a) the FS against liquefaction is one when the N_L is one and (b) that the ratio of a motion's acceleration to PGA is equivalent to the ratio of shear stress to the maximum shear stress (e.g., $\frac{\alpha}{\alpha_{max}} = \frac{\tau}{\tau_{max}}$). However, Green and Terri (2005) showed that neither assumption has any effect on the calculation of N_{eq}. Thus, similar methods (discussed in detail in the following section) are used in the creation of weighting factor curves for equivalent number of uniform cycles in earthquakes.
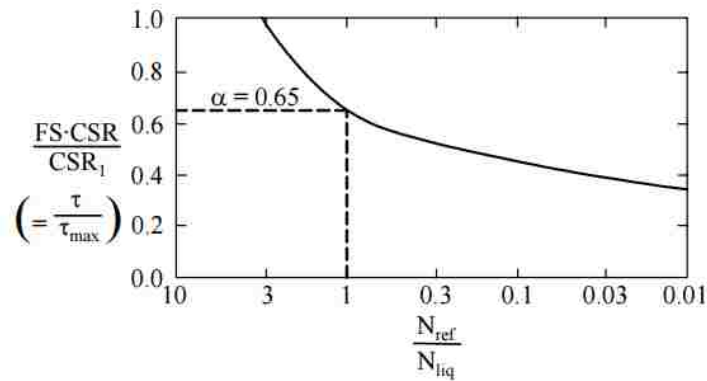
Figure 48: Weighting factor curve for calculation of N_{ref} by Seed et al. (1975). Figure after Green & Terri (2005).

Several methods have been proposed to account for the irregularity of peaks in an earthquake motion. Seed et al. (1975) suggested that a motion's equivalent uniform harmonic test can be conducted at a shear stress amplitude of 65% of the peak shear. In his calculation of N_{eq}, Seed disregarded shear stress peaks with amplitudes below 35% of FS(CSR)/CSR₁ as he considered these small amplitude shear stress pulses to have negligible effects on excess pores pressure. While theoretically sound, the empirical methods proposed by Seed et al. (1975) takes a generalized approach over the entire ground motion which may not be useful in the detailed analysis of a single cycles.

The effects of two-dimensional earthquake loading have been studied to a lesser extent than one-dimensional effects. Seed et al. (1975) simplified the effects of two-dimenisonal loading by assuming that the CSR in the field was roughly 90% of that calculcated in a one-dimensioanl simple shear (e.g., $CSR_{field} = 0.9 * CSR_{lab}$). Studies in two-dimensional loading show that pore pressure and shear strain response in one direction are influenced to various degrees by initial static shear stresses in an orthogonal direction (Krammerer et al., 2004; Boulanger & Seed, 1995;

Ishihara & Yasmazaki, 1980). This may account for some discrepancy between the results of this one-dimensional laboratory study and true in-situ seismic response.

Pore pressure response in transient loading

Liquefaction models assess an earthquake's intensity by as many methods: energy quantification, cycle tracking, peak counting, or assignment of equivalent uniform cycles. However, the precise point of liquefaction triggering is difficult to predict, thus the tests in this report provide good data for the assessment of liquefaction models. The parametric studies in Chapter 4.2 capture some distinct pore pressure trends which are important for any pore pressure generation liquefaction model to address.

A test on medium-dense Nevada sands in level conditions is shown in Figure 49. The excess pore pressure tends to build slowly—even remain relatively constant—in periods of low or constant shear (i.e., Range O-A and B-C). Logically, there exists more rapid pore pressure generation following high levels of shear stress (i.e., Range A-B and D-E). Rapid shear stress transitions between low to higher magnitude of shear can cause incremental 'jumps' in excess pore pressure. This effect is seen in Figure 49 as the absolute amplitude of the shear stress jumps at Points A, C, and D resulting in incremental jumps in r_u. The magnitudes of these increments are largely dependent on loading history. A 'pulse' of shear stress which occurs in the beginning of a motion (i.e., Point A) will likely cause immediate, significant generation of excess pore pressure, whereas an equal shear stress pulse is likely to affect the pore pressure to a lesser degree if it occurs at a higher pore pressure state like those later in the motion (Point D). Pulses after the initiation of liquefaction will not increase the effective stresses greatly as they are already at near-zero levels, but degradation of the fabric of the sand produces additional softening that leads to increased

strains. Dilation after liquefaction, however causes periodic instances of pore pressure drops with accompanying stiffness increases. Several asymmetric cyclic test studies investigate the effects of the order of shear stress pulses on pore pressure generation further also exhibit these behaviors (Kwan, 2015; Krammerer, 2002).
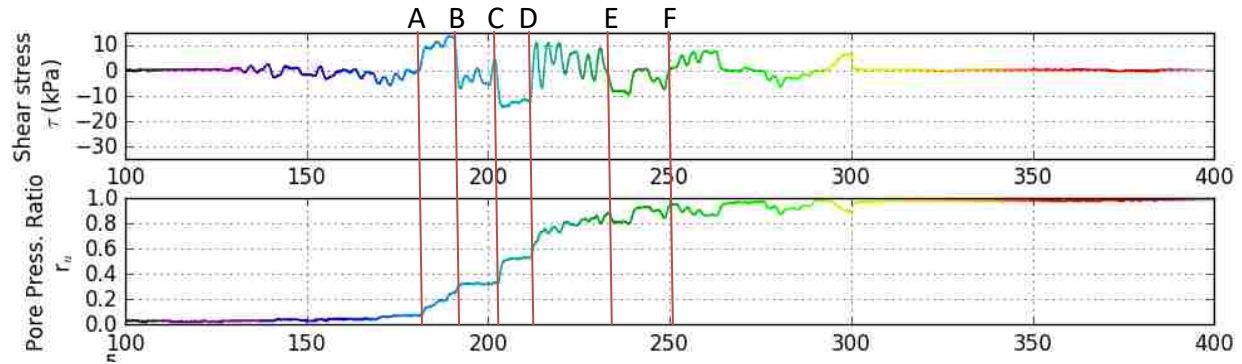

Figure 49: Typical pore pressure response in a test without initial shear stresses. Test N0407, Palm Spring motion on Nevada sand, Dr = 65%, CSR = 0.15, α = 0, σ_{vo} =100 kPa.

Similar behavior is observed in relatively flat slopes. Figure 50 shows tests conducted at increasing levels of initial static shear stress. Both the zero and low initial static shear stress tests liquefied at the same point (around shear stress jump at Point D). In large initial static shear stress conditions, however, the soil has already been subject to higher levels of past shear stress, thus the stress caused from a motion can serve to either (a) increase the shear stress to greater degree than would be seen in level conditions and cause increased rate of excess pore pressure generation, or (b) decrease the amplitude of the shear stress and cause reduced rate of excess pore pressure generation. An example of case (a) can be evidenced by the negative shear stress pulse at Point D causing the greatest rate of excess pore pressure generation in the test with the highest α. Case (b) is evidenced by the decreasing slopes of r_u with increasing level of α in range A to B. In addition, the history of shear stress in steeply sloping conditions may cause a reduction in the amplitude of

jumps at each shear stress pulse (i.e., Points A and D), resulting in smaller final excess pore pressures in steeper sloped tests than a test without initial shear stresses.
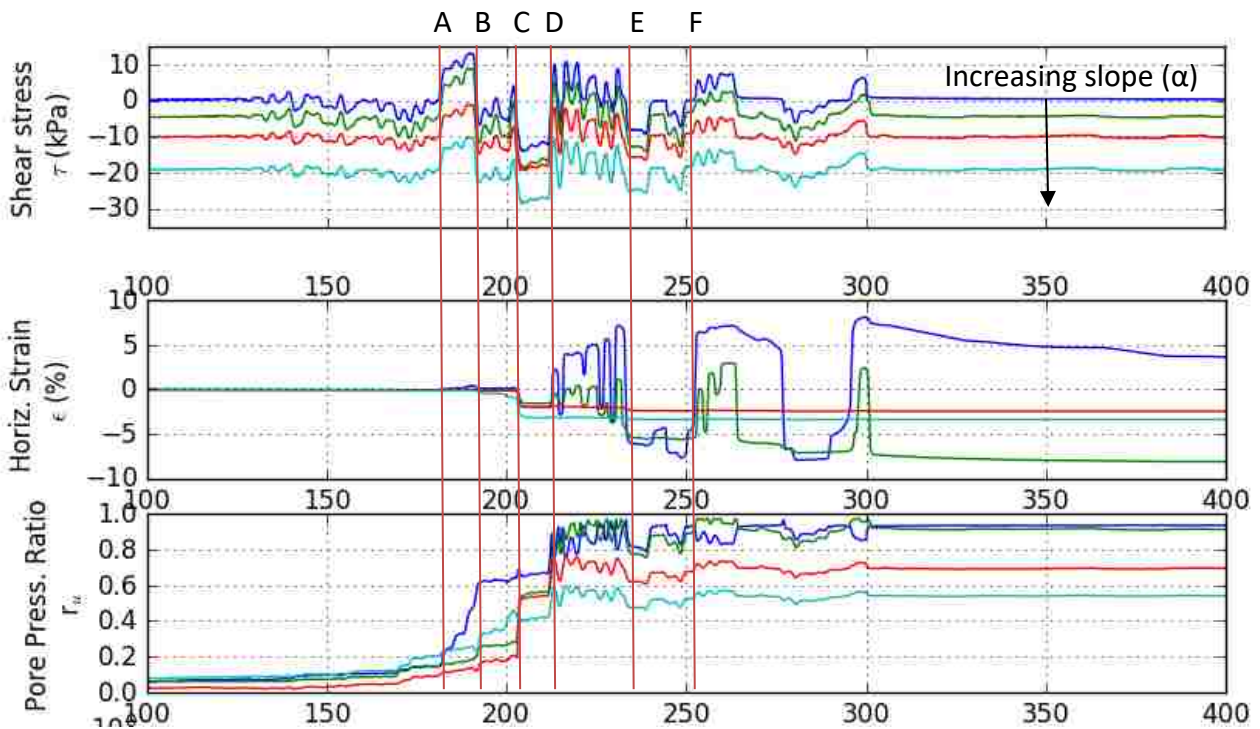

Figure 50: Pore pressure generation and strain response from similar tests in loose conditions and increasing levels of slope. Figure taken as a clip of Figure 25, shown here for ease of reference. Dark blue test represents level conditions, green is tested at α<CSR, red at α=CSR, and light blue at α>CSR.

Figure 50 shows tests conducted with the shear stress loading from the motion parallel to the direction of the initial static shear stress. In cases of two-directional loading, it is possible to have the shear stress act in an orthogonal direction to the initial static shear. This would entail that the effects of shear stress levels and pulses on excess pore pressure generation as discussed previously would be expected to be greatly reduced. The behavior of in-situ soils subject to an earthquake would be expected to be somewhere in between these two cases. Thus, the pore pressure generation in the 1-D tests of this report could be thought of as extreme-case scenarios.
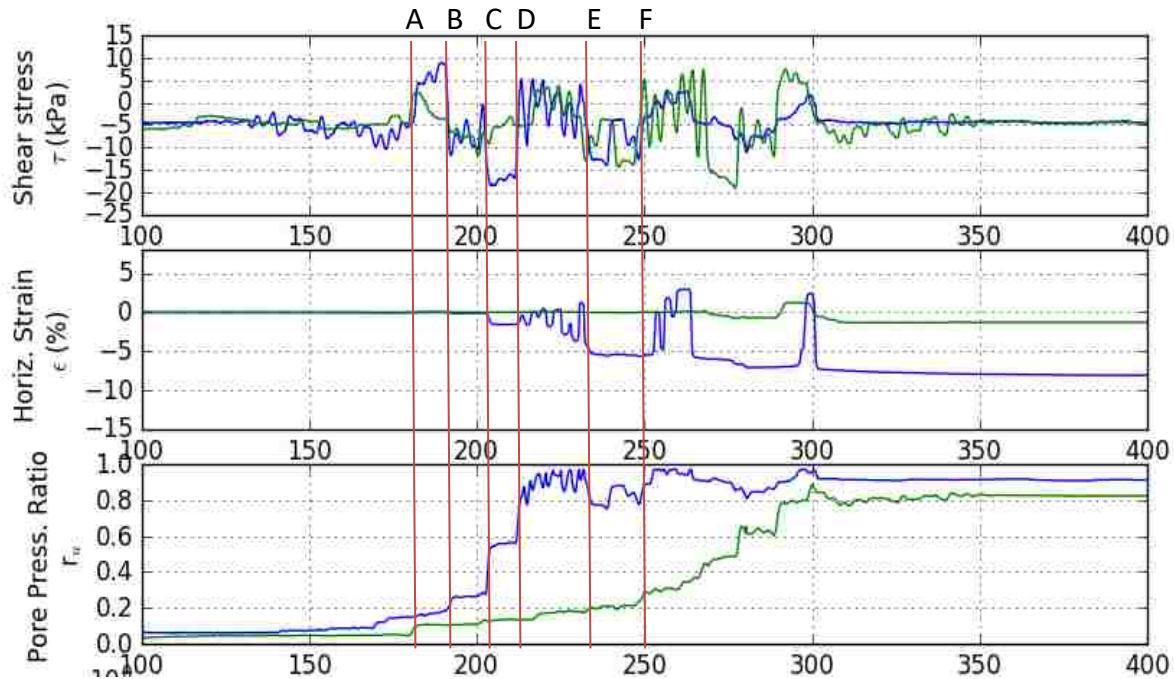
Figure 51: Forward (blue) versus reverse (green) Palm Springs motion with respect to time. Figure taken as a clip of Figure 39, shown here for ease of reference. Tests on loose soils (Dr<45%) and low sloping conditions (α = 0.45).

Order of loading presents another complexity of transient loading. Large amplitude pulses at the beginning of a motion are likely to cause liquefaction to happen sooner. An example is shown in Figures 51 in which the same motion is tested in reverse with respect to time. This figure is taken from a clip of Tests N0404 in Figure 39. The motions have the same intensity measures and maximum shear stress, and peak-counting models or those which rely on full-motion intensity measures such as magnitude of PGA might predict a symmetrical pore pressure response and equal final r_u values for both tests. However, it is apparent that the forward motion generates excess pore pressure at a greater rate than the reverse motion as the largest shear stress pulses (Points A and C) occur first. The reverse motion does not reach liquefaction at all. At very high pore pressure levels (blue test, Points D-F), subsequent shear loading can cause periodic dilation and contraction

that correspond to pore pressure drops and jumps which roughly mirror the shape of the load. Thus, liquefaction triggering predictions should not be based on full-motion intensity indexes but rather with cumulative measures over time.

Shear strain response in transient loading

Figure 52 is a zoomed in illustration of the stress-strain response of a test without initial shear stress under irregular earthquake loading. The scale of Figure 52 is such that the small-strain soil response before initiation of liquefaction can be observerd. Deformations which occur before the initiation of liquefaction are minor compared to deformation after initiation. The following are observations which support the predictions made by exisitng stress-strain models with an example of each labelled in Figure 52:

A. Initial large pulses can be seen to follow the shape of the initial backbone curve.

B. Subsequent unloading moves along an unloading and reloading curve.

C. If a reloading curve crosses a past cycle's curve, it follows the backbone curve of the last cycle until the next stress reversal.

D. Shear modulus nonlinearity apparent by decreased slope of unloading/reloading curves as test progresses.

In addtion to the pore pressure response, Figure 50 illustrates the strain response properties of a transient test as it evolves with time. Similar to the results of cyclic studies, transient tests such as this show that there are dramatic development of shear strains at very high levels of excess pore pressure, i.e., after Point D in tests of zero and low initial static shear stress. The greatest deformations occur as the effective stresses go to zero, i.e., when the shear stress switches signs (ex. Points D, E, and F for flat and low sloping tests). Therefore, tests with higher initial static shear stresses exhibit growing permanent strains in a single direction (red and light blue tests). The

instantneous pulses in strain at or after failure were not as great as they would be in zero or low

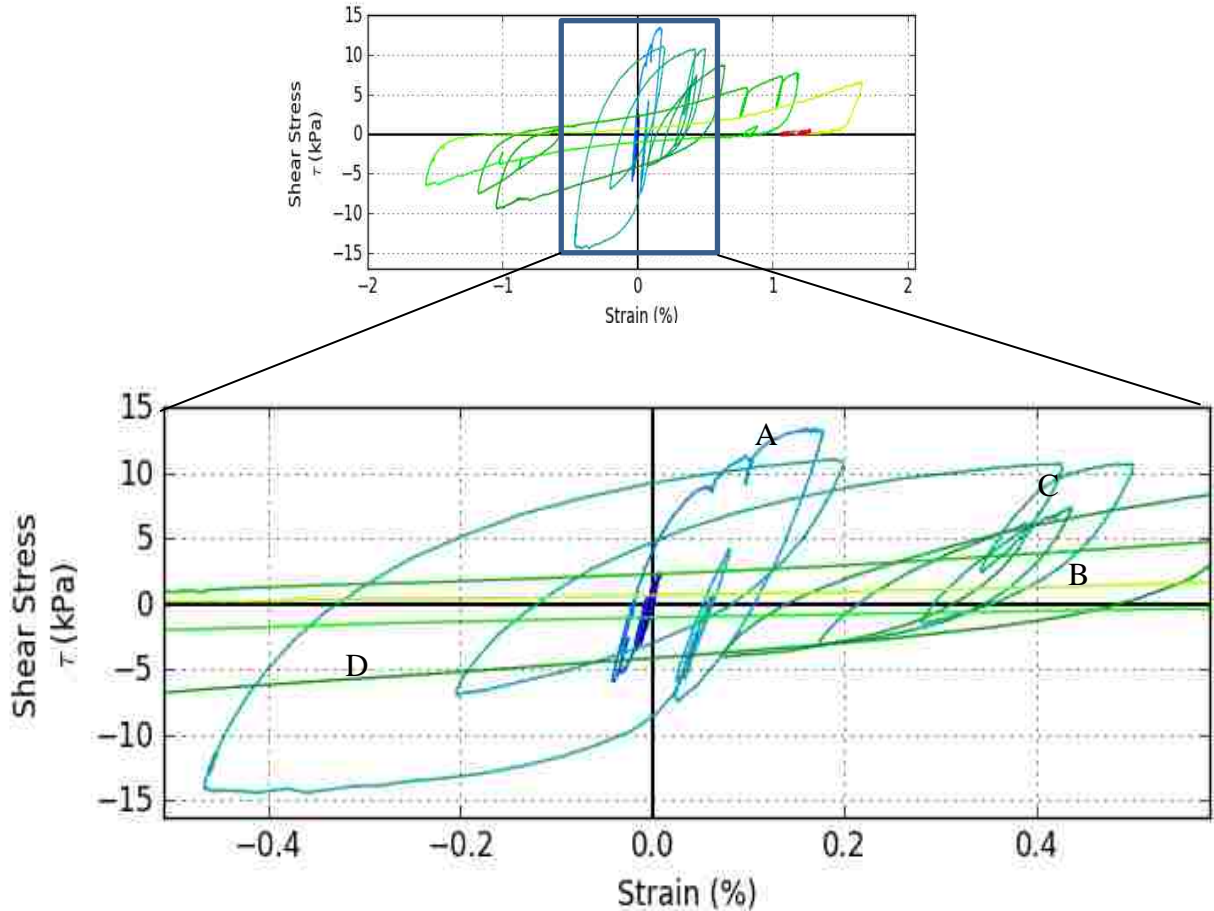levels of initial static shear stress.

Figure 52: Transient shear test per the time history in Figure 49. Test liquefies around 200 seconds. Full tests (top) and zoomed in version shown to observe small-strain behavior. Initial estimated backbone curve is shown in black. Test N0407, Palm Spring motion on Nevada sand, Dr = 65%, CSR = 0.15, α = 0, σ'$_{vo}$ =100 kPa.

5.4 Investigation of K_α

The effects of static shear on liquefaction potential can be expressed in the K_α-α space.

5.4.1 K_α under uniform cyclic testing

The CRR of a simple harmonic test is determined as the CSR resulting in liquefaction at a given

number of cycles. For an earthquake with a magnitude of 7.5, Seed and Lee (1966) defined CRR

as the CSR that would result in liquefaction after 15 cycles while Ishihara (1993) used 20 cycles. K_α is defined in Equation 10 as the ratio of resistances (i.e., a CRR ratio) of a test with initial static shear to an identical specimen tested with no initial static shear. The CRR for each test can be found by creating cyclic strength curves (recall that CRR $= a * N_L^{-b}$ for each test) for each level of initial static shear stress, e.g., empirically fitting parameters $a_{\alpha=0}$ and $b_{\alpha=0}$ (for the level cyclic strength curve) and $a_{\alpha>0}$, and $b_{\alpha>0}$ (for all other cyclic strength curves). K_α can take the form:

$$K_\alpha = \frac{[a_{\alpha>0} * N_L^{-b_{\alpha>0}}]}{[a_{\alpha=0} * N_L^{-b_{\alpha=0}}]} = \left(\frac{a_{\alpha>0}}{a_{\alpha=0}}\right) * N_L^{b_{\alpha>0}-b_{\alpha=0}} \qquad \text{Equation 25}$$

The question then becomes one of defining N_L for each test. The form of the CSR term can be inverted as $N_L = \left(\frac{CSR}{a}\right)^{1/b}$ and substituted into Equation 25. Thus, K_α is reduced to:

$$K_\alpha = \left(\frac{a_{\alpha>0}}{a_{\alpha=0}}\right) * \left[\left(\frac{CSR_{\alpha=0}}{a_{\alpha=0}}\right)^{\frac{1}{b_{\alpha=0}}}\right]^{b_{\alpha>0}-b_{\alpha=0}}$$

$$= \left(\frac{a_{\alpha>0}}{a_{\alpha=0}}\right) * \left[\frac{CSR_{\alpha=0}}{a_{\alpha=0}}\right]^{\frac{b_{\alpha>0}}{b_{\alpha=0}}-1} \qquad \text{Equation 26}$$

This was calculated for each test in the cyclic program which reached liquefaction and the results plotted on Figure 54. The K_α form can also be directly compared to past studies, as seen in Figure 55 which overlays the Seed and Harder 1990 model and the Boulanger 2003 corrections.
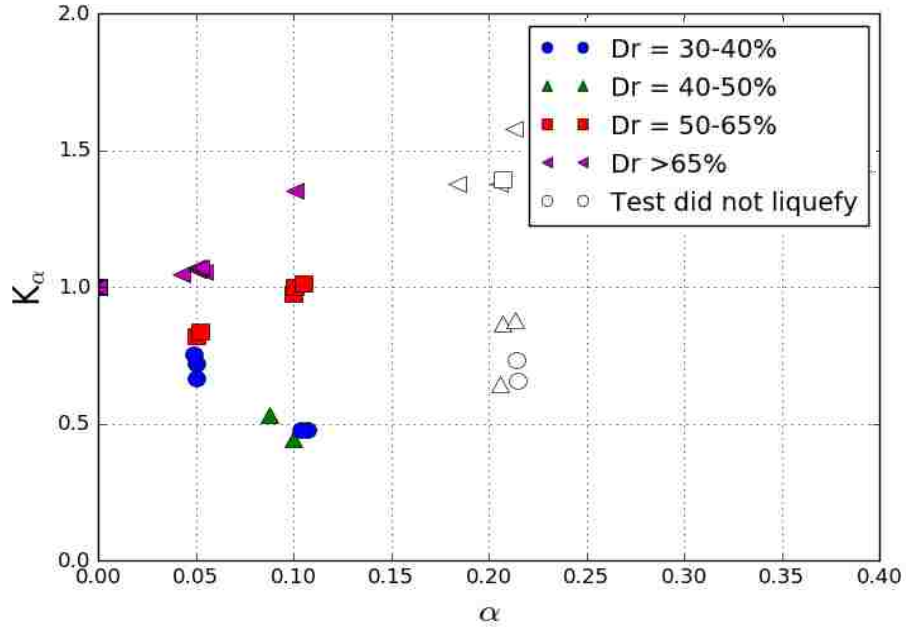
Figure 53: K_α on Siri sands in σ_{vo} = 100 kPa. The point of liquefaction triggering is taken as r_u = 1.0 (for cases which did not fail in liquefaction, failure considered to point at which r_u reaches peak threshold)
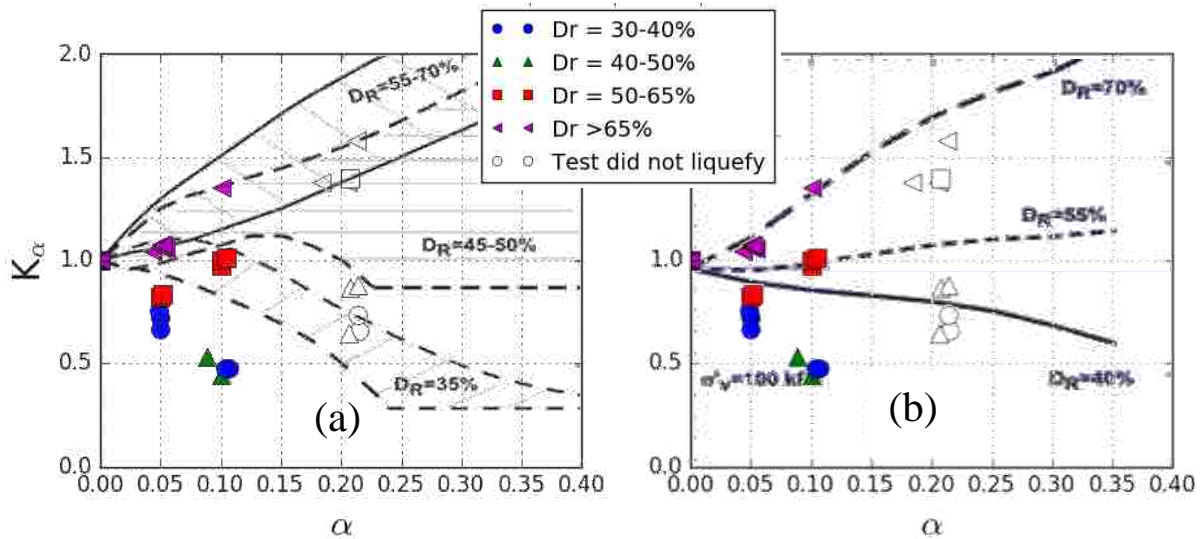

Figure 54: CSS tests of σ'_{vo} =100 kPa from Figure 49 are then overlaid with (a) K_α form of Seed and Harder 1990, and (b) Boulanger 2003. The point of liquefaction triggering is taken as r_u = 1.0 (for cases which did not fail in liquefaction, failure considered to point at which r_u reaches peak threshold)

The results of this CSS program reveal a wider range of K_α behavior for loose soils than those proposed by Seed and Harder (1990) and Boulanger (2003) models. Therefore, a new K_α form for shallow slopes as a function of relative density is proposed in Figure 49. This model is

based on a regression analysis of the CSS testing results. Tests which did not undergo initial liquefaction are included in the figure for reference only and were not considered in the regression analysis. This form is recommended for values of D_r between 30% and 80% and $0 < \alpha < 0.25$. The form of the equation is a second order polynomial function of relative density and initial static shear stress:

$$K_\alpha = 1 + A\alpha + B\alpha^2 \qquad\qquad \text{\textit{Equation 27}}$$

$$A = a_1 + a_2 D_r + a_3 D_r^2$$

$$B = b_1 + b_2 D_r + b_3 D_r^2$$

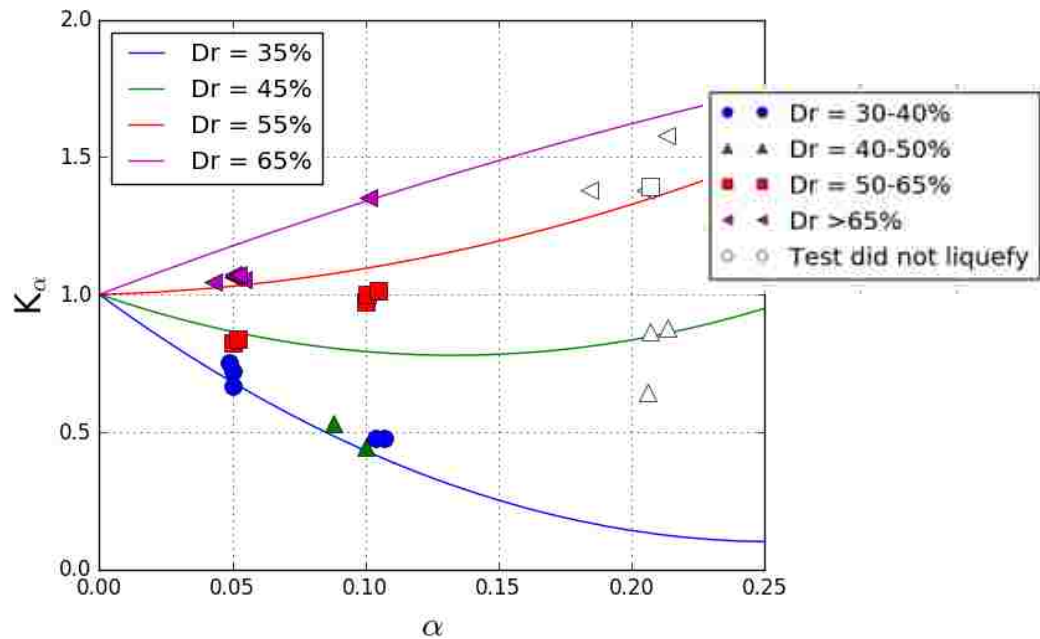| a1	a2	a3	b1	b2	b3
-21.535	0.443	-0.00085	-13.792	1.518	-0.02075

Figure 55: Proposed model of K_α for clean sands of σ'_{vo} = 100 kPa.

Direct comparisons of the K_α regression model to Seed & Harder's (1975) and the Boulanger's (2003) model are plotted in Figure 56. The regression model's intermediate density soils fall between the two models: it is more a conservative estimate than Seed & Harder's

predicted range but a less conservative estimate than Boulanger's prediction. There is good

agreement in the high-density soils between all three models, but this study's regression model

predicts liquefaction resistance for low density soils less than those of both literature models. One

potential reason for the greater disagreement between models in the low density soils versus the

high density soils involves testing procedures. A dense specimen is forgiving of minor jostling

during the sample preparation, placement, or consolidation stages of testing. However, it is

exceptionally easy to slightly jostle a loose specimen at 30-40% relative density which can

rearrange the loose soil fabric. Therefore, simply having a different equipment or lab technician

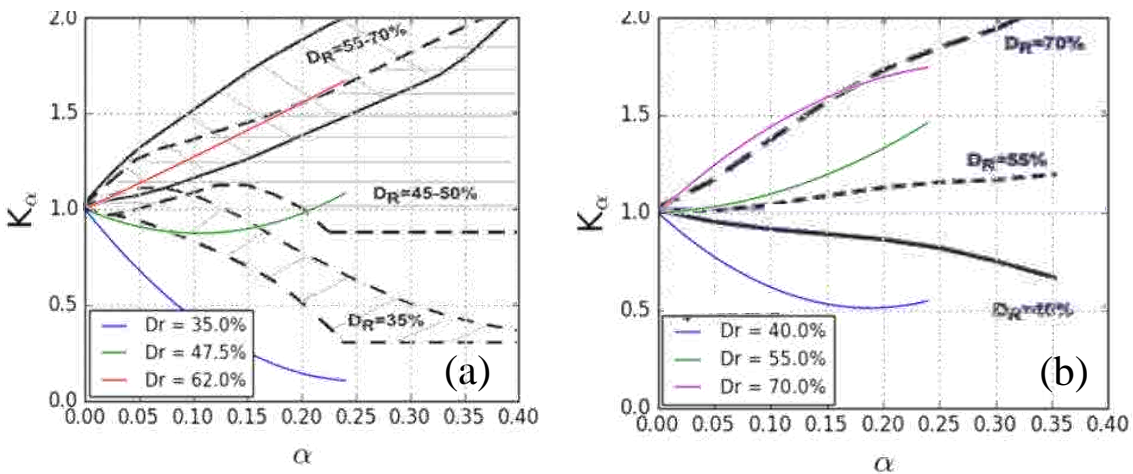perform the same test may lead to different test results.

Figure 56: Results of cyclic regression of K_α in this study shown in color, compared to (a) Seed & Harder's (1975) model and (b) Boulanger's (2003) model shown in black. All models compare tests at $\sigma'_{vo} = 100 \ kPa$.

5.4.2 K_α for use in one-dimensional transient loading

Interpreting K_α for transient and dynamic loading is more complicated than it is for cyclic testing

programs. If we assume that the factor of safety against liquefaction is 1.0 at the point of

liquefaction and $FS_L = CSR/CRR(K_\alpha)(MSF)$, then it follows that K_α at liquefaction can take the following form:

$$K_{\alpha,transient} = \frac{CRR_{\alpha \neq 0}}{[CSR/(MSF)]_{\alpha=0}}$$

Equation 28

CSR and MSF are defined as for the transient tests in Table 6, and the CRR can be defined as the peak past shear stress at the point of liquefaction divided by the vertical effective stress.

Uniform cyclic tests simply take this peak shear stress index as the amplitude of the shear load, but this is not sufficient to capture the magnitude variability of shear stress in earthquake loading. Therefore, this report uses a modified version of a peak-counting method (Liu & Stewart, 2001; Dowling, 1972) to develop a relationship between a transient shear stress history and an equivalent number of cycles at any point in the record. To analyze an acceleration record (analogous to a shear stress record) over the course of the full motion, Liu & Stewart (2001) used the peak ground acceleration (PGA_m) normalized by magnitude scaling factor of each cycle in the motion. The PGA_m and number of equivalent cycles can be tracked over the full motion. Applying this PGA_m analysis method to a shear stress loading history requires a substitution for the PGA_m with a peak shear stress normalized by the magnitude of the loading cycle, $\tau_{peak,m}$. An example of tracking the $\tau_{peak,m}$ and cycle number N as it evolves with time is shown in Figure 57.

There is a slight modification to this procedure for calculating $\tau_{peak,m}$ and N. In Liu and Stewart's method, cycles are counted by zero crossings and those with an amplitude less than 35% of the max shear acceleration are discounted. However, this method only works for shear records with no initial shear stress. These methods count cycles at every point which the zero-shear stress line is crossed. Therefore, with higher initial static shear stresses we would count fewer cycles—or even no cycles. This is not reflective of the motion intensity. Thus, this method for counting

cycles must be analyzed on a record such that $\tau_{ananlyzed} = \tau_{record} - \tau_o$ and $\tau_{peak,m}$ and N values

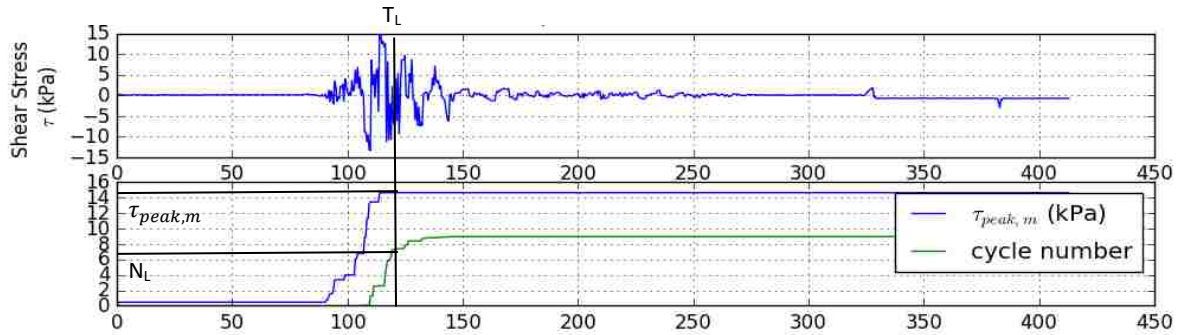calculated from analysis of $\tau_{ananlyzed}$.

Figure 57: Method for finding equivalent number of uniform stress cycles at liquefaction, N_L. Adapted from Liu and Stewart (2001). T_L is the time at which the test liquefied. The $\tau_{peak,m}$ and N_L can then be assessed. These have values of 14.4 kPa and 6.78 respectively for this test.

As data is available to identify the point of liquefaction, a $\tau_{peak,m}$ at liquefaction can be

identified at N_L for every test, as seen in Figure 57. The values of $\tau_{peak,m}$ at liquefaction are

reported for each test in Table A.1 in Appendix A. Assuming $CRR = a * N_L^{-b}$, the CRR of each

test can be plotted against N_L to create an equivalent weighting factor curve for each level of initial

static shear stress. As CRR is defined as the CSR at liquefaction, these values can be substituted

into Equation 28 and the form of K_α for transient tests can be written as:

$$K_{\alpha,transient} = \frac{\left[a * N_L^{-b}\right]_{\alpha \neq 0}}{\left[\frac{CSR}{MSF}\right]_{\alpha = 0}} \qquad \text{Equation 29}$$

Figure 58 compares the calculated K_α values from the transient program to the curves created from

the cyclic testing program. It is apparent from Figure 58 that the $K_{\alpha,transient}$ model predicts similar

liquefaction resistances for low levels of slope inclination (α= 0.05) to those obtained from the

cyclic tests. For steeper slopes, the values of K_α calculated in the transient tests are consistently

lower than that predicted in the cyclic model.

A regressive form can be created to fit the K_α transient test data. This form will add an additional term to the second order polynomial of Equation 27. The terms A and B are defined using the a_i and b_i parameters calculated from the cyclic program, and C is defined using another regression to determine the c_i factors. This equation for the curves fitted $K_{\alpha, transient}$ transient data is shown graphically in Figure 59 and takes the form:

$$K_{\alpha, transient} = 1 + A\alpha + B\alpha^2 + C\alpha^3 \qquad \text{Equation 30}$$

$$A = a_1 + a_2 D_r + a_3 D_r^2$$

$$B = b_1 + b_2 D_r + b_3 D_r^2$$

$$C_T = c_1 + c_2 D_r + c_3 D_r^2$$

a1	a2	a3	b1	b2	b3	c1	c2	c3
-21.535	0.443	-0.00085	-13.792	1.518	-0.02075	274.980	-10.001	0.06945

This form is created using limited data as only tests of $\alpha \leq 0.1$ liquefied. Therefore, this form is only recommended for values of $0 < \alpha < 0.12$.
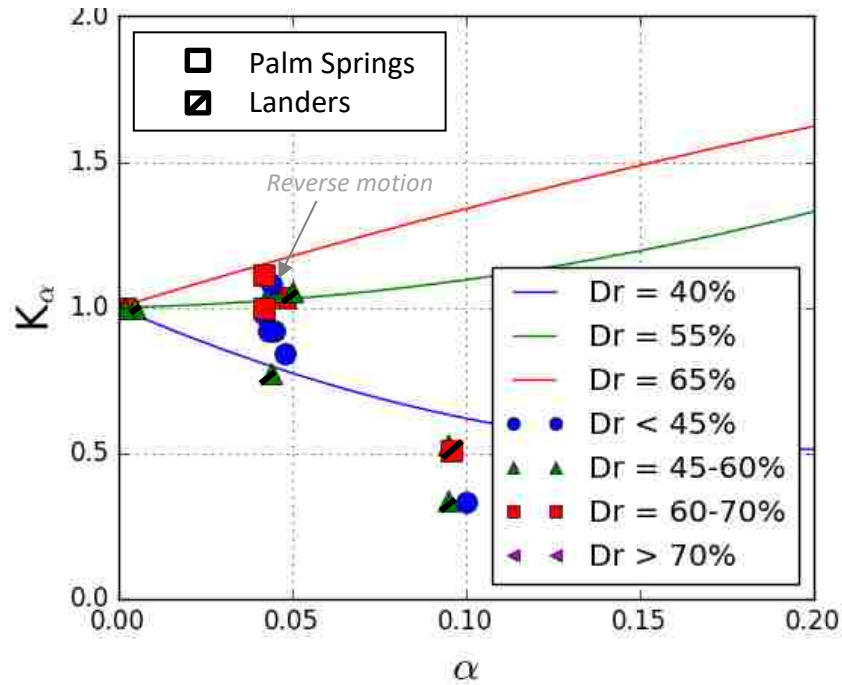
Figure 58: Transient K_α values from testing program on Nevada sands at σ_{vo} =100 kPa, CSR = 0.15 overlaid with the K_α form calculated in the cyclic program. The data points corresponding to tests subject to the Landers motions are marked with a bold line and the Palm Springs motion which was run in reverse with respect to time is marked by an arrow.
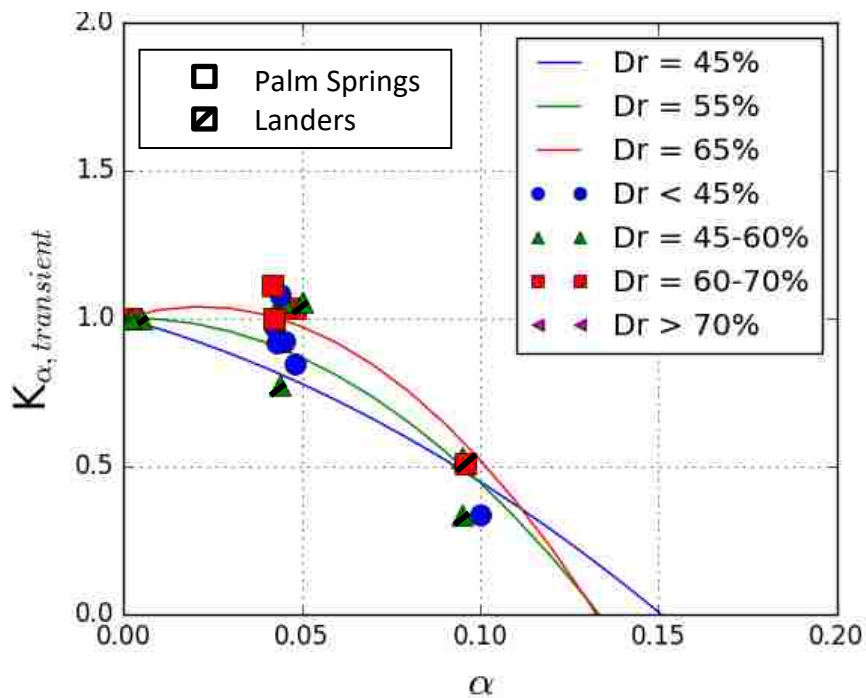

Figure 59: Transient K_α values from testing program on Nevada sands at σ_{vo} =100 kPa, CSR = 0.15 overlaid with form of K_α corrected for transient loading from Equation 30.

The results of the transient regression indicate that the resistance to liquefaction may be lower for higher slopes than a cyclic testing program would suggest.There are several possible explanations to the differences observed here.

First, this study has indicated that loading history may play a larger role in determining liquefaction resistance than currently considered, as shown by the dissimilar point of liquefaction initiation for identical tests run in both forward and reverse direction. Uniform cyclic tests do not capture these effects. One way to assess the possibility that loading history is the reason for the discrepancy between the cyclic and transient regressive forms is to look at the differences between motions. The Landers motion can almost be characterized by a cyclic uniform test of a low cycle period and a shear stress amplitude around 40% of the max shear stress. The Palm Springs motion is better approximated by a small amplitude, high period cyclic test with two large, directionally opposite pulses toward the beginning of the motion. K_α is theoretically independent of shear stress amplitude. The Landers motion would therefore be expected to exhibit a $K_{\alpha,transient}$ similar to that calculated by an equivalent cyclic test ($K_{\alpha,cylcic}$). in the Palm Springs motion, 'jumps' in excess pore pressure are likely to occur at the shear stress pulses, leading to an earlier liquefaction initiation. Thus, the Palm Springs tests may exhibit a smaller $K_{\alpha,transient}$ than $K_{\alpha,cylcic}$ in cases which α is significantly less than the CSR. The reversed Palm Springs motion would be expected to behave similarly, with perhaps a moderately higher resistance than its normal counterpart as the shear stress pulses appear later in the motion. Although these hypotheses are supported in the data in Figure 58, there is an insufficient amount of data to draw firm conclusions regarding the causes of the slight differences between tested motions. Further study is warranted to isolate the true sources.

Another reason for the difference between cyclic and transient K_α behavior involves the choice of ground motion intensity measure used in the calculation of $K_{\alpha,transient}$. The soil liquefaction resistance measure, CRR, was found using a magnitude-modified peak-counting method but other measures to quantify earthquake intensity could be used to draw alternative outcomes to the value of $K_{\alpha,transient}$, i.e., energy methods. Other explanations for the differences in behavior include a combination of factors such as the effects of rate of loading or testing device. Further study is warranted to understand the true cause, as the transient test results suggest that continued use of initial static shear stress models developed using uniform cyclic tests may lead to unconservative estimates of earthquake liquefaction resistance.

The factor of safety model presented by the Simplified Procedure presents a black-and-white picture of the likelihood of triggering liquefaction but says nothing about the permanent strains that may develop on slopes regardless of liquefaction triggering. However, most engineering analyses desire approximations of the peak or final strains during a seismic event to better estimate liquefaction damages. The following are generalized observations and recommendations for liquefaction analyses in liquefiable, sloped soil deposits based on the results of the transient tests.

Strain response in slopes:

Given liquefaction, shallow slopes are likely to exhibit smaller cyclic strains than level slopes but may have similar peak or final strains. Steep slopes (where τ_o is greater than a motion's τ_{peak}) are unlikely to liquefy, but large final strains can still be expected as the slope 'ratchets' downhill under cyclic loading. In some cases, excess strain these may lead to flow liquefaction or slope failures.

Point of liquefaction triggering:

It is recommended to consider the FS_L calculated in a cyclic testing program to be unconservative (i.e. higher than the in-situ value) if:

a) *…the design motion spectra reveal the presence of low frequency (f < 0.3 Hz), large amplitude pulses anywhere in the motion.*

    o Pulses of low shear stress frequencies are amplified in the pore pressure generation of soft soils.

b) *…there are large or multiple initial pulses in the design motion of a deposit on a shallow slope.*

    o The order of shear stress pulses in an earthquake loading history play a large role in the point of liquefaction initiation, and therefore better predictions of initiation can be made if a representative time history is available to analyze. On flat or shallow slopes, if a given motion is seen to have a large pulse near the peak loading amplitude, the point of liquefaction triggering may be significantly sooner than the case where the same pulse was seen towards the end of a motion. An earlier initiation would imply that the cyclic and peak strains are likely to be much greater.

c) *...there is a high rate of intensity buildup in the design ground motion.*

    o The rate of intensity buildup in a ground motion's time history is also important. Given liquefaction occurs in two events of equivalent magnitude, high rates of cumulative intensity buildup will tend to cause liquefaction triggering sooner than one of a slower intensity buildup but longer duration. This has significant consequences on cyclic and peak strains. Several tests in this study revealed the

final strain state of a specimen to be three to five times greater in the case where

liquefaction is triggered early in the motion.

CHAPTER 6. SUMMARY

To summarize, this study reveals the need for the inclusion of slope factors in professional practice liquefaction analyses. In the presence of even minor slopes, the factor of safety against liquefaction can halve in loose soils or double in dense soils. Furthermore, the results of the transient program indicate that the resistance to liquefaction may be lower for higher levels of initial static shear stress than a cyclic testing program would suggest. Continued use of models developed via uniform cyclic testing methods could therefore lead to unconservative estimates of earthquake liquefaction resistance.

The cyclic testing data was processed and compiled for an investigation of the Simplified Procedure's initial shear stress factor, K_α which was found to agree with forms calculated from empirical cyclic studies. However, the results of the transient testing program indicate that K_α has a greater dependence on loading history and state than previously thought. General suggestions are made in Chapter 5 regarding the effects of common ground motion characteristics on K_α calculated from a cyclic testing program but further study is warranted to develop empirical relationships between principal ground motion characteristics and liquefaction resistance.

This thesis presents two databases on simple shear testing of sands investigating both cyclic and transient slope effects on liquefaction triggering. Key differences between in-situ soil behavior in an earthquake and the results gathered from a standard cyclic liquefaction analyses were highlighted through a study of transient loading on sands. The raw transient simple shear testing data is intended to fill gaps in the NGL project's laboratory database regarding initial static shear

stress effects on liquefaction resistance. It is intended for use in the testing and calibration of clean-sand liquefaction models to better the geotechnical practice of natural hazard analyses.

APPENDIX A – Graphical Representation of Simple Shear Tests

A.1 Transient Simple Shear Tests

The transient program is recorded in the *NGI_CSS_Trans_2016.db* database described in Appendix C. Tables 9 and 10 outlines the test parameters of all transient tests performed and indexes their location in this Appendix A.1. All transient tests are recorded here for visual inspection. Raw digital data is available upon request to the author.

Some tests required transposed raw data to reflect accurate initial shear stresses. Additionally, due to equipment limitations, all motions were split into 100 second intervals. The first raw data point logged at each interval is logged incorrectly to be much higher than reality. This misreading is suppressed in these tests by assuming the first point of each interval is equivalent to the last data point in the interval before.

The calculation of instantaneous shear modulus, G_{tan}, is shown in these sections in its raw format. In cases in which the increment of strain $\gamma_i - \gamma_{i-1}$ is zero, this will cause the value of G_{tan} to go to infinity. These effects can be minimized using various smoothing filters on the raw data of shear load and vertical strain.

Some tests did not reach conclusion due to equipment failures. The figures in this appendix show the tests up to the point of failure in the specimen. Table A.1 summarizes the results of each test in this appendix and Table A.2 summarizes the supplemental harmonic tests conducted on the EMDCSS device.

Table A.1: Summary of transient and dynamic simple shear tests on Nevada sands. Test graphically shown in Appendix A at given index. All transient tests run at one quarter of real-time speed, dynamic tests at real-time.

GROUND MOTION	TEST ID	RELATIVE DENSITY (%)	COMMENTS	MSF	α	CSR	CSR/MSF	N_L
PALMSPR_MVH135	N0403	55.1	(e)	1.24	0	0.148	0.120	3.33
	N0404	45.6		1.24	0.042	0.147	0.118	3.69
		44.0	(b)	1.24	0.045	0.152	0.122	6.09
		42.1	(d)	1.24	0.044	0.154	0.124	3.05
		69.6	(a)	1.24	0.048	0.127	0.102	3.97
	N0405	42.0		1.24	0.100	0.130	0.105	3.91
	N0406	43.8		1.24	0.199	0.128	0.103	5.59
	N0407	65.1		1.24	0.002	0.149	0.120	5.08
	N0408	62.9		1.24	0.042	0.149	0.120	2.87
	N0409	64.3		1.24	0.092	0.148	0.119	6.18
	N0410	64.7		1.24	0.193	0.155	0.125	4.26
	N0423	91.1	(e)	1.24	0.101	0.151	0.122	4.34
	N0419	43.9		1.24	0.042	0.057	0.046	4.78
	N0420	39.7		1.24	0.043	0.097	0.078	6.22
	N0421	63.9		1.24	0.042	0.147	0.118	3.97
	N0422	73.3		1.24	0.045	0.020	0.016	2.66
LANDERS_MCF_000	N0411	59.8		1.05	0.004	0.115	0.109	8.02
	N0412	62.7		1.05	0.047	0.098	0.093	8.48
	N0413	62.2		1.05	0.096	0.137	0.130	12.62
	N0414	58.2		1.05	0.213	0.168	0.16	5.01
	N0415	55.6		1.05	0.002	0.143	0.136	8.71
	N0416	59.1		1.05	0.044	0.153	0.146	7.93
	N0417	60.7		1.05	0.100	0.118	0.112	11.45
	N0418	55.6		1.05	0.187	0.135	0.129	10.88

COMMENTS:

(a) Dynamic Test, run at real-time, but with low logging resolution
(b) Run in reverse
(c) Pre-sheared at 20 cycles and 0.05 kPa
(d) Run to test repeatability
(e) Consolidated past target density

Table A.2: Supplemental cyclic harmonic tests on Nevada Sands

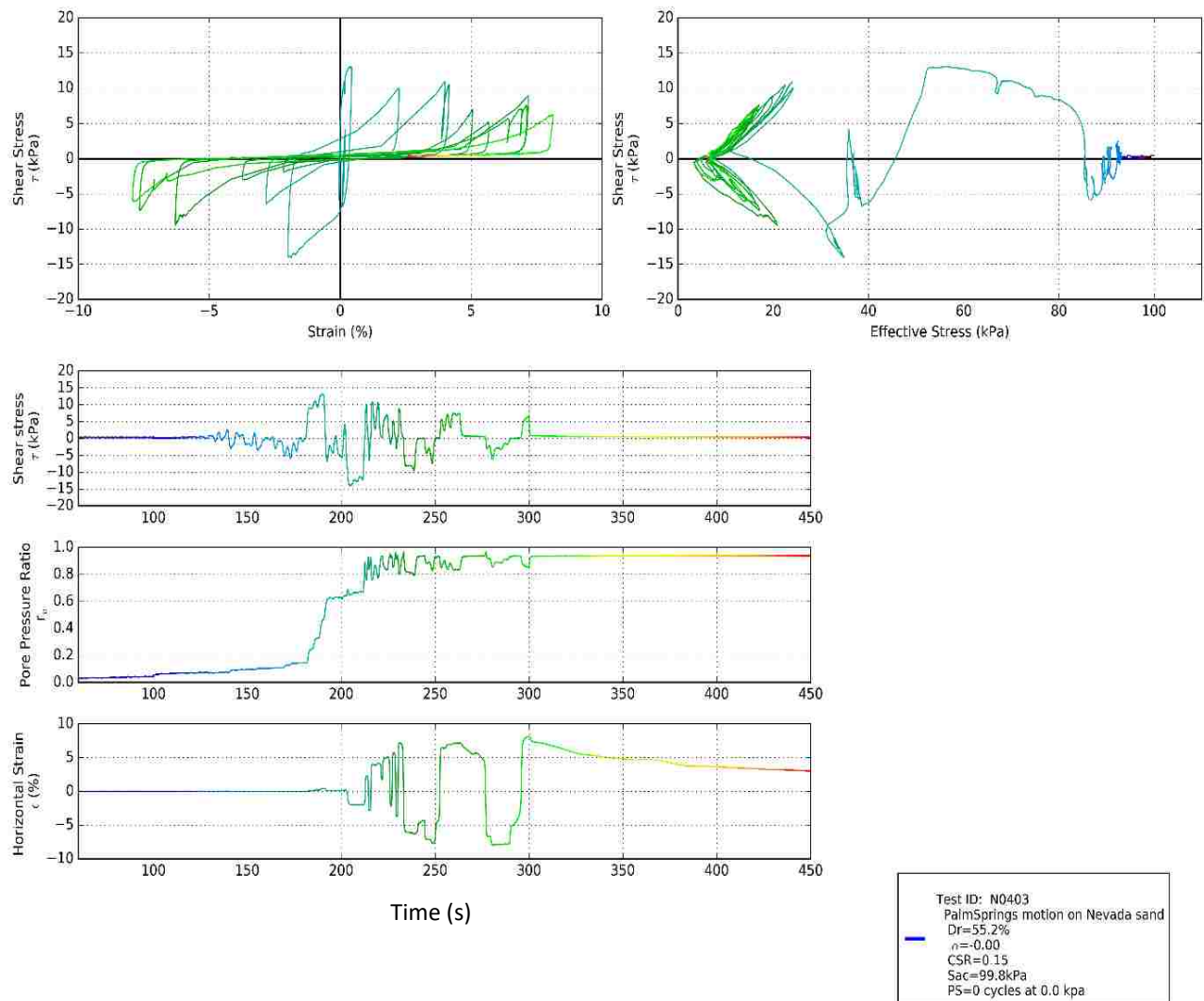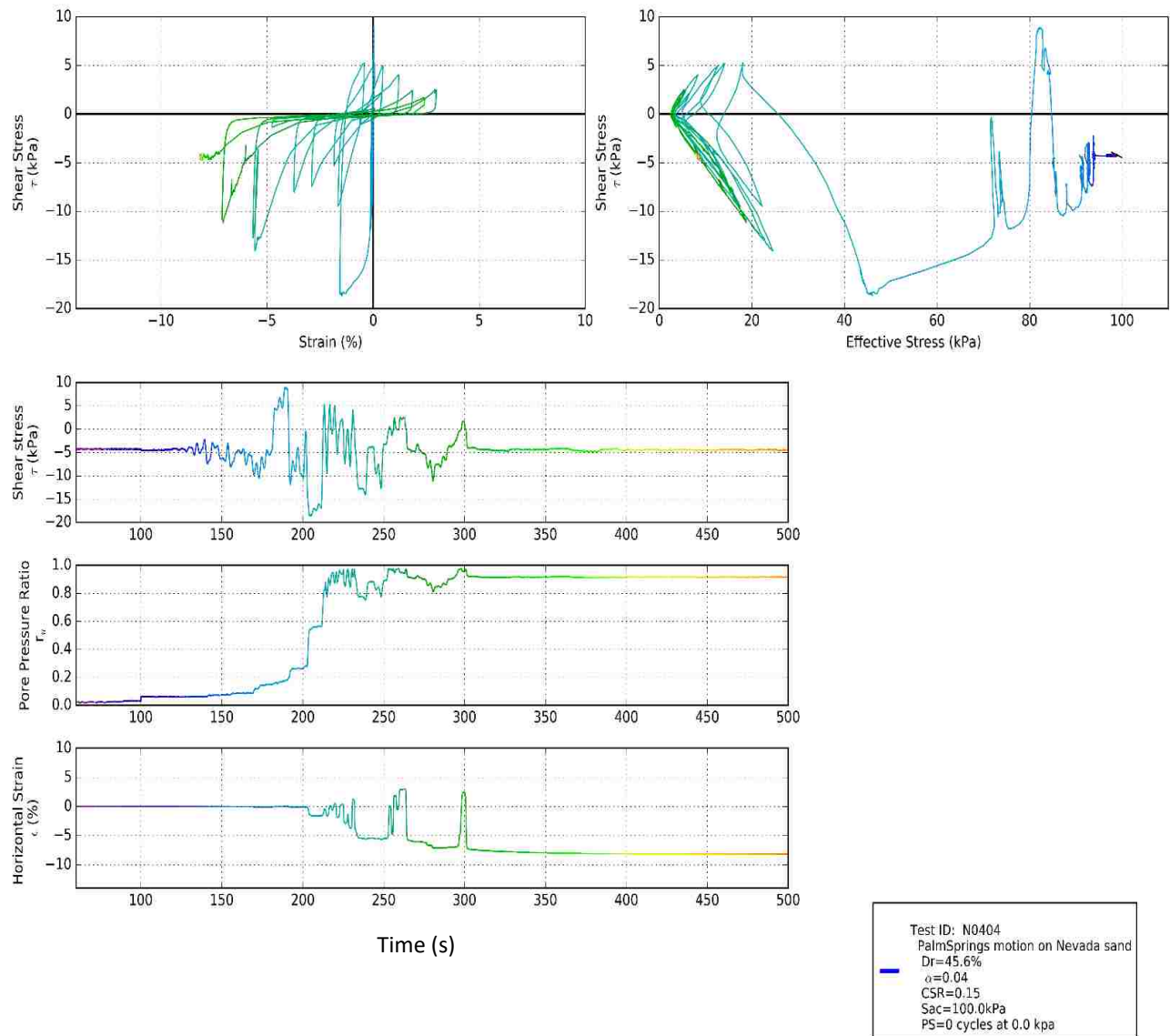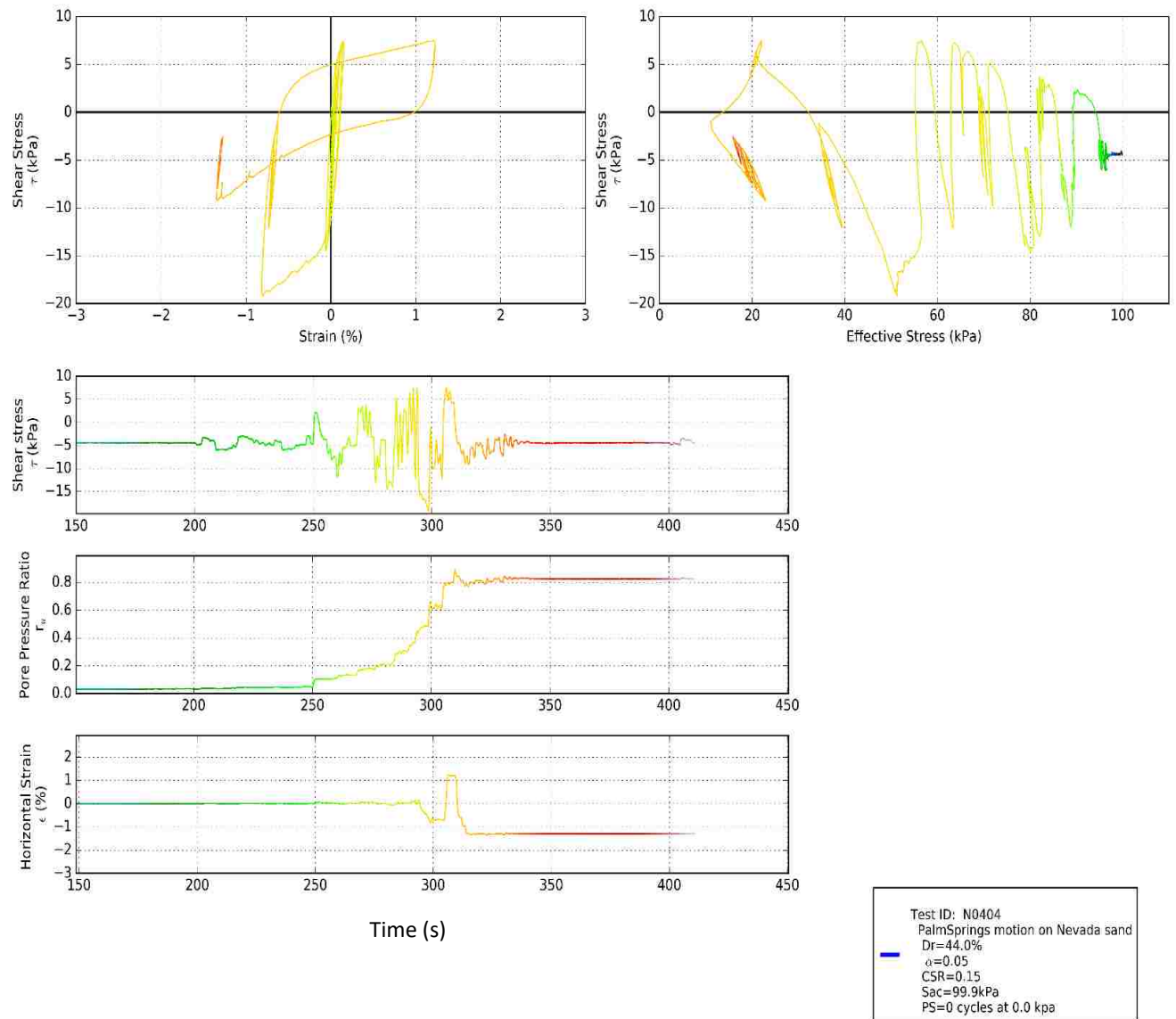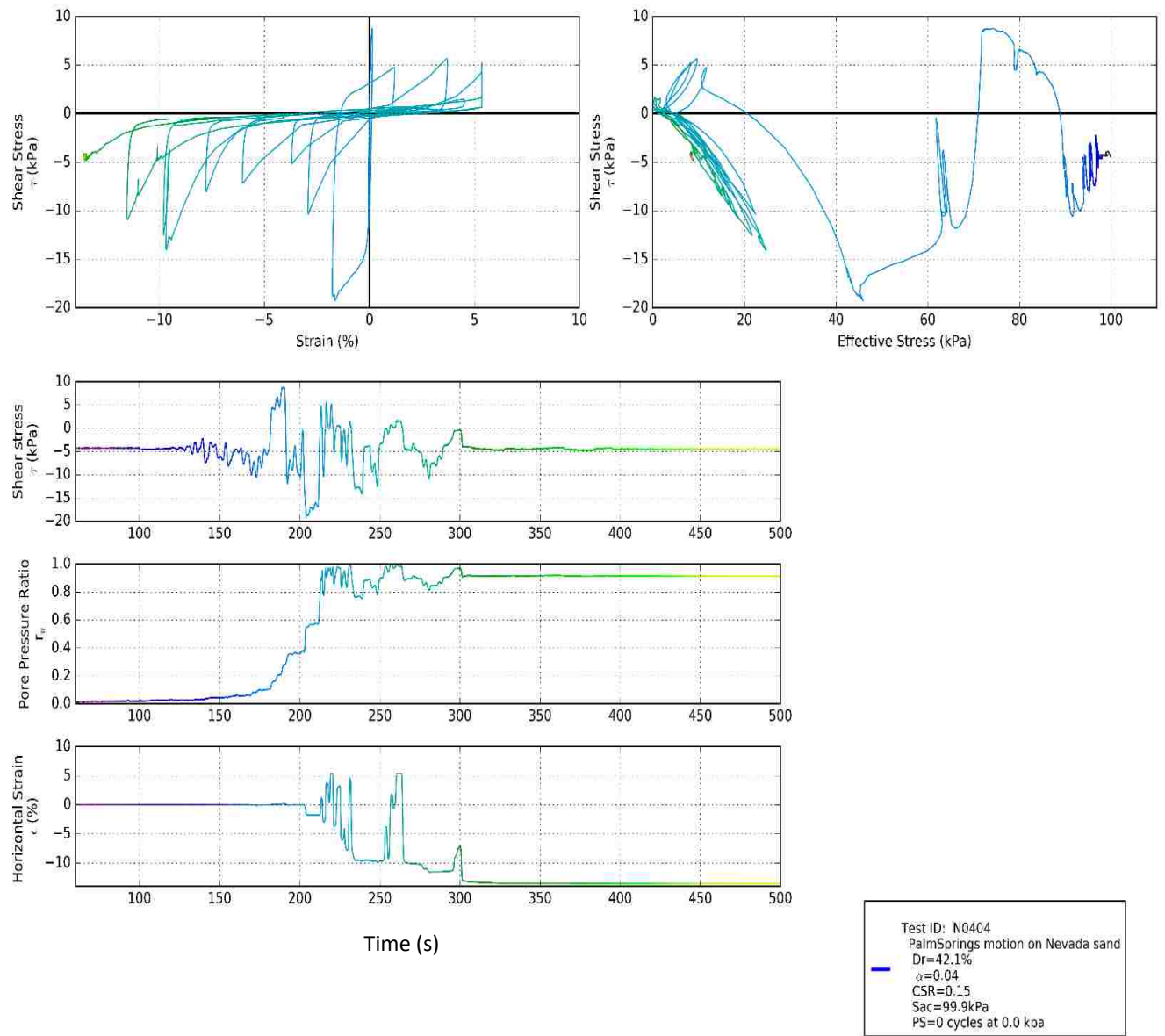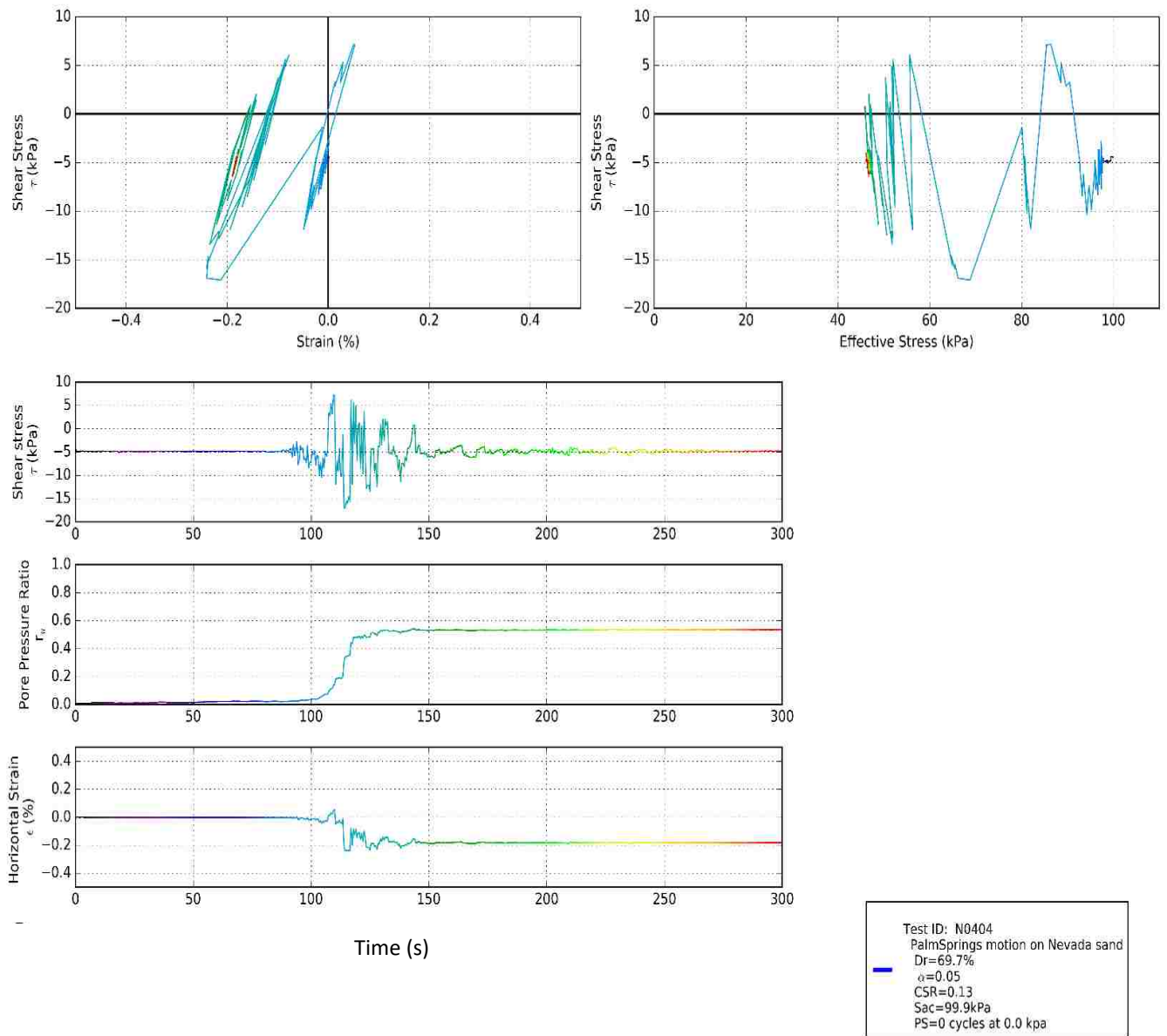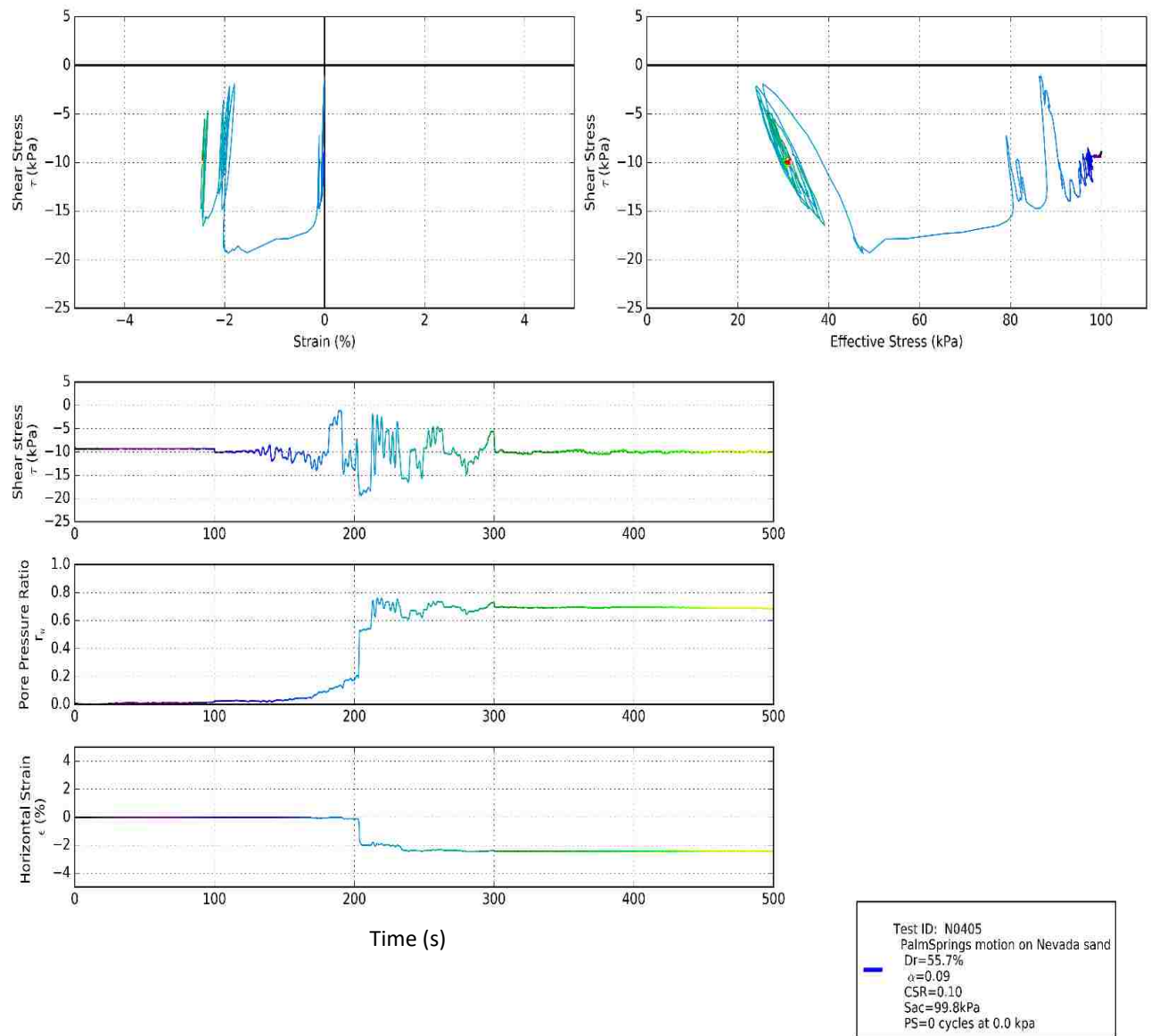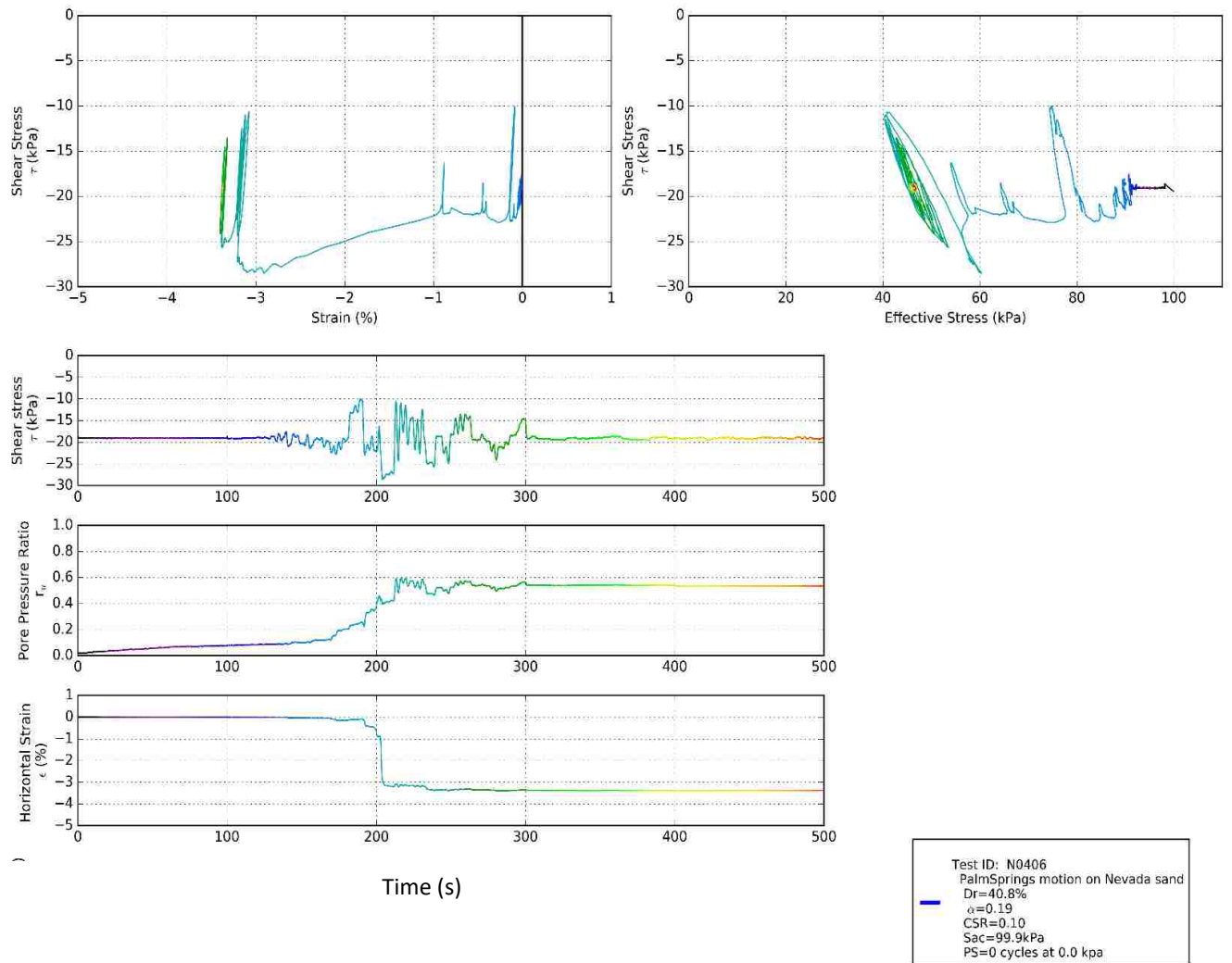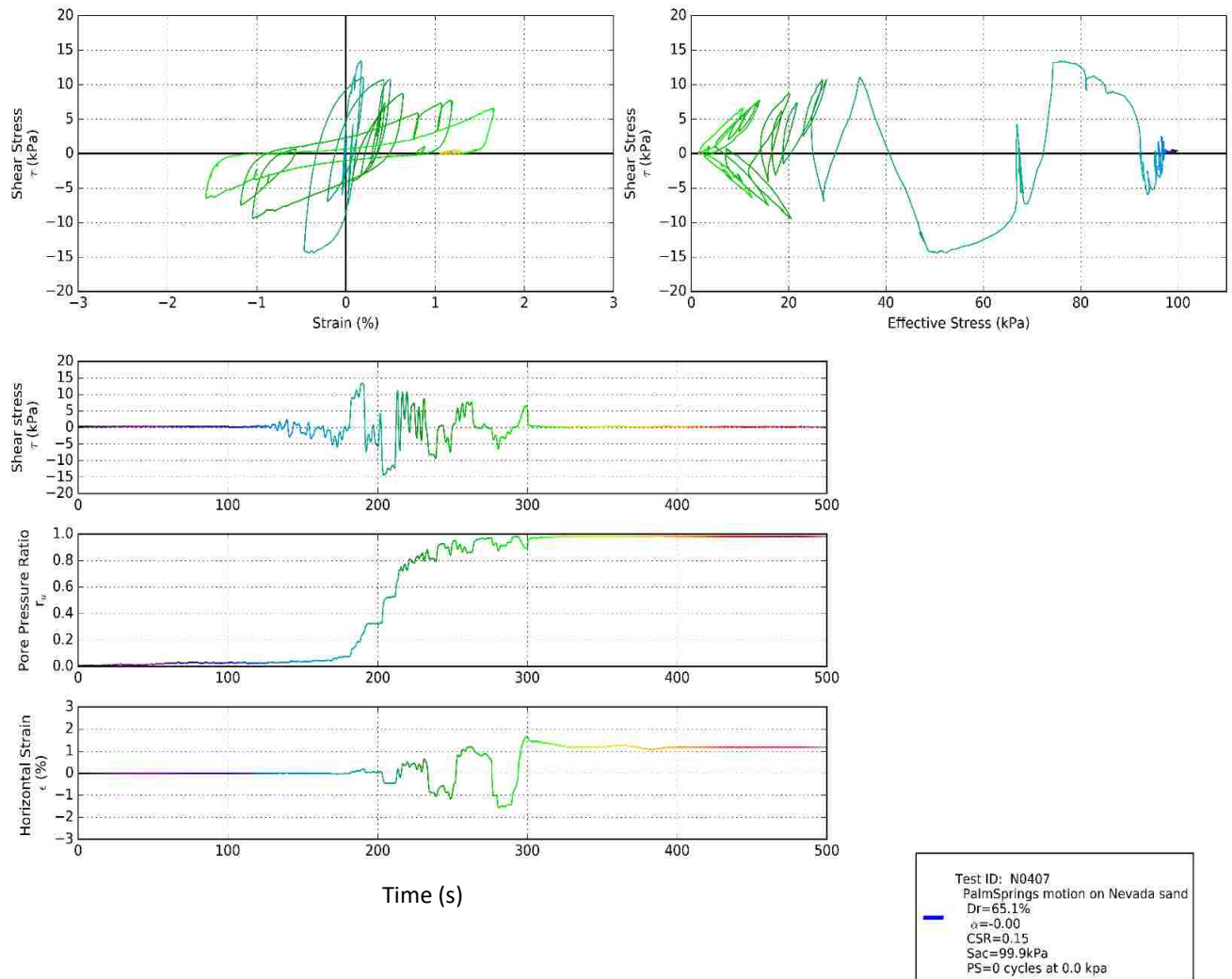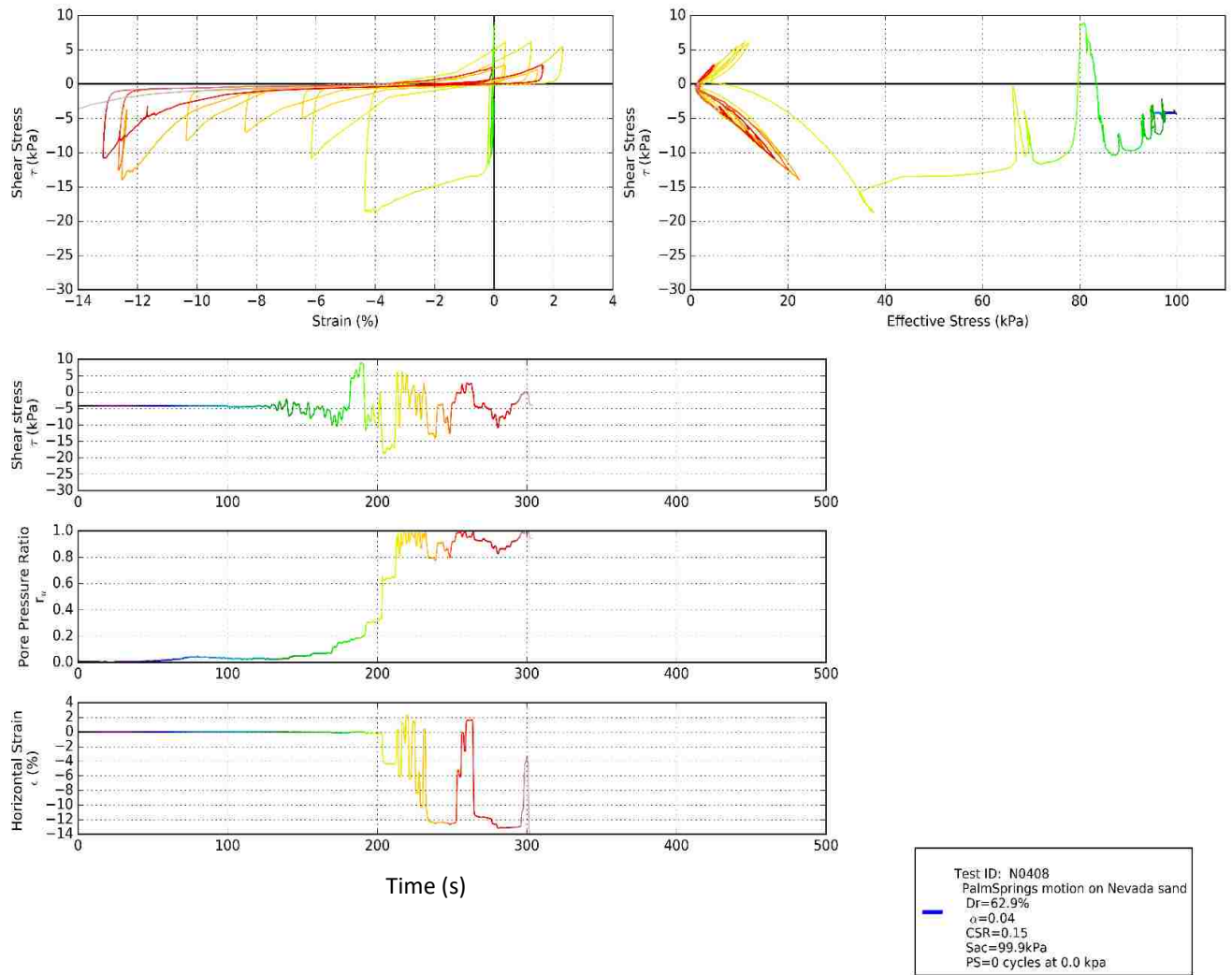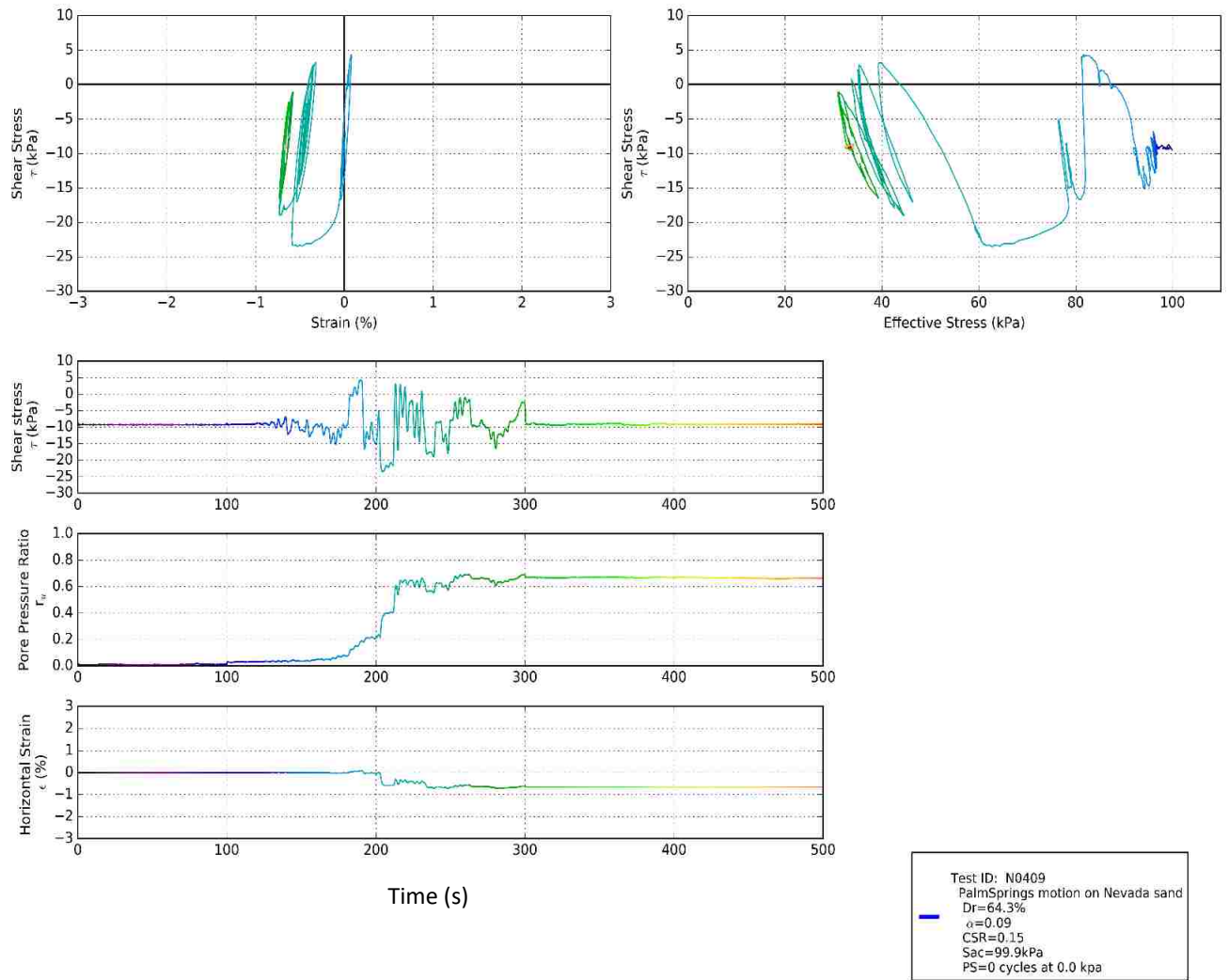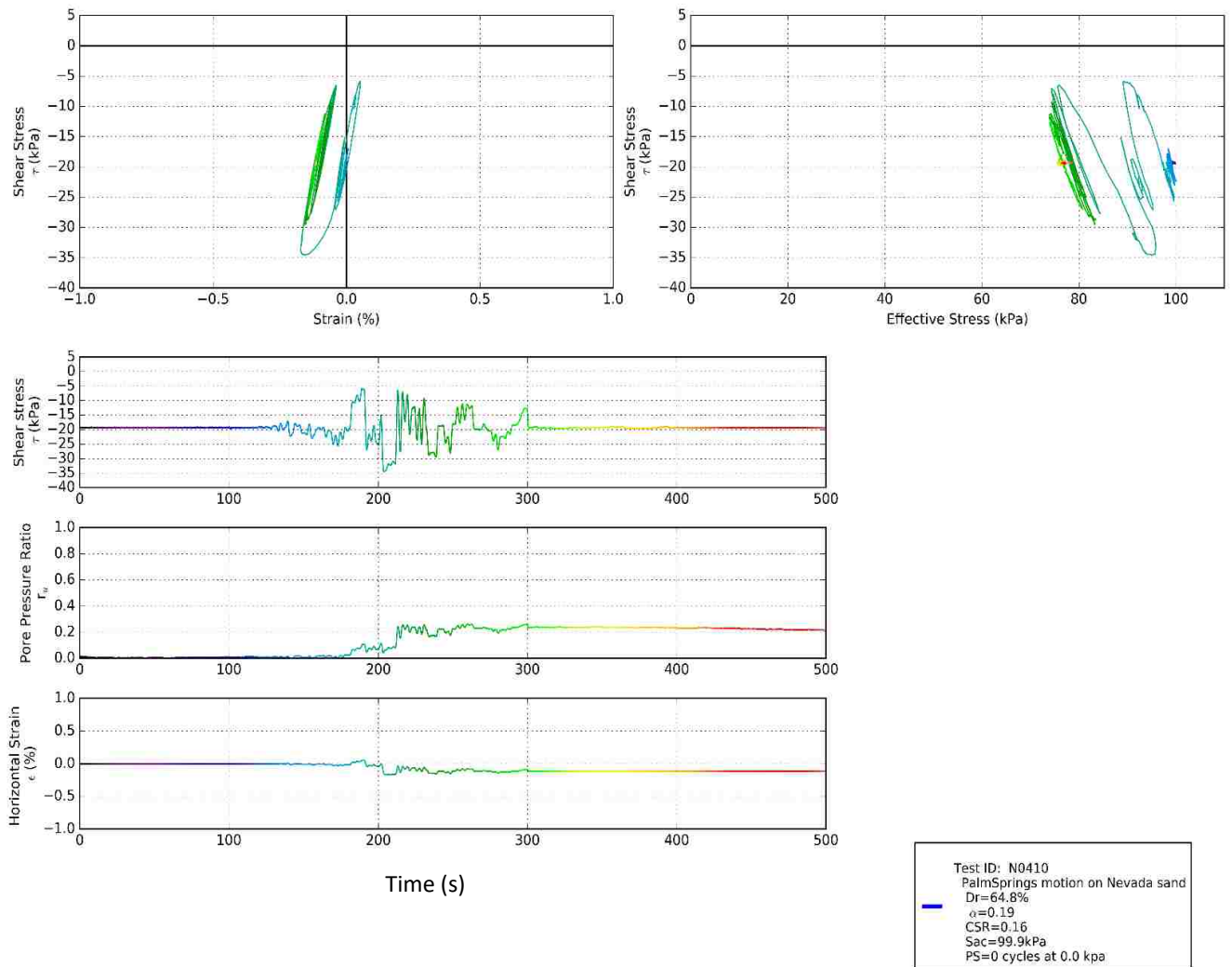| TEST ID	RELATIVE DENSITY (%)	CSR	α
N0500	50.5	*0.10*	0.0
N0501	87.4	*0.09*	0.0
N0502	46.7	*0.045*	0.112
N0503	58.7	*0.045*	0.112

Figure A.1

Figure A.2

Figure A.3

Figure A.4

Test ID: N0404
PalmSprings motion on Nevada sand
Dr=69.7%
α=0.05
CSR=0.13
Sac=99.9kPa
PS=0 cycles at 0.0 kpa

Figure A.5

Figure A.6

Test ID: N0405
PalmSprings motion on Nevada sand
Dr=55.7%
α=0.09
CSR=0.10
Sac=99.8kPa
PS=0 cycles at 0.0 kpa

Figure A.7

Test ID: N0406
PalmSprings motion on Nevada sand
Dr=40.8%
α=0.19
CSR=0.10
Sac=99.9kPa
PS=0 cycles at 0.0 kpa

Figure A.8

Test ID: N0408
PalmSprings motion on Nevada sand
Dr=62.9%
∂=0.04
CSR=0.15
Sac=99.9kPa
PS=0 cycles at 0.0 kpa

Figure A.9

Figure A.10

Figure A.11

Test ID: N0410
PalmSprings motion on Nevada sand
Dr=64.8%
ⱥ=0.19
CSR=0.16
Sac=99.9kPa
PS=0 cycles at 0.0 kpa

Figure A.12

Test ID: N0411
Landers motion on Nevada sand
Dr=60.0%
α=-0.01
CSR=0.10
Sac=99.9kPa
PS=0 cycles at 0.0 kpa

Figure A.13

Test ID: N0412
Landers motion on Nevada sand
Dr=54.4%
α=0.05
CSR=0.15
Sac=99.9kPa
PS=0 cycles at 0.0 kpa

Figure A.14

Test ID: N0413
Landers motion on Nevada sand
Dr=48.6%
α=0.10
CSR=0.13
Sac=99.9kPa
PS=0 cycles at 0.0 kpa

Figure A.15

Test ID: N0414
Landers motion on Nevada sand
Dr=54.2%
α=0.19
CSR=0.13
Sac=95.4kPa
PS=0 cycles at 0.0 kpa

Figure A.16

Figure A.17

Figure A.18

Figure A.19

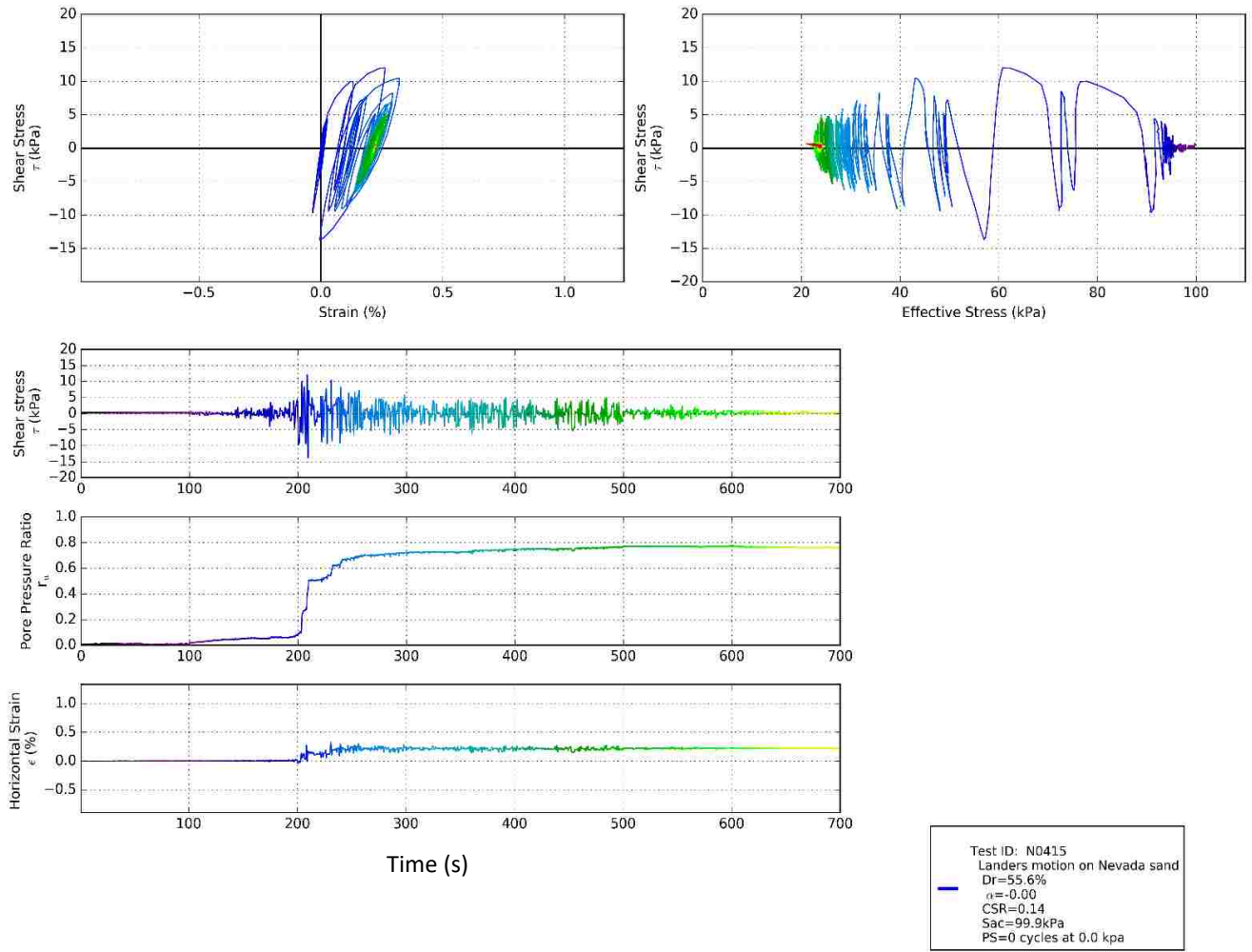Test ID: N0418
Landers motion on Nevada sand
Dr=55.6%
α=0.19
CSR=0.13
Sac=95.5kPa
PS=0 cycles at 0.0 kpa

Figure A.20

Test ID: N0419
PalmSprings motion on Nevada sand
Dr=43.9%
α=0.04
CSR=0.06
Sac=99.9kPa
PS=0 cycles at 0.0 kpa

Figure A.21

Test ID: N0420
PalmSprings motion on Nevada sand
Dr=39.7%
α=0.04
CSR=0.10
Sac=99.9kPa
PS=0 cycles at 0.0 kpa

Figure A.22

Test ID: N0422
PalmSprings motion on Nevada sand
Dr=73.8%
α=0.05
CSR=0.20
Sac=99.8kPa
PS=0 cycles at 0.0 kpa

Figure A.23

Test ID: N0423
PalmSprings motion on Nevada sand
Dr=91.1%
α=0.10
CSR=0.15
Sac=95.5kPa
PS=0 cycles at 0.0 kpa

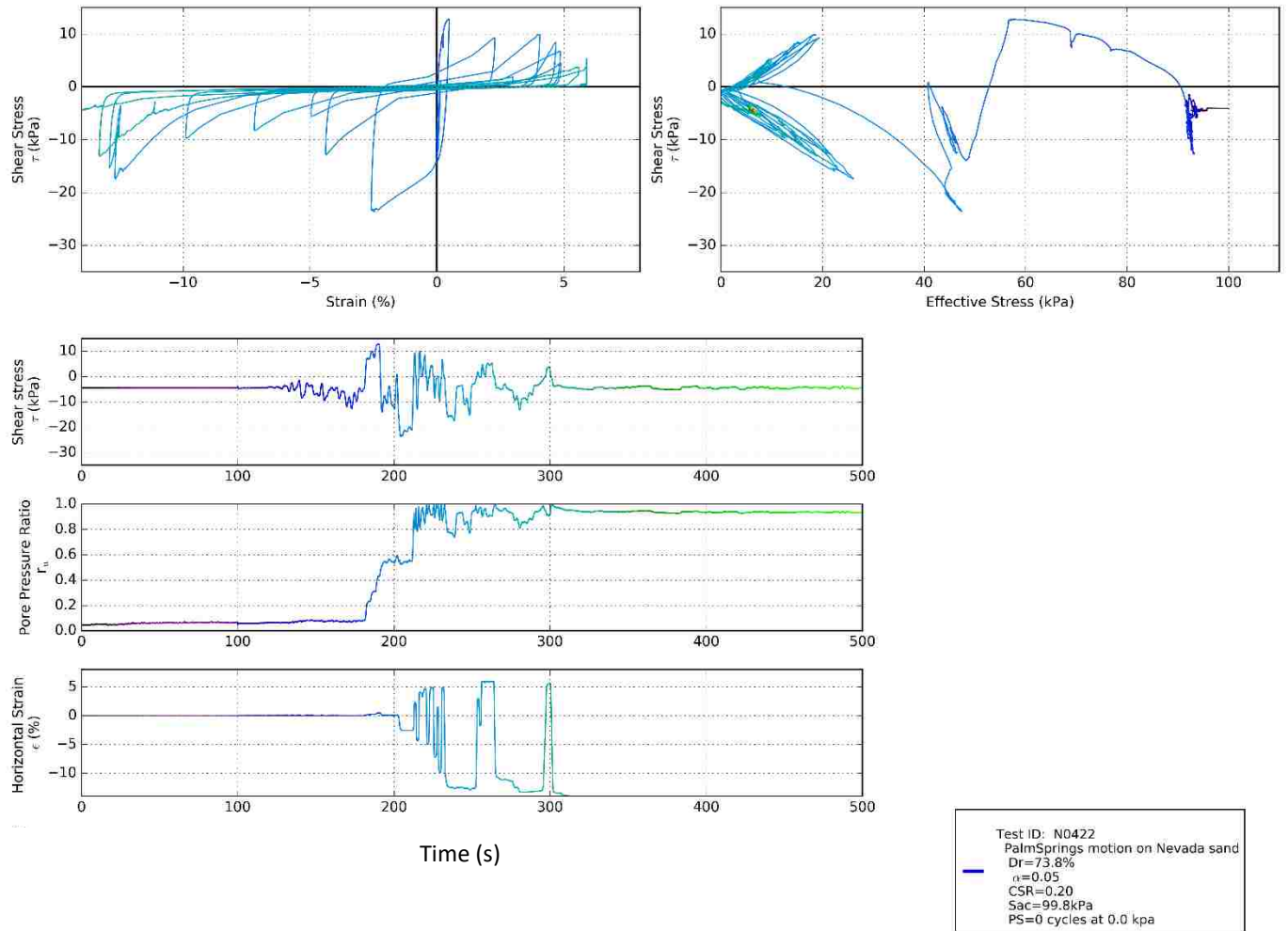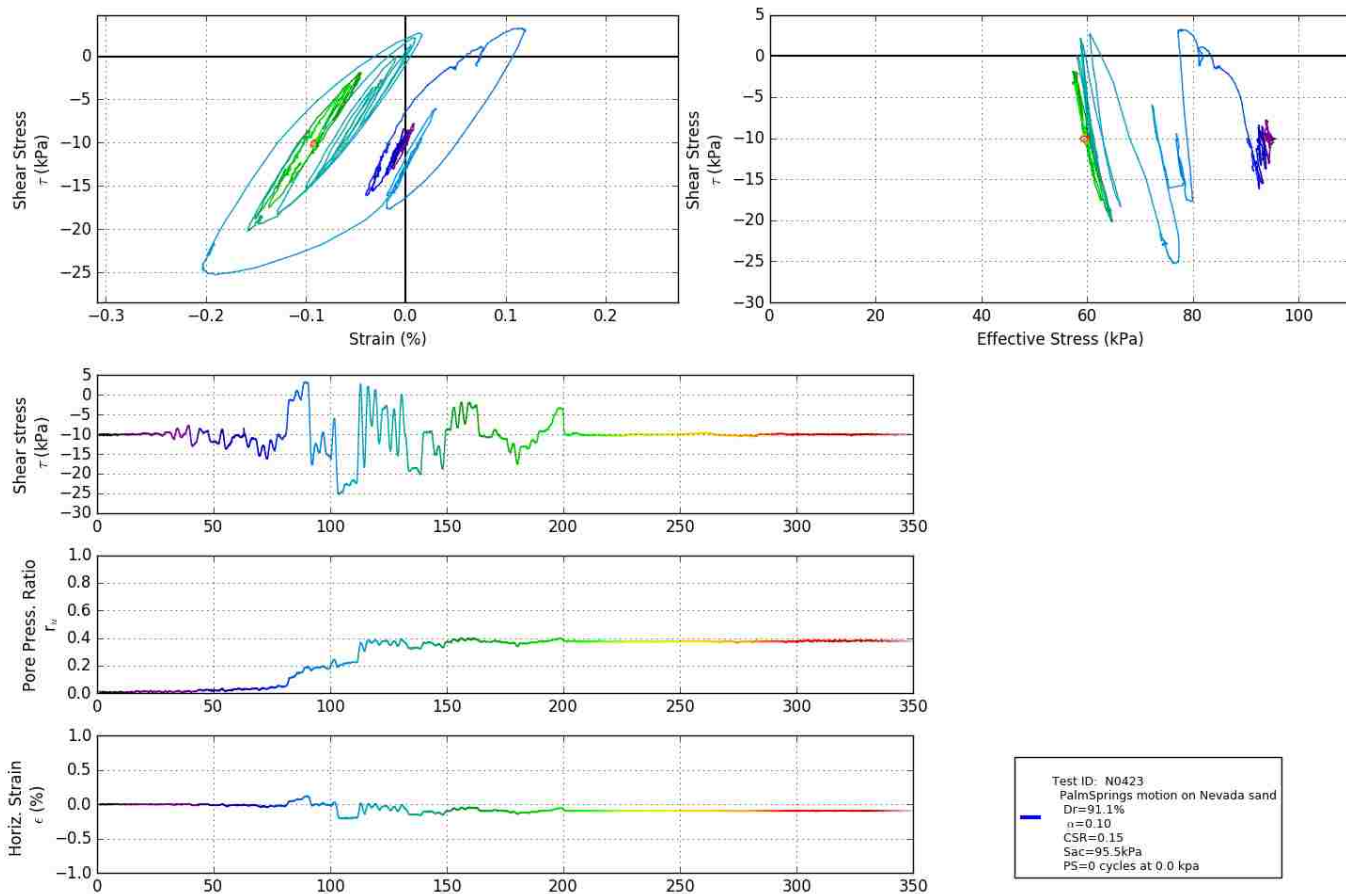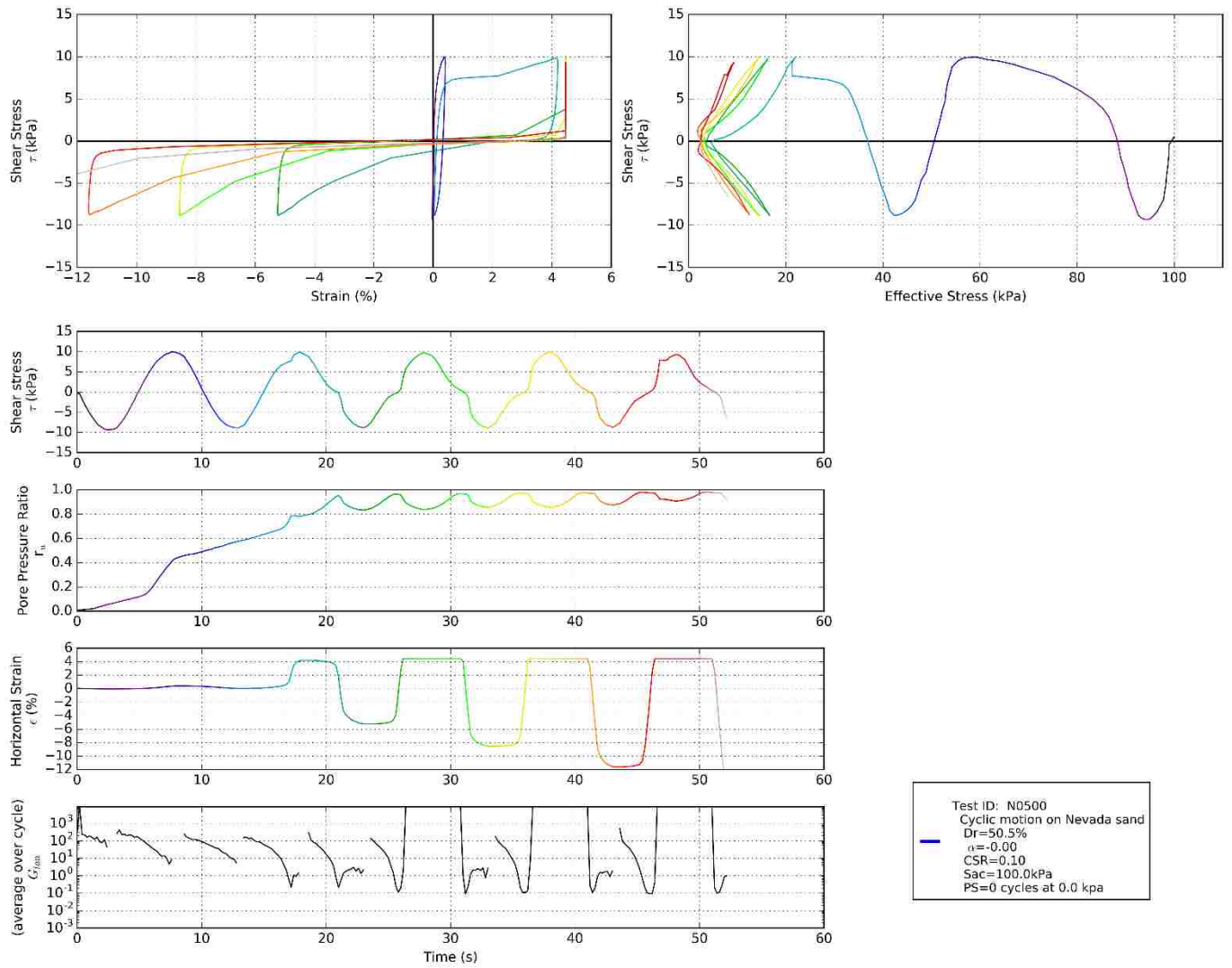Figure A.24: NOTE- limited strain threshold at +4% strain due to testing error.
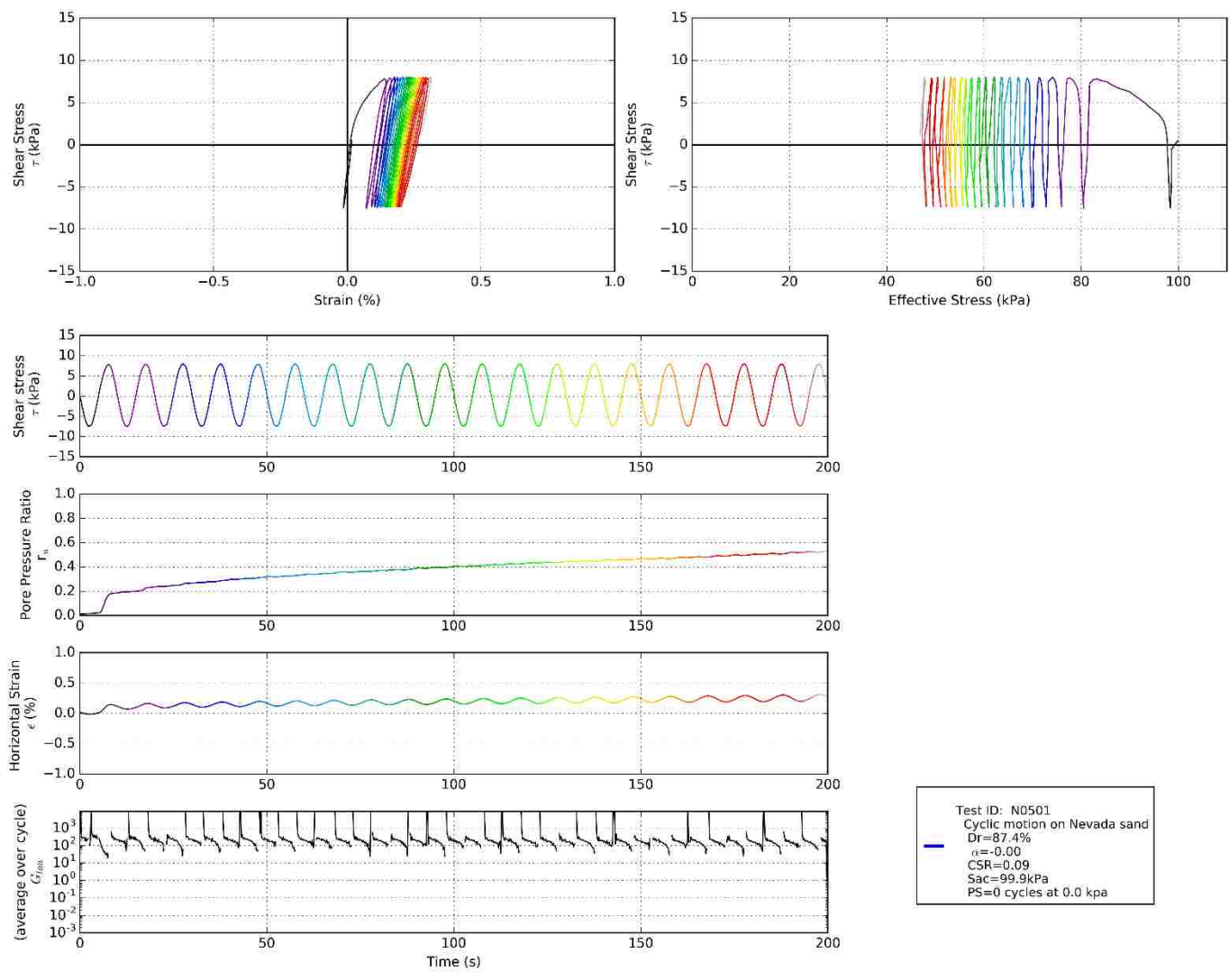
Figure A.25
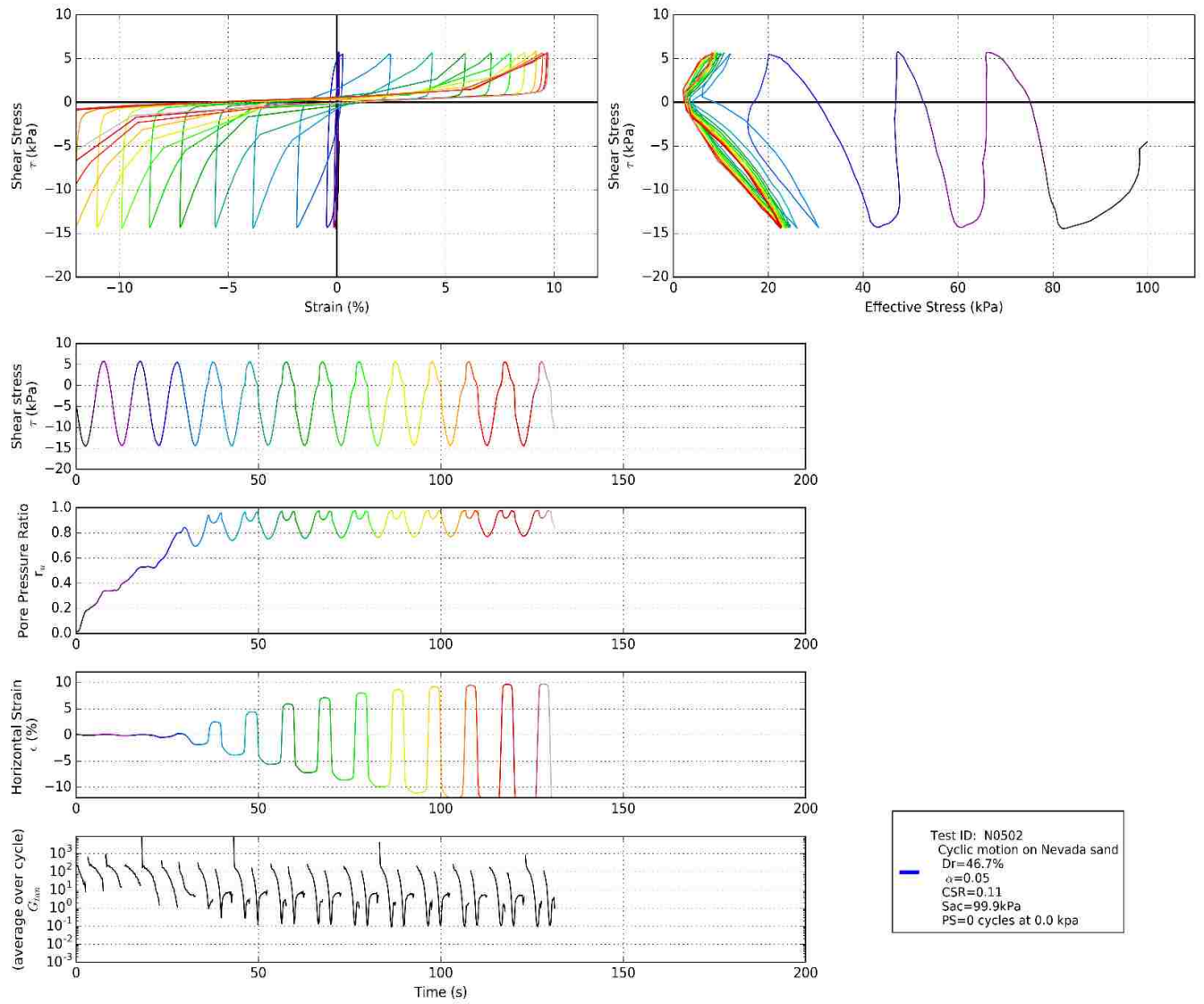
Figure A.26
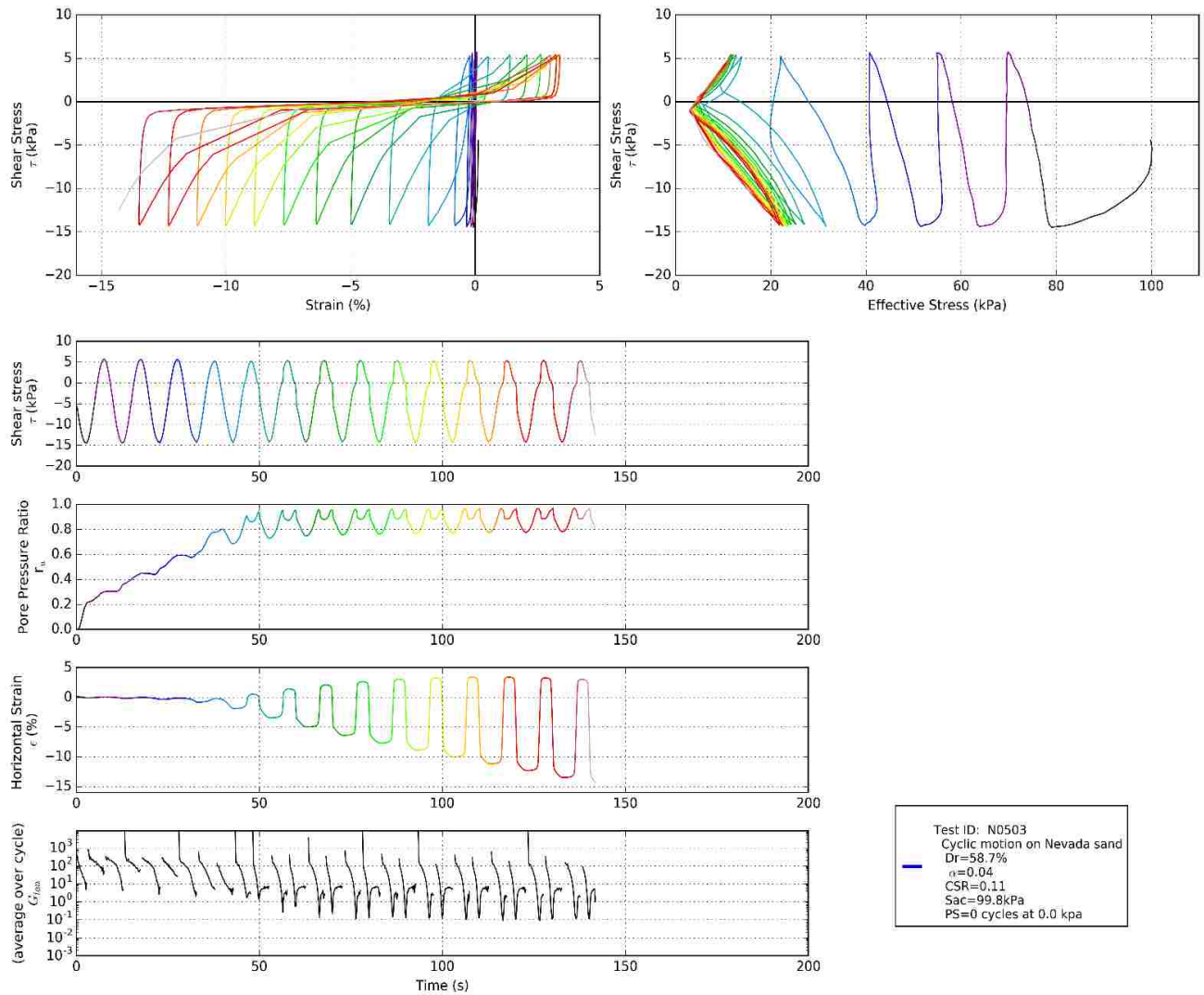
Figure A.27

A.2 Consolidation

Each test was preceded by a period of consolidation. Figure A.28 shows a typical consolidation curve for Nevada sands on the GDS device. Specimens were loaded to 100 kPa at a constant rate over the course of 10 minutes, then allowed to rest for two hours before shearing.
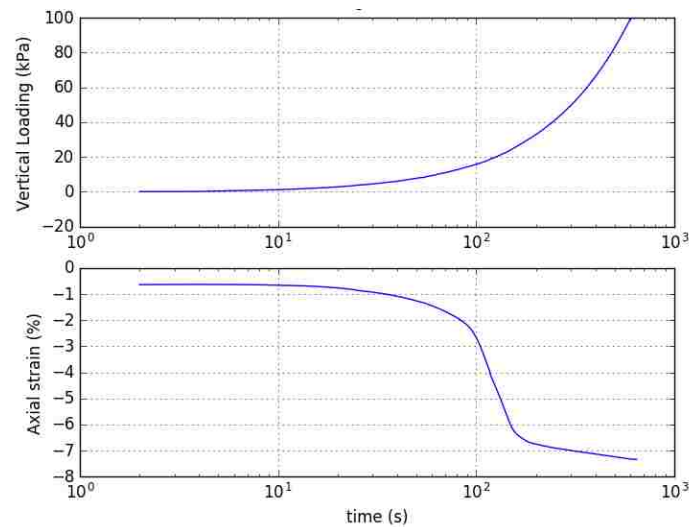
Figure A.28: Sample consolidation curve for Nevada sands in GDS device. Loaded to vertical stress of 100 kPa over 10 min.

A.3 Cyclic simple shear program

The cyclic simple shear tests referenced in this test to create the proposed form of K_α in Equation 28 can be accessed upon request to the author.

APPENDIX B – Transient Waveforms

Six transient acceleration records were referenced in this testing program. Stress histories are scaled versions of each of these, scaled to a peak stress of 15 kPa.

| Motion	PEER NGA#	Location	Year
GREECE_PLK_NS	484	Pelekanda, Greece	1987
PALMSPR_MVH135	527	North Palm Springs, USA	1986
KOCAELI_CNA000_H2	1157	Koaceli, Turkey	1999
LANDERS_MCF_000	880	Landers, USA	1992
COYOTELK_G04360	149	Coyote Lake, USA	1979
HECTOR_MMP090	1761	Hector Mine, USA	1999

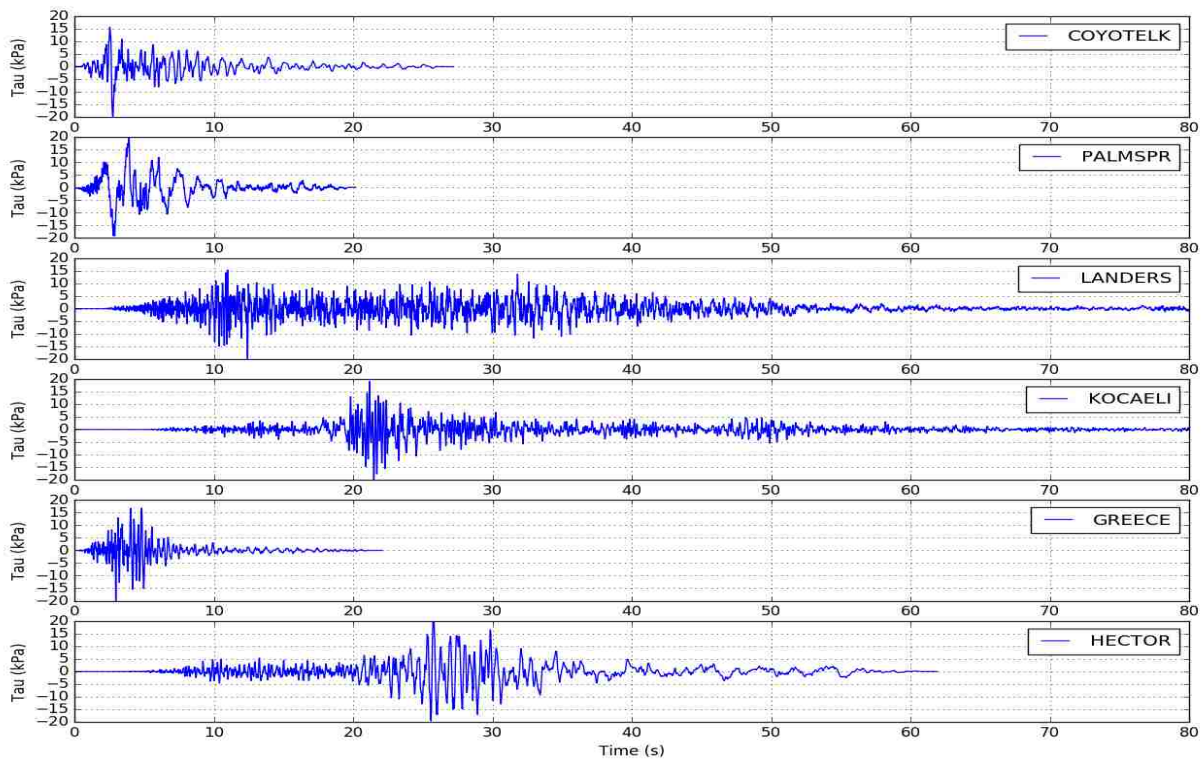|	Magnitude	PGA unscaled (g)	Arias intensity	CAV$_5$	τ peak scaled (kPa)
GREECE_PLK_NS	5.00	0.75	0.22	1.21	20
COYOTELK_G04360	5.74	0.46	0.50	2.61	20
PALMSPR_MVH135	6.06	1.01	0.62	2.57	20
HECTOR_ MMP090	7.13	1.05	0.23	2.40	20
LANDERS_MCF_000	7.28	0.49	0.36	3.93	20
KOCAELI_CNA000_H2	7.51	1.09	0.48	3.85	20

Figure B.1: Transient waveforms of six historical earthquake motions

APPENDIX C – NGI Cyclic and Transient Simple Shear Database

The transient tests conducted in this parametric study on effects of K_α on liquefaction resistance in clean sands are saved to the SQL database entitled *NGI_Trans_Kalpha_2016.db*. All tests in this database were performed by Katherine deLaveaga at the Norwegian Geotechnical Institute in 2016. Access to the database is available upon request: kdelaveaga1@gmail.com.

Appendix C includes a description of the NGI_CSS_Kalpha_2016.db database scripts used for post-processing and data display.

Programs required for database access

MySQL or sqlite3:

Query language module for raw data access. Use pip install to add chosen SQL module to Python.

Sqlite3 can be downloaded at the following site:

http://www.codegood.com/archives/129

Python 2.7 or higher:

Access to processed data and scripts to filter and display data

C.1 Database formatting

The SQL Database NGI_Trans_Kalpha_2016.db contains the raw data and test parameters of all simple shear tests conducted at NGI described in this report. This database is composed of five tables including variables which store various aspects of the test.

Each table is linked, and therefore easily queried, by the variable 'TestID' and/or 'Sand'. Each Linked object between tables are color-coded in the tables below.

I.   Test Parameters as described in ProgramSummary.xlsx

TABLE: TestInfo

Variable Name	Entry type	Units	Description
TestID	int		Ncy number of test (i.e. If test is ncy101, TestID = 101)
TestName	str		Test name as defined by ProgramSummary.xlsx (i.e. S0103)
Date	dd.mm.yyyy		
Sand	str		'Siri' or 'Nevada' sand
TypeTest	str		'Control', 'Cyclic', or 'Transient'
alpha	float		Shear deadload/normal deadload
AreaSpec	float	cm²	Area of specimen
HeightInitial	float	mm	Initial Height of specimen before consolidation and shearing
HeightBeforeShear	float	mm	Height of specimen after consolidation (and preshear) before test begins
CSR	float		Critical stress ratio = peak applied cyclic shear stress / overburden stress
Dr	float	%	Relative density
TauCyclic	float	kPa	Cyclic shear stress amplitude
AxialNormalStress	float	kPa	Normal shear stress applied
MembCorr	float	kPa	Membrane correction factor of wire framed membrane
MembThickness	float	mm	Membrane thickness
WaterContent	float	%	Water content at end of test
SamplePrepMethod	str		'Wet Pluviation','Dry Tamping'
NumPreshearCycles	int		Number of cycles during preshearing stage
PreshearLevel	float	kPa	Stress applied during preshearing

II.   Raw, unprocessed data logged during test

TABLE: RawData

Variable Name	Entry type	Units	Description
TestID	int		Ncy number of test (i.e. If test is ncy101, TestID = 101)
Time	float	s	
gamma	float	%	Horizontal strain by time
EffSig	float	kPa	Effective normal stress, normal stress - pore pressure
tau	float	kPa	Applied shear stress (not including deadload)
u	float	kPa	Pore pressure (in CCV tests, u is considered equal to the vertical stress required to keep the top platen at a constant height)
ru	float		Pore pressure ratio = u/overburden stress

III.   Failure state at test conclusion and general test performance

TABLE: TestOutcomes

Variable Name	Entry type	Units	Description
TestID	int		Ncy number of test (i.e. If test is ncy101, TestID = 101)
Nf	int		Number of cycles until sample 'fails' or reaches liq. (by definition of ru = 1) in cylcic tests, else equivalent number of cycles until failure in transient tests
RuFinal	float		Final Ru reached
TestQuality	str		Qualitative analysis of test results based on test process and initial visual Inspection of data. 'Good', 'Fair', or 'Poor'

IV. Logging calibration factors (kN/volt) and zero readings (volt)

TABLE: SensorCalibration

Variable Name	Entry type	Units	Description
TestID	int		Ncy number of test (i.e. If test is ncy101, TestID = 101)
AxialLoadCalib	float	N/volt	Axial load calibration factor
AxialLoadZero	float	volt	Axial load zero reading
ShearLoadCalib	float	N/volt	Shear load calibration factor
ShearLoadZero	float	volt	Shear load zero reading
AxialDispCalib	float	N/volt	Axial displacement calibration factor
AxialDispZero	float	volt	Axial displacement zero reading
ShearDispCalib	float	N/volt	Shear displacement calibration factor
ShearDispZero	float	volt	Shear displacement zero reading

V. Geotechnical characteristics of tested sands

TABLE: SandInfo

Variable Name	Entry type	Units	Description
Sand	str		Name of sand: 'Siri' or 'Nevada'
emax	float		
emin	float		
SG	float	kN/m^3	Specific gravity
MaxDensity	float	kN/m^3	
MinDensity	float	kN/m^3	
Cu	float		Coefficient of curvature

VI. Log of consolidation tests which preceded shearing

TABLE: Consolidation

Variable Name	Entry type	Units	Description
TestID	int		Ncy number of test (i.e. If test is ncy101, TestID = 101)
time	float	s	0,6,15 seconds after each increment of load is added every 30 min. 4 stages total
load	float	kg	Load on specimen
VerticalDeformation	float	mm	Vertical deformation after consolidation is logged

APPENDIX D – Shear Testing Equipment

D.1 EMDCSS GDS device

The EMDCSS device has been modified in the NGI labs to use wire-reinforced membranes as opposed to stacked rings these are the same wire reinforced rubber membranes that are used in the NGI DSS devices. The machine uses constant volume conditions using Active Height Control. The full device specs can be found on the GDS website at the URL:

http://www.gdsinstruments.com/__assets__/Products/00028/EMDCSS_Datasheet.pdf
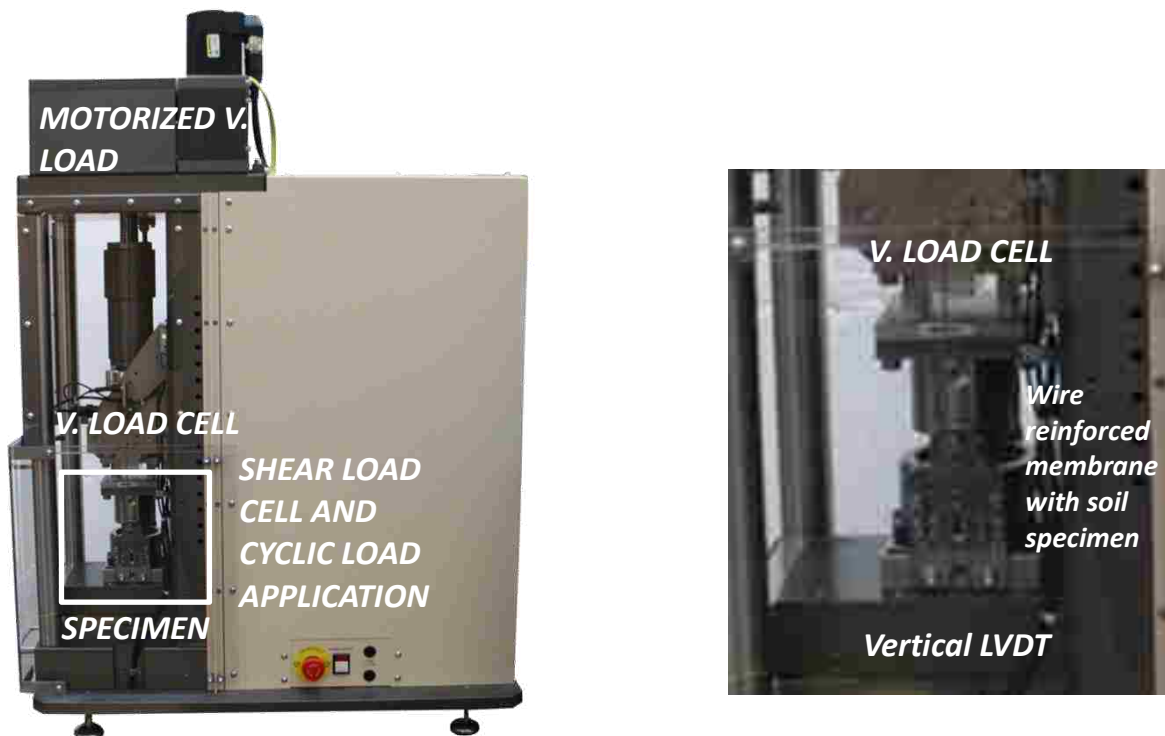

Figure D.1: EMDCSS device (left) and specimen set-up (right)

NOTATION

PARAMETER	NAME
α	Static shear stress ratio, τ_o/σ_{vo}
CAV_5	Cumulative average velocity over 5 cm/s
CRR	Critical resistance ratio used in Simplified Method
CSR	Critical stress ratio used in Simplified Method
D_r	Relative density (%)
e	Void ratio
e_c	Critical void ratio
e_{max}	Maximum void ratio obtained through compaction
e_{min}	Minimum void ratio obtained through loose pluviation/deposition
E_{secant}	Secant shear modulus
$E_{tangent}$ or E_{tan}	Tangent shear modulus
FC	Fines content (%)
G_{cyclic}	Average shear modulus over a full cycle
G_{secant} or G_{sec}	Secant shear modulus
$G_{tangent}$ or G_{tan}	Instantaneous or tangent shear modulus
F_{bb}	Stress-strain backbone curve function
FS_L	Factor of safety against liquefaction
H	Height of specimen
γ or ϵ	Strain (%)
γ_c	Equivalent cyclic strain (%)
I_r	Dilatancy index
I_s	Stress intensity
$I_{s,n}$	Normalized stress intensity
K_α	Static shear stress correction factor
K_σ	Overburden stress correction factor
K_0	Membrane confining stress
K_T	Transient static shear stress correction factor
LL	Liquid limit
MSF	Magnitude scaling factor
N_{eq}	Number of equivalent uniform cycles
N_f	Number of cycles to failure
N_L	Number of cycles to liquefaction
PGA	Peak ground acceleration
ϕ	Friction angle
ϕ_{cv}	Constant volume friction angle
r_d	Depth reduction factor
r_u	Pore pressure ratio, or excess pore pressure/σ_{vo}
Sa	Spectral acceleration
σ_v', p', or σ_{3c}'	Effective stress, or σ_{vo}- pore pressure
σ_{vo} or S_{ac}	Initial vertical effective stress
τ	shear stress
τ_{cy}	Cyclic shear stress amplitude
τ_α or τ_o	Initial static shear stress datum
U_p	Permanent average accumulated pore pressure
Δu	Excess pore pressure
ψ, or ξ_R	State parameter
Z	Depth (m)

REFERENCES

Alacon-Guzman, Leonards, G., & Chameau, J. (1988). Undrained monotionic and cyclic loading of sands. *Journal of Geotechnical Engineering ASCE Vol. 114 No 10*, 1089-1108.

Anderson, K. (1976). Behavior of clay subjected to undrained cyclic loading. *Int. Conf. on Behaviour of Offshore Struct.* (pp. 392-403). Trondheim, Norway: BOSS'76.

Anderson, K. (1991). *Cyclic Loading of Soils, From Theory to Design.* Blackie & Son Ltd. .

Andrews, D., & Martin, G. (2000). Criteria or Liquefaction of Silty Soils. *12th World Conference on Earthquake Engineering.* Auckcland, New Zealand.

Arango, I. (1996). Magnitude scaling factors for soil liquefaction evaluations. *J. Geotech. Engrg., ASCE*, 122(11). 929-936.

Been, K., & Jefferies, M. (1985). A State Parameter for Sands. *Geotechnique. Vol 35. No 2. *, 99-112.

Bjerrum, L., & Landva, A. (1966). Direct Simple-Shear Test on a Norwegian Quick Clay. *Geotechnique Vol. 16, No. 1*, 1-20.

Blaker, O., & Anderson, K. (2015). Shear strength of dense to very dense Dogger Bank sand. *Int Symposium on Frontiers in Offshore Geotechnics, ISFOG.* Oslo, Norway.

Bolton, M. (1986). The strength and dilatancy of sands. *Geotechnique 36.1 *, 65-78.

Boulanger, & Idriss. (1991). Earthquake groung motions at soft soil sites. *Proceedigns, 2nd International Conference on Recent Advances in Geotechnical Earthquake Engineering and Soil Dynamics, Vol. III *, (pp. 2265-2271).

Boulanger, & Kulasingam. (2004). Strength loss and localization at silt interlayers in slopes of liquefied sand. *Journal of Geotechnical and Geoenvironmental Engineering 130.11*, 1192-1202.

Boulanger, R. (2003). Relating Kα to Relative State Parameter Index. *Journal of Geotechnical and Geoenvironmental Engineering. ASCE 129(8)*, 770-773.

Boulanger, R., & Idriss, I. (2015). CPT-Based Liquefaction Triggering Procedure. *American Society of Civil Engineers*. doi:10.1061/(ASCE)GT.1943-5606.0001388

Boulanger, R., Wilson, D., & Idriss, I. (2011). Examination and Reevalaution of SPT-Based Liquefaction Triggering Case Histories. *Journal of Geotechnical and Geoenvironmental Engineering 138.8*, 898-909.

Bray, J., & Sancio, R. (2006). Assessment of the liquefaction susceptibility of fine-grained soils. *Journal of geotechnical and geoenvironmental engineering 132.9*, 1165-1177.

Brylawski, E., & Berre, T. (1992, rev. 1997). *Membrane Correction - DSS Apparatus.* GEONOR Inc.

Casagrande. (1936). Characteristics of cohesionless soils affecting the stability of slopes and earth fills. *Journal of the Boston Society of Civil Engineers*.

Cetin, K., & Bilge, H. (2015). Stress Scaling Factors for Seismic Soil liquefaction engineering problems: A performance-based approach. In A. Atilla, & M. Sakr, *Perspectives on Earthquake Geotechnical Engineering* (pp. 113-140). Springer International Publishing.

Chiang, D. (1999). The generalized Masing Models for Deteriorating hystersis and cyclic plasticity. . *Institute of Aeronautics and AStronautics. .*

Darendeli, M. (2001). *Development of a new family of normalized modulus reduction and material damping curves .* PhD Thesis, Dept. of Civil Eng. Univ. of Texas Austin.

DeAlba, P., Seed, H., & Chan, C. (1976). Sand Liquefactionin large scale simple shear tests. *Journal of Getechnical Engineering Div. ASCE 102(GT9)*, 909-27.

Dobry, Ladd, Yokel, Chung, & Powell. (1982). *Prediction of pore pressure buildup and liquefaction of sands during earthquakes by the cyclic strain method.* Washington D.C: National Bureau of Standards. U.S. Department of Commerce.

Dobry, R., Ladd, R., Yokel, F., Chung, R., & Powell, D. (1982). Prediction of pore water pressure buildup and liquefaction of sands during earthquakes by the cyclic strain method. *NBBS Building Scinece Series 138* (pp. 1487-1520). Gaithersburg, Maryland: National Bureau of Standards.

Doroudian, & Vucetic. (1995). A Direct Simple Shear Device for Measuring Small Strain Behavior. *Geotechnical Testing Journal GTJODJ Vol. 18, No. 1*, 69-85.

Dyvik, R. (1984). *Influence of Consolidation Shear Stresses and Relative Density on Threshold Strain and Pore Pressure During Cyclic Straining of Saturated Sand.* United States Arpmy Corps of Engineers, Rensselaer Polytechnic Inst., NY: US Army Engineer Waterways Experiment Station.

Dyvik, R., Berre, T., Lacasse, S., & Raadim, B. (1987). Comparison of truly undrained and constant volume direct simple shear tests. *Geotechnique, Vol.37, No.1*, 3-10.

El Mohtar, C. ,. (2013). Combined Resonant Column and Cyclic Triaxial Tests for Measuring Undrained Shear Modulus Reduction of Sand With Plastic Fines. *Geotechnical Testing Journal, Vol. 36, No. 4.*

Eseller-Bayat, Gokyer, Yegian, Ortakci, & Alshawabkeh. (2013). Design and Application of Simple Shear Liquefaction Box. *Geotechnical Testing Journal 36.3*, 322-330.

Finn, W., Lee, L., & Martin, K. (1977). An effective stress model for liquefaction. *Journal of Geotechnical Engineering. Vol 103, No.6*, 517-553.

Frank, F. (1965). On dilatancy in relation to seismic sources. *Reviews of Geophysics 3.4* , 485-503.

GDS (n.d.). (Retrieved 2016). from http://www.gdsintruments.com/shear_testing.htm.

Green, R., & Terri, G. (2005). Number of Equivalent Concept for Liquefaction Evaluations - Revisited. *Jour. of Geotech. and Geoenviron. Eng.* , 131.

Harder, L., & Boulanger, R. (1997). Application of Ksig and Ka correction factors. *Proceedings, NCEER Workshop on Evaluation of Liquefaction Resistance of Soils* (pp. 167-90). National Center for

Earthquake Engineering Research, SUNY, buffalo, NY: Youd and Idriss, Eds. Techinical Report NCEER-97-0022.

Hoeg, D., Dyvik, R., & Sandbaekken, G. (2000). Strength of undisturbed versus reconstituted silt and silty sand specimens. *ASCE J. geotech and Geoenv. Engineering 126(7)*, 606-617.

Idriss, & Boulanger. (2003). Estimating Ka for use in evaluating cyclic resistance of sloping ground. *8th Proceedings of US-Japan Workshop on Earthquake Resistant Design of Lifeline Facilities and Countermeasures against liquefactions.* Mulitdisciplinary Center for Earthquake Engineering Research, SUNY Buffalo, Buffalo, N.Y.

Idriss, & Boulanger. (2008). Static Shear Correction Factor. In Idriss, & Boulanger, *Soil Liquefaction druing Earthquakes* (pp. 96-113). Oakland, CA: Earthquake Engineering Research Institute.

Idriss, I. (2004). Semi-empirical procedures for evaluating liquefaction potential during earthquakes. *11th International Conference on Soil Dynamics & Earthquake Engineering, Proceedings of the 11th ICSDEE & 3rd ICEGE.* Berkeley, California.

Ishihara, K. (1993). Liquefaction and flow failure during earthquakes. *Geotechnique. Vol 43 No. 3*, 351-415.

Iverson, R. M. (2003–2012). Regulation of landslide motion by dilatancy and pore pressure feedback. *Journal of Geophysical Research: Earth Surface* , 110.F2 .

Kjellman, W. (1951). Testing the Shear Strength of Clay in Sweden. *Geotechnique, Vol. 2*, 225-232.

Konrad, J. (1988). Interpretation of flat plate dilatometer tests in sands in terms of the state. *Geotechnique 38(2)*, 263-277.

Kramer, S. L. (1996). Geotechnical Earthquake Engineering. University of Washington: Pearson Education Inc. .

Krammerer. (2002). *Undrained Response of Monterey 0/30 Sand Under Multidirectional Cyclic Simple Shear Loading Conditions.* Berkeley: Univ. of Califonia Berkeley.

Kwan, W. (2015). *Laboratory Investigation into Evaluation of Sand Liquefaction under Transient Loadings.* Dissertation, Austin, TX.

Liu, A., Stewart, J., Abrahamson, N., & Moriwaki, Y. (2001). Equivalent Number of Uniform Stress Cycles for Soil Liquefaction Analysis. *J. of Geotech. Geoeviron. Eng.* , 127: 1017-1026.

Liu, Stewart, Abrahamson, & Moriwaki. (2001). Equivalent Number of Uniform Stress Cycles for Soil Liquefaction Analysis. *ASCE Journal of Geotechnical and Geoenvironmental Engineering*, 127(12).

Masing, G. (1926). Eigenspannungen und Verfestigung Bim Messing. *2nd International Congress on Applied Mechanics.* Zurich.

Mortezaie, Mladen , & Vucetic. (2012). Small strain cyclic testing with standard NGI simple shear device. *Geotechnical Testing Journal 35.6*, 935-948.

Moss, R., Seed, R., Kayen, R., Stewart, J., Kiureghian, A. D., & Cetin, K. O. (2006). CPT-Based Probabilistic and Deterministic Assessment of In Situ Seismic Soil Liquefaction Potential. *10.1061(ASCE)*.

Mulilis, Seed, H., Chan, C., Mitchell, J., & Arulanandan, K. (1977a). Effects of sample preparation on sand liquefaction. *ASCE Journal of Geotechnical Engineering 103(2)*, 91-108.

Pocino, D., Maraciano, V., & Nicola, V. (2009). Influence of cyclic pre-shearing on undrained behavior of carbonate sand in simple shear tests. In *Geomenchanics and Geoengineering* (pp. 42, 151-161,).

Poulos, S., Castro, G., & Fran, J. (1985). Liquefaction evaluation procedure. *Journal of Geotechnical Engineering 111.6*, 772-792.

Reimer, M., Bray, W., & Arango, I. (1994). *Effects of loading frequency and control of the liquefaction behavior of clean sands.* UC Berkeley: Geotechnical Engienering Report No. UCB\GT\94-07.

Roscoe, K. H. (1953). An Apparatus for the Application of Simple Shear to Soil Samples. *roceedings of the 3rd International Conference on Soil Mechanics and Foundation Engineering* (pp. 189-191). Zurich: Vol 1.

Seed, H. B., & Harder. (1985). Influence of SPT Procedures in Soil Liquefaction Resistance Evaluations. *ASCE Geotechnical Journal*.

Seed, H., & Idriss, I. (1971). Simplified Procedure for Evaluating Soil Liquefaction Potential. *Journal of the Soil Mechanics and Foundations Division, ASCE*, Vol 97, No SM9, Proc. Paper 8371, 1249-1273.

Seed, R. (2003). *Recent advances in soil liquefaction engineering: a unified and consistent framework.* Long Beach, CA: Proceedings of the 26th Annual ASCE Los Angeles Geotechnical Spring Seminar.

Seed, R., & Harder, L. (1990). SPT-based analysis of the cyclic pore pressure generation and undrained residual strength. *Proceedings, H. Bolton Seed Memorial Symposium* (pp. 351-376, Vol. 2). University of California, Berkeley: J.M Duncan ed.

Silver, M., Chan, C., Ladd, R., Lee, K., Tiedemann, townsend, . . . Wilson. (1976). Cycli triaxial strength of standard test sand. *ASCe H. of Geotechnical Engineering. 102(5)*, 511-524.

Stokoe, N. (1984). In situ shear wave velocities from Sprectral Analysis of Surface Waves. *Proceedings from the 8th World Conference of Earthquake Engineering* (pp. Vol II, 31-38). Englewood Cliffs, New Jersey: Prentence-Hall Inc.

T.L. Youd, R. A., Arango, I., Castro, G., Chistian, J., Dobry, R., Finn, W. L., & Harder, L. (2001). *Liquefaction resistance of soils: Summary report from the 1996 NCEER\NSF workshops on Evaluation of Liquefaction resistance of soils.* Journal of Geot. and Geoenviron. Eng.

Tatsuoka, Toki, Miura, Kato, Okamoto, Yamada, . . . Tanizaw. (1986a). Some Factors affecting cyclic undrained triaxial strength of sand. *Soils and Foundations 26(3)*, 99-116.

Teara.govt.nz. (2015). Historic Earthquakes. *Te Ara Encyclopedia Of New Zealand*.

Tika, T. E., Caughan, P., & Lemos, L. (1996). Fast shearing of pre-existing shear zones in soil. *Geotechnique 46.2*, 197-233.

Vaid, Sivathayalan, & Stedman. (1999). Influence of specimen reconstitution method on the undrained response of sand. *ASTM Geotech. Testing Journal 22*, 187-195.

Vaid, Y., & Sivthayalan, S. (1996). Static and cyclic liquefaction potential of Fraser Delta sand in simple shear and triaxial tests. *Jouranl of Geotechnical Engineering, 33*, 281-89.

Van Asch, J. M. (2007). "Techniques, advances, problems and issues in numerical modelling of landslide hazard".

Wang. (1979). *Some Findings in Soil Liquefaction.* Bejing: Water Conservancy and Hydroelectric Power Scientific Research Institute.

Wood, D. M. (2003). *Geotechnical modelling. Vol. 1.* CRC Press.

Woods, R. D. (1978). Measurement of Dynamic Soil Properties, Vol 1. *Proceedings of the ASCE Geotechnical Engineering Division Specialty Conference* (pp. 91-178). Pasadena, CA: ASCE Geotechnical Engineering Devision, New York, NY.

Yoshimi, Tokimatsu, & Hasaka. (1989). Evaluaiton of Liquefaction resistance of clean sands based on high quality undisturbed samples. *Soils and Foundations, Vol 29 No. 1*, 93-104.

Yoshimine, M., & Ishihara, K. (1998). Flow potential of sand during liquefaction. *Soils and foundations 38(3)*, 177-186.

Youd. (1991). Mapping of earthquake induced liquefaction for seismic zonation. *Proceedings, 4th International Conference on Seismic Zonation, Earthquake Engineering Research Institute*, (pp. 111-147 Vol. 1). Stanford University, CA.

Youd, & Idriss. (2001). Liquefaction resistance of soils: summary report from the 1996 NCEER and 1998 NCEER/NSF workshops on evaluation of liquefaction resistance of soils. *Journal of geotechnical and geoenvironmental engineering* .

Youd, T. (1984). Recurrence of liquefaction at the same site. *8th World Conference on Earthquake Engineering* (pp. Vol 3, pp 231-238). Proceedings.

Ziotopoulou, K. (2014). *A Sand Plasticity Model for Earthquake Engineering Applications.* PhD Thesis, Davis, California.